2018

Temporal Coordination Of Mitotic Chromosome Alignment And Segregation: Structural And Functional Studies Of Kif18a

Haein Kim
University of Vermont

TEMPORAL COORDINATION OF MITOTIC CHROMOSOME ALIGNMENT AND SEGREGATION: STRUCTURAL AND FUNCTIONAL STUDIES OF KIF18A

A Dissertation Presented

by

Haein Kim

to

The Faculty of the Graduate College

of

The University of Vermont

In Partial Fulfillment of the Requirements
for the Degree of Doctor of Philosophy
Specializing in Cellular, Molecular, and Biomedical Sciences

October, 2018

Defense Date: May 15, 2018
Dissertation Examination Committee:

Jason K. Stumpff, Ph.D., Advisor
Sylvie Doublié Ph.D., Chairperson
Chrisopher L. Berger, Ph.D.
Alan K. Howe, Ph.D.
David M. Warshaw, Ph.D
Cynthia J. Forehand, Ph.D., Dean of the Graduate College

ABSTRACT

Chromosome alignment is highly conserved in all eukaryotic cell divisions. Microtubule (MT) -based forces generated by the mitotic spindle are integral for proper chromosome alignment and equal chromosome segregation. The kinetochore is a multi-subunit protein complex that assembles on centromeric regions of chromosomes. Kinetochores tether chromosomes to MTs (K fibers) that emanate from opposite poles, in a process called biorientation. This linkage translates K fiber dynamics into chromosome movements during alignment and segregation. Stable, high-affinity kinetochore attachments promote spindle assembly checkpoint (SAC) silencing, which is active when unattached kinetochores are present. During chromosome alignment, 1) K fiber plus-end dynamics decrease, confining chromosome movements near the spindle equator, and 2) electrostatic interactions between kinetochore proteins and MTs increase. Chromosome segregation occurs as soon as all chromosomes are stably attached to microtubules and the SAC has been silenced. SAC silencing and chromosome alignment are temporally coordinated during normal divisions, implying that the mechanisms regulating *K fiber dynamics* and *kinetochore affinity* must be linked. Interestingly, HeLa cells depleted of a kinesin-8 motor Kif18A, known for its role in promoting chromosome alignment, display a SAC-dependent mitotic delay due to kinetochore-MT attachment defects. This is puzzling, as Kif18A's function in chromosome alignment is to suppress MT growth by stably associating with MT plus-ends. Whether Kif18A is required for attachment in all cells and how it promotes kinetochore microtubule linkages are not understood.

The work presented in this dissertation supports a model in which Kif18A functions as a molecular link that coordinates chromosome alignment and anaphase onset. We find that Kif18A is required to stabilize kinetochore-MT attachments during mammalian germline development, as germline precursor cells in Kif18A mutant mice are unable to divide during embryogenesis due to an active SAC. However, while all cell types require functional Kif18A for chromosome alignment, mouse primary somatic cells can still divide with normal timing. This finding indicates a cell-type specific dependence on Kif18A for stabilizing kinetochore-MT attachments, and provides evidence that this function might be separate from Kif18A's known role in chromosome alignment. Consistent with this idea, we find that an evolutionarily conserved binding motif for protein phosphatase 1 (PP1) is required for Kif18A's novel role in regulating kinetochore microtubule attachments. Kif18A-PP1 interaction is required for Kif18A-mediated dephosphorylation of the kinetochore protein Hec1, which enhances attachment. However, Kif18A's interaction with PP1 is dispensable for chromosome alignment. Thus, point mutations that disrupt PP1 binding separate Kif18A's role in stabilizing kinetochore attachments from its function in promoting chromosome alignment. Additionally, through structure function studies of the motor domain, we identified a long surface loop (Loop2) that is required for Kif18A's unique MT plus-end binding activity, which is essential for its function in confining chromosome movements. Taken together, we find that Kif18A is molecularly tuned to provide temporal control of chromosome alignment and anaphase entry.

CITATIONS

Material from this or dissertation has been published in the following form:

Czechanski, A., Kim, H., Byers, C., Greenstein, I., Stumpff, J., and Reinholdt, L.G.. (2015). Kif18a is specifically required for mitotic progression during germ line development. Developmental biology 402, 253-262.

Kim, H., Fonseca, C., and Stumpff, J.. (2014). A unique kinesin-8 surface loop provides specificity for chromosome alignment. Molecular biology of the cell 25, 3319-3329.

Material from this dissertation has been submitted for publication on April 14, 2018 in the following form:

Kim, H. and Stumpff, JK.. Kif18A promotes Hec1 dephosphorylation to coordinate chromosome alignment with kinetochore-microtubule attachment. (2018). Submitted.

Material from this dissertation has been submitted to BioRxiv on April 18, 2018 in the following form:

Kim, H., and Stumpff, J.K.. (2018). Kif18A promotes Hec1 dephosphorylation to coordinate chromosome alignment with kinetochore microtubule attachment. bioRxiv.

DEDICATION

I would like to dedicate this dissertation to my parents. I will always remember the time when I was having a quarter-life crisis and almost considered not going to graduate school, and they gently nudged me to reconsider. They always know my strengths and what my passions are, even when I don't think I do. Pursuing a career in science was the best decision I have made for myself, and I have my parents to thank for that. They always encouraged me to enjoy the journey, and not think too much about how long it may take. I am forever grateful for their patience and unending support, and this dissertation would not have been possible without them.

ACKNOWLEDGEMENTS

I would like to thank my mentor and advisor, Dr. Jason K. Stumpff, for giving a biochemist like me a chance to learn about cell biology and mitosis. He has provided me with all the tools to become an independent scientist and to think critically. Most importantly, he showed me how to truly enjoy what you are doing. Any amount of the success I had as a scientist is all due to his mentorship and guidance. I also would like to thank my thesis committee members Dr. Alan Howe, Dr. Sylvie Doublié, Dr. Christopher Berger, and Dr. David Warshaw for their insightful suggestions and encouragement throughout my Ph.D process. I would like to thank the Stumpff lab members Cindy Fonseca, Dr. Heidi Malaby, Leslie Sepaniac, Alex Thompson, Carolyn Marquis, Chris Kruglik, and Lisa Wood, and the rest of the Berumpff (Berger-Stumpff) lab members for making office life much more enjoyable. I would also like to thank the MPBP department, for giving me a home, and also for all of the thoughtful suggestions. Huge thanks to the CMB program for their support, especially Jessica Deaette and Carrie Perkins for keeping my non-academic life in order. I also would like to thank Dr. Jamie Stern and Vicki DeVault for being awesome classmates. Lastly, I have to give a big shoutout to my weekly trivia buddies for being my non-UVM support network and helping me enjoy life outside of school.

TABLE OF CONTENTS

Page

CHAPTER 1: INTRODUCTION

Chromosome alignment, a highly conserved aspect of eukaryotic cell division, is required for proper chromosome segregation and ensures genomic stability with each division. During the cell cycle, the cell prepares to form two genetically identical cells. Each daughter cell must inherit a full set of chromosomes during the cell division process to maintain a stable genome throughout subsequent divisions. Thus, two of the major components of the cell cycle involve duplicating the genome (S phase) and equally distributing the genomic material to each daughter cell (M phase/Mitosis). The gap phases (G1 and G2) provide ample time for the cell to grow and prepare for the next phase of the cell cycle. These gap phases also provide important checkpoints between different phases of the cell cycle. For instance, G1/S and G2/M checkpoints guarantees that the cell transitions to S or M phases only when the cell is fully committed to enter the next phase of the cell cycle. This further ensures that the cell cycle only occurs unidirectionally. Mitosis assures that each daughter cell receives all of the genetic information required to carry out the rest of the cell cycle efficiently and accurately. Despite only occupying a small fraction of time during the cell cycle, mitosis is a highly dynamic process, which necessitates precise coordination of events for its fidelity.

Cells utilize a microtubule-based molecular machine known as the mitotic spindle to align and segregate chromosomes (McEwen et al., 1997). Spindle microtubules generate pushing and pulling forces necessary to align chromosomes and pull apart sister chromatids upon anaphase onset (McEwen et al., 1997). Attachments

between chromosomes and spindle microtubules require specialized protein structures called kinetochores, which assemble at the centromeric region of each chromosome (Bernat et al., 1991; Earnshaw et al., 1991). Efficient use of spindle forces necessary for chromosome alignment and equal segregation requires (1) robust, bioriented attachments between spindle microtubules and sister kinetochore pairs, and (2) precise control of kinetochore microtubule (K fiber) dynamics (McEwen et al., 1997; Stumpff et al., 2008). As equal chromosome segregation requires proper attachments between kinetochores and microtubules, a checkpoint pathway is activated to prevent cells from mitotic progression until every kinetochore is attached (Chen et al., 1998; Rieder et al., 1994). During normal cell division, the checkpoint is silenced and chromosome segregation initiates as soon as all chromosomes are confined at the spindle midzone. Despite decades of study, it remains unclear how chromosome alignment and attachment are temporally coordinated during division.

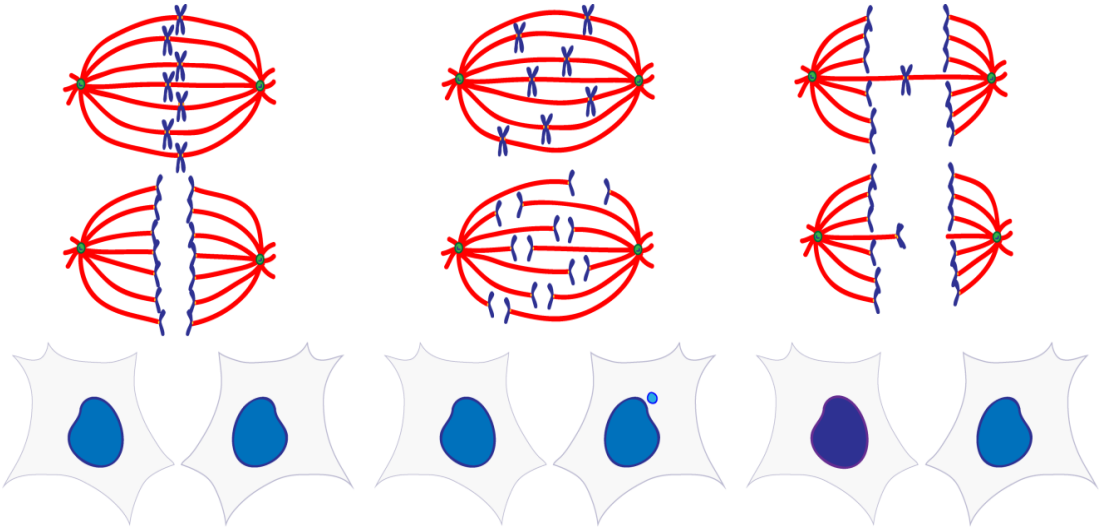

Figure 1-1. Possible consequences for loss of coordination between chromosome alignment and chromosome segregation. During normal cell division, chromosomes segregate only when chromosome alignment is established, ensuring that genomes are equally distributed between each daughter cell (left). When cells segregate chromosomes without alignment, some sister chromatids have to travel long distances to reach the corresponding pole. These chromatids cannot be reincorporated into the main nucleus, and form a micronucleus (middle). When a kinetochore is attached to microtubules from both poles, and the error is not resolved prior to segregation, this results in a lagging chromosome and one daughter cell with abnormal chromosome number, or aneuploidy (right).

What happens when chromosome alignment is not coordinated with anaphase entry?

Divisions that occur with chromosome alignment or attachment errors increase the likelihood of genomic instability in daughter cells, which directly affects the daughters' viability during subsequent cell cycles (Uetake and Sluder, 2010). Chromosome segregation without alignment leads to micronucleus formation (Figure 1-1, center) (Fonseca, et al., 2018). A micronucleus contains chromosome fragments or whole chromosomes that are isolated from the main nucleus. This isolated genetic material can undergo catastrophic rearrangement due to incomplete DNA replication (Crasta et al., 2012; Zhang et al., 2015). On the other end of the spectrum, chromosome segregation in the presence of erroneous attachments between kinetochores and microtubules can result in formation of either micronucleated or aneuploid daughter cells, which contain an abnormal number of chromosomes (Figure 1-1, right) (Cimini et al., 2001; Salmon et al., 2005). Aneuploidy is one of the leading causes of spontaneous abortions during early stages of pregnancy, is the molecular cause of trisomy syndromes such as Down syndrome, and is even used as a measure of malignancy in certain types of cancers (Hogge et al., 2003; Lengauer et al., 1997; Nagaoka et al., 2012).

The kinetochore-microtubule attachment process during early mitosis is often error prone and these errors must be corrected for equal distribution of genomic material (Cimini et al., 2003). Sister kinetochore pairs must be attached to microtubules from opposite poles, or bioriented, to ensure equal segregation (Figure 1-2, 1.). Intermediate attachment states that occur during the process of biorientation can

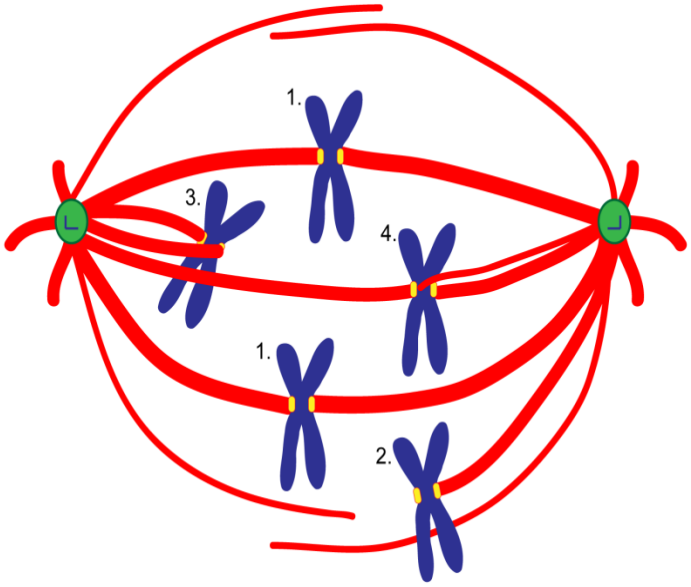

Figure 1-2. Schematic of kinetochore microtubule attachments within the spindle. For faithful chromosome segregation, replicated sister chromatids must attach to microtubules from opposite spindle poles to achieve a bioriented attachment (1.). Erroneous attachments are common during early mitosis, resulting in monotelic attachments, in which only one kinetochore of a sister pair is attached (2.), or syntelic attachments in which both sister kinetochores attach to microtubules that emanate from the same pole (3.). Merotelic attachments occur when microtubules from opposite poles attach to the same kinetochore (4.)

result in segregation errors if they are not corrected. For instance, a single kinetochore from the sister pair typically binds to microtubules *first*, resulting in a monotelically attached kinetochore pair (Figure 1-2, 2.) Sister kinetochores closer to the spindle poles, where the microtubule density is high, can also connect with microtubules that emanate from the same pole, forming a syntelic attachment (Figure 1-2, 3.). Merotelic attachments, or microtubule attachments from both poles to a single kinetochore, can also arise. Merotelic attachments are known to be significant contributors to aneuploidy (Figure 1-2, 4.) (Cimini et al., 2001). Mechanisms that prevent aneuploid cells from entering the next division cycle are in place to prevent the propagation of chromosome segregation mistakes. For example, unaligned chromosomes, which could contribute to missegregation, are post-translationally modified via phosphorylation of histone H3.3 (Hinchcliffe et al., 2016). This phosphorylation results in activation of a p53-dependent DNA damage checkpoint pathway and cell cycle arrest in the daughter cells (Hinchcliffe et al., 2016). Similarly, micronucleated chromosomes are prone to DNA damage and DNA replication errors (Crasta et al., 2012; Zhang et al., 2015), which can trigger the DNA damage checkpoint and arrest the cells in G1 (Lewis and Golsteyn, 2016).

1. Nuclear envelope breakdown

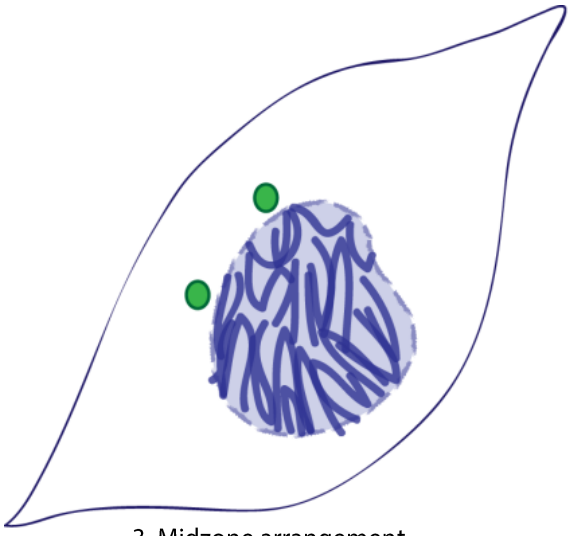

2. Rosette formation

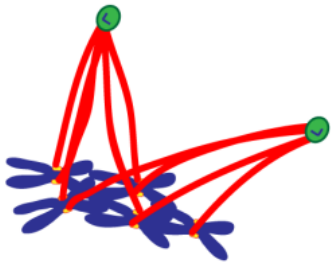

3. Midzone arrangement

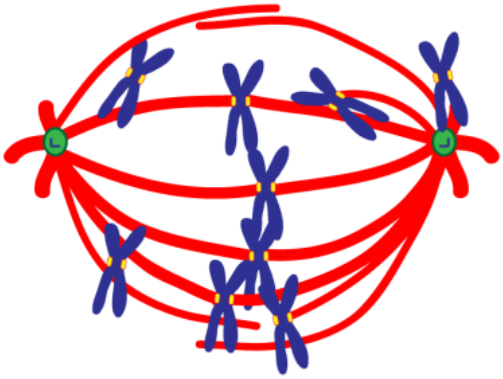

4. CENP-E dependent movement towards the equator

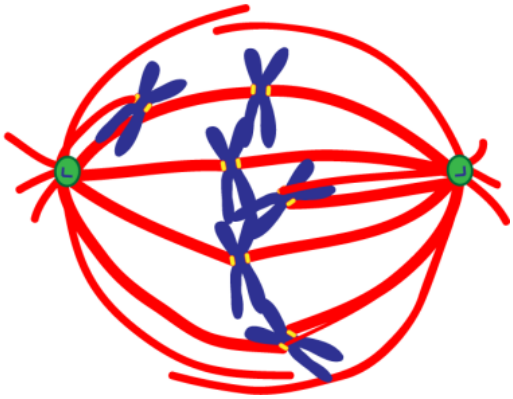

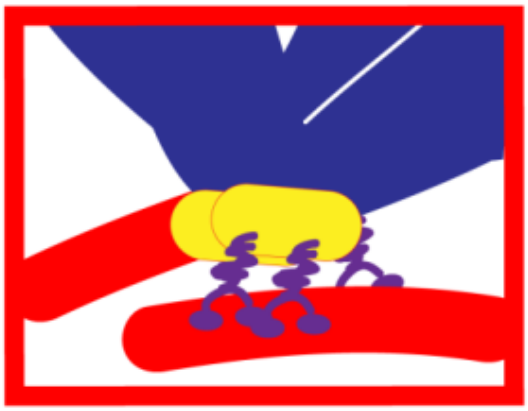

Figure 1-3. Schematic showing how the spatial arrangement of chromosomes, kinetochore geometry, and motor activity facilitate biorientation. 1) As the nuclear envelope breaks down, the spindle poles already started to migrate to opposite ends of the cell. 2) Chromosomes are organized in a rosette with arms facing out and kinetochores facing inward, which promotes interactions between kinetochores and microtubules nucleated from the spindle poles. 3) Bipolar spindle formation spatially arranges microtubule plus-ends towards the middle of the cell. Lateral contacts are made between the kinetochore and microtubules. 4) CENP-E dependent lateral kinetochore (yellow) attachment brings pole proximal chromosome (arrow) to the midzone. Lateral attachments are initially made by the motor CENP-E (red square, CENP-E motors in purple).

In order to promote equal segregation of chromosomes, cells regulate sister kinetochore geometry, the spatial arrangement of chromosomes at the onset of mitosis, and the bipolar nature of the spindle to favor the formation of bioriented attachments. During prophase, the nuclear envelope breaks down as spindle poles migrate towards opposite sides of the nucleus, initiating the formation of a bipolar spindle with the replicated chromosomes in the center (Figure 1-3, 1.). Next, chromosomes are organized into what is known as a prometaphase rosette, which promotes kinetochore contact with spindle microtubules (Figure 1-3, 2.) (Cai et al., 2009; Itoh et al., 2018; Kapoor et al., 2006; Magidson et al., 2011; Nagele et al., 1995). The bipolar nature of the spindle directs microtubule plus-ends towards the middle of the spindle, also enhancing biorientation (Figure 1-3, 3.) (Loncarek et al., 2007). Sister kinetochore pairs face away from each other, towards opposite spindle poles, geometrically biasing the kinetochore interface to engage with microtubules from a single spindle pole (Loncarek et al., 2007; Magidson et al., 2011; Wollman et al., 2005; Zaytsev and Grishchuk, 2015). Chromokinesins that decorate the chromosome arms are known to play a role in maintaining the kinetochore geometry (Brouhard and Hunt, 2005; Levesque and Compton, 2001; Magidson et al., 2011). Additionally, kinetochore architecture changes from a diffuse airy disc to a more punctate disc as microtubules are bound, spatially restricting the microtubule binding sites to prevent microtubule attachments from both poles (Magidson et al., 2015). Kinesins that decorate the chromosomes such as Kid, a part of kinesin-10 family, generate pushing forces that maintains sister kinetochore pairs to be parallel to the spindle pole axis (Brouhard and Hunt, 2005; Drpic et al.,

2015; Yajima et al., 2003). Initial contact between kinetochores and microtubules typically involves association with the lateral surface of a spindle microtubule (Figure 1-3, 4., red square). This lateral interaction is facilitated by CENP-E, a kinesin motor that is part of kinesin-7 family. Initial attachments to the kinetochore are stabilized through tension applied across the sister kinetochore pair. Exactly how this tension is generated is not well understood. However, an example of tension generation that has been observed is when a monotelically attached sister kinetochore is pulled towards the spindle pole, while its laterally attached sister starts moving towards the center of the spindle (Figure 1-3, 2.). This tension is a net result of the opposing forces generated by non-chromatin interacting microtubules exerting pushing forces via PEFs, and the pulling forces generated by the depolymerizing K fiber on the monotelically attached kinetochore. While lateral attachments can be geometrically bioriented and induce tension across sister kinetochores, these attachments are insufficient to silence the spindle assembly checkpoint, which prevents the metaphase to anaphase transition (Kuhn and Dumont, 2017). The plus-end directed motility of CENP-E and PEFs promote the transition from lateral to end-on attachments, which are able to silence the checkpoint and support chromosome segregation (Drpic et al., 2015; Shrestha and Draviam, 2013).

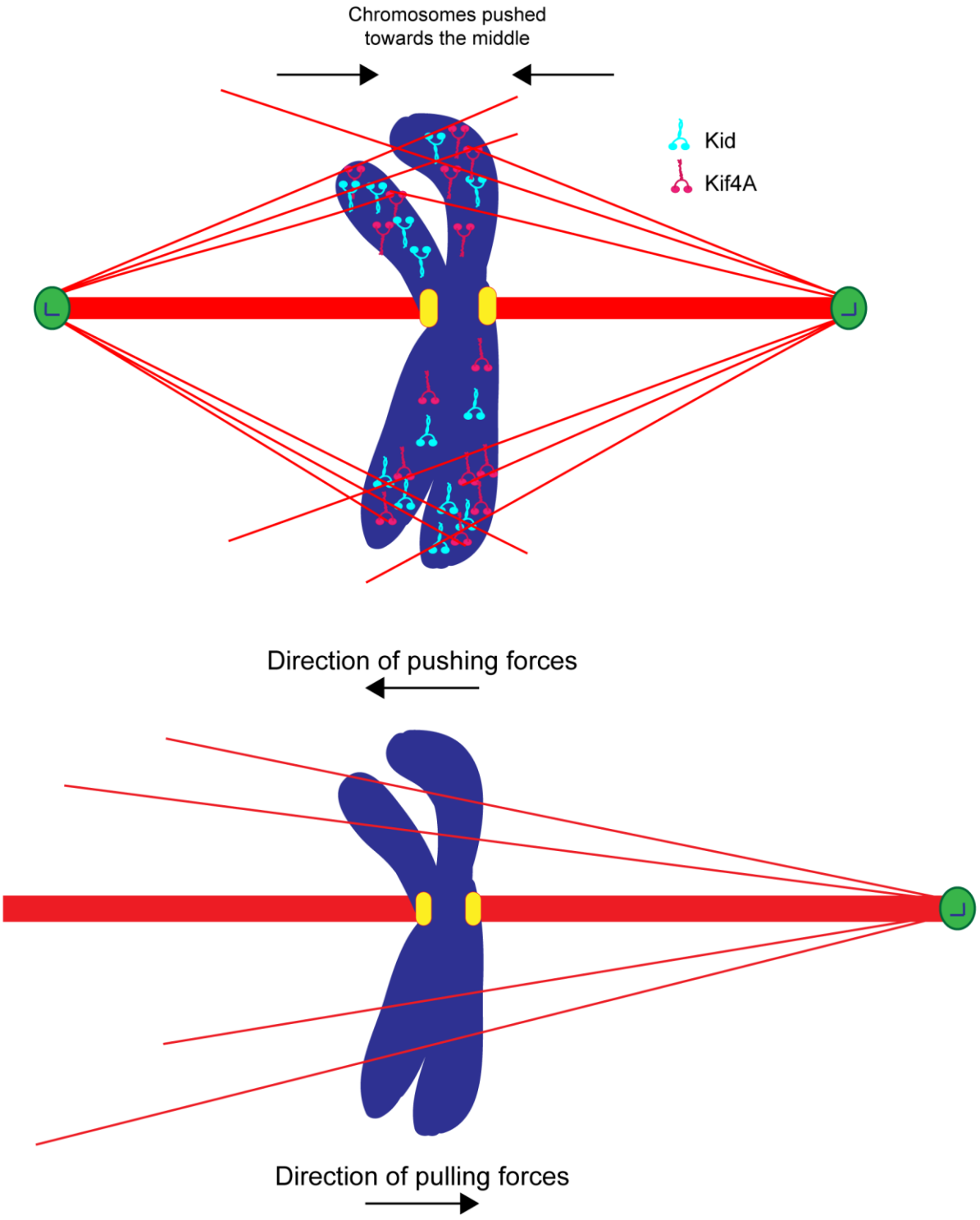
Chromosomes pushed
towards the middle
Kid
Kif4A
Direction of pushing forces
Direction of pulling forces

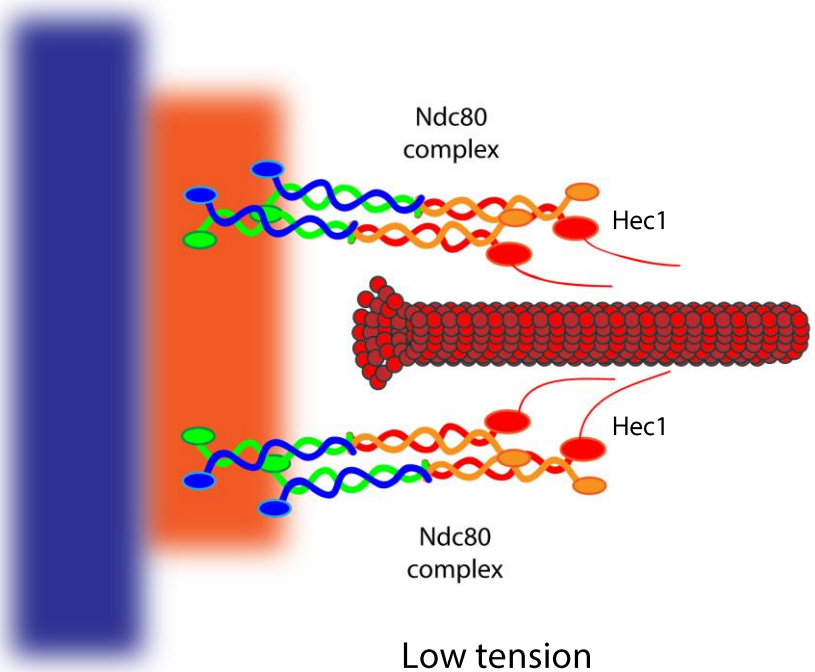

Low tension

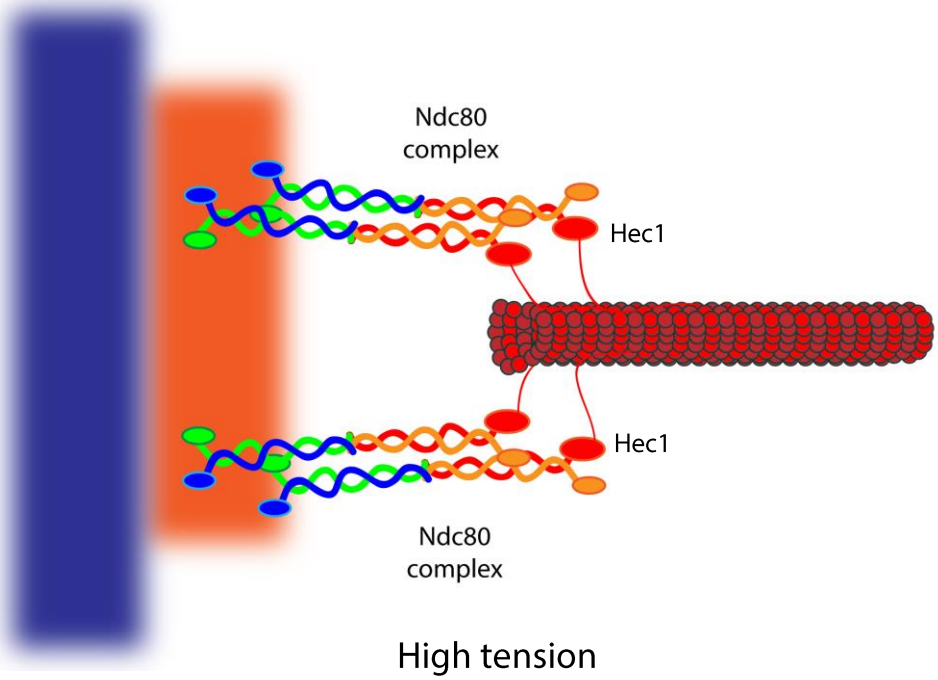

High tension

Figure 1-4. Schematic depicting how opposing microtubule based forces can stabilize end-on microtubule attachments. Chromokinesins Kif4A and Kid contain DNA binding motifs in the C-terminal tail. Kif4A limits the growth of microtubules that contact the chromosome arms, and Kid exerts pushing forces against the chromosome interacting microtubules. Together, they confine the chromosome arms towards the center of the spindle. These pushing forces oppose the pulling forces generated by the depolymerizing microtubules on the poleward moving K fiber, putting tension on the kinetochore. Under low tension, the N -terminal tail of Hec1 may not be in direct contact with the microtubule lattice. Under high tension, Hec1 interacts with the microtubule lattice with higher affinity, stabilizing the interaction.

Kinetochore-microtubule attachment stability and regulation

The kinetochore itself is a multi-subunit protein complex which links chromosomal DNA with microtubules that make up the K fiber. This physical connection to the spindle microtubules translates spindle generated pushing and pulling forces to chromosome movements observed during mitosis (Cassimeris et al., 1990; Maiato et al., 2004; McEwen et al., 1997). The kinetochore is roughly divided into two separate components: the inner and the outer kinetochore (Figure 1-5). Proteins that directly bind to centromeric DNA are part of the constitutive centromere associated network, or CCAN (Figure 1-5) (Przewloka et al., 2011; Screpanti et al., 2011; Sullivan et al., 1994). The outer kinetochore includes proteins that directly contact the microtubule, such as KNL1, Mis12, and Ndc80 network, or KMN (Figure 1-5) (Cheeseman et al., 2006; Petrovic et al., 2010; Rosenberg et al., 2011; Screpanti et al., 2011). It also includes other centromeric associated proteins that respond to tension, which bridge the gap between the centromere associated, and microtubule binding proteins, such as CENP-T and Mis12 complexes (Figure 1-5) (Screpanti et al., 2011).

The inner kinetochore contains proteins that are constitutively associated with the centromere (Screpanti et al., 2011; Sullivan et al., 1994). CENP-A, or centromeric protein A, a variant of histone H3, becomes deposited into the centromeric nucleosome during S phase of the cell cycle (Sullivan et al., 1994). CENP-A provides a template on which the rest of the kinetochore can assemble (Sullivan et al., 1994). CENP-C has been shown to enhance the recruitment of outer kinetochore proteins such as KNL1 and Mis12, which in turn provides a scaffold for microtubule binding proteins within the

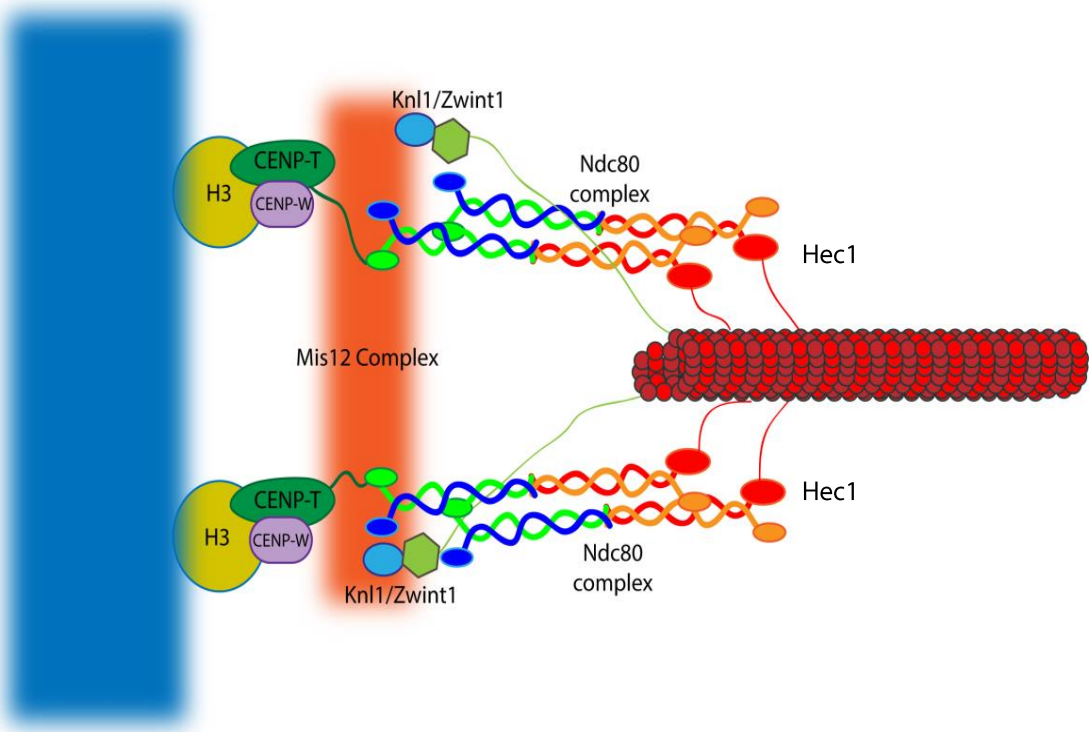

Figure 1-5. A schematic depicting CCAN (constitutive centromere associated network) and the microtubule binding KMN (KNL1, Mis12 Ndc80) network. CENP-A is first deposited, which recruits other kinetochore components. CENP-T contains a histone fold which allows for DNA binding. The N-terminal tail of CENP-T can interact with the Mis12 complex, or the NDC80 complex, linking the inner and the outer kinetochore complexes. The NDC80 complex, Hec1 in particular, directly interacts with the microtubule, providing a physical link between the chromosome and spindle microtubules.

Ndc80 complex to assemble (Przewloka et al., 2011; Screpanti et al., 2011). CENP-T and CENP-C help to recruit the Ndc80 complex by interacting with Mis12 to bridge the inner centromeric proteins to the microtubule binding proteins at the outer kinetochore (Przewloka et al., 2011; Screpanti et al., 2011).

The proteins that make up the outer kinetochore provide a direct connection between the chromosome and the microtubule lattice. The KNL1 complex, which consist of Knl1 and Zwint, can bind to the Mis12 complex and the microtubules, contributing to chromosome segregation (Cheeseman et al., 2004; Kline et al., 2006). KNL1 recruits many signaling molecules that are necessary for an active spindle assembly checkpoint pathway, and also affect microtubule binding by modulating Aurora B kinase activity (Caldas et al., 2013). While the KNL1 complex can certainly associate with microtubules, the heterotetrameric Ndc80 complex is predominantly responsible for the end-on attachments of kinetochores (Ciferri et al., 2005; DeLuca et al., 2005; Sundin et al., 2011). The Ndc80 complex consists of Spc24/25, Nuf2 and Hec1, and provides the primary linkage between the kinetochore and the microtubule (Ciferri et al., 2005; DeLuca et al., 2005; DeLuca et al., 2006; Sundin et al., 2011). Cells depleted of KNL1 can still make bioriented attachments, as opposed to Hec1 depleted (Cheeseman et al., 2004) cells, which cannot form robust K fibers (Caldas et al., 2013).

Ensuring faithful chromosome segregation relies heavily on maintaining stable, high affinity attachments between K fiber microtubules and kinetochores. Cells take advantage of electrostatic interactions between kinetochore components directly

contacting the microtubule, and microtubule surfaces, to secure end-on attachments (Cheeseman et al., 2006; Ciferri et al., 2005; DeLuca et al., 2005; DeLuca et al., 2006; DeLuca et al., 2011; Sarangapani et al., 2013; Umbreit et al., 2012). As part of the Ndc80 complex, Hec1 provides the physical tether to microtubules, and its affinity is under phosphoregulation by Aurora B kinase and protein phosphatase 1 (PP1) (Figure 1-6) (Cimini et al., 2006; Liu et al., 2010a). Hec1 is heavily phosphorylated by Aurora B during early mitosis, and is subsequently dephosphorylated, with significantly low levels seen in metaphase and anaphase (Figure 1-6, left) (DeLuca et al., 2011). Several PP1 recruitment mechanisms have been described, and a role for PP1 in general antagonization of Aurora B activity is well established. However, the mechanisms underlying direct dephosphorylation of Hec1 have not been determined (Figure 1-6, right) (Liu et al., 2010a; Sivakumar et al., 2016).

Aurora B and PP1 activities are regulated by other proteins that are at the kinetochore. Like other phosphatases, PP1 requires the binding of a regulatory subunit for its catalytic activity. A short peptide of just 4 residues containing the canonical binding motif RVXF is sufficient for PP1's phosphatase activity (Tappan and Chamberlin, 2008). Aurora B kinase autophosphorylation activates the kinase, and PP1/PP2A have been shown to inactivate Aurora B (Qian et al., 2015). While KNL1 contains a PP1 binding site (RVXF) and recruits PP1, KNL1-dependent PP1 recruitment is not required for the regulation of Aurora B activity (Caldas et al., 2013) However, KNL1 recruits Bub1 kinase to increase Aurora B activity at the outer kinetochore through several Bub1 binding (MELT) motifs (Caldas et al., 2013) .

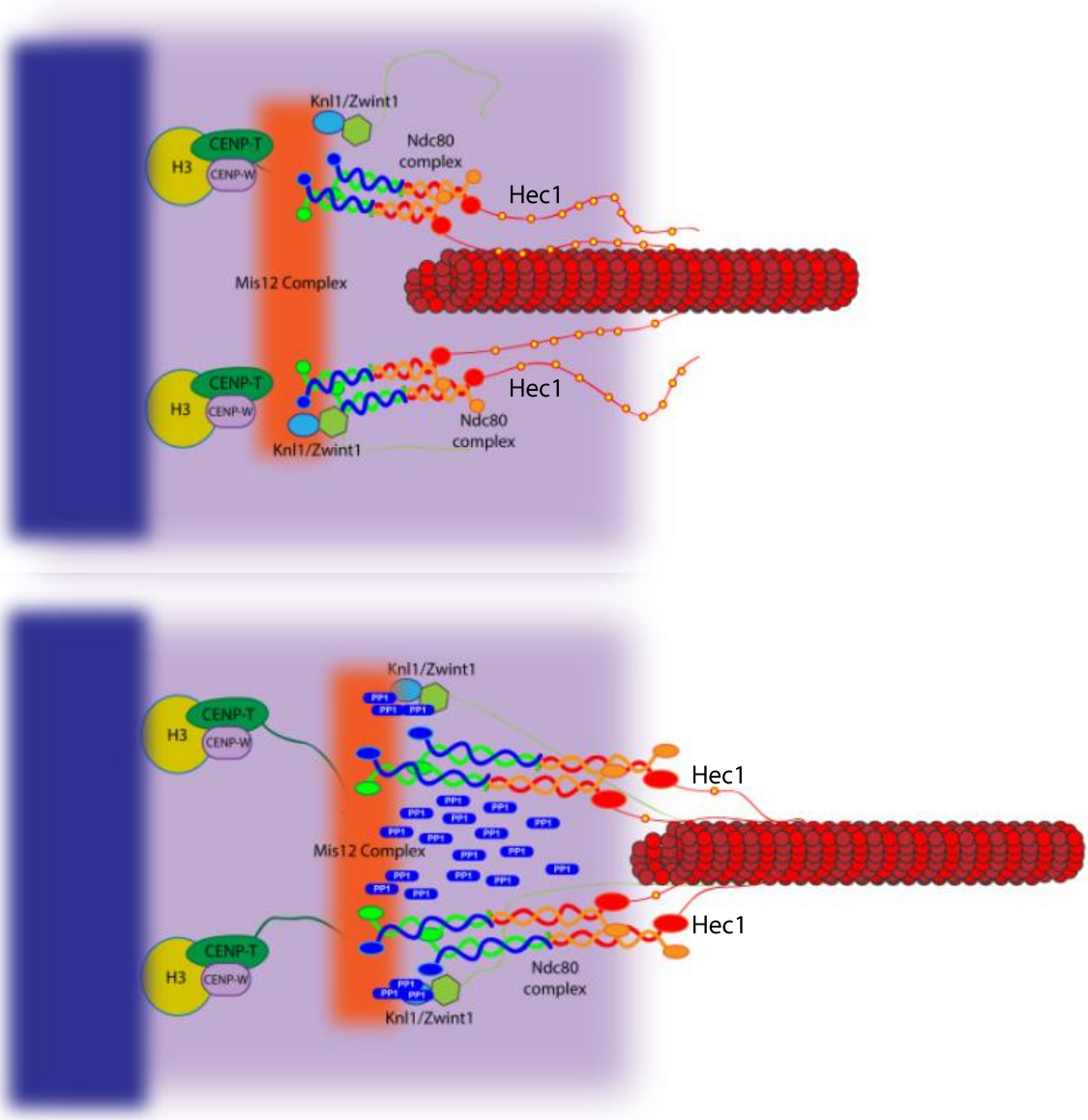
Knl1/Zwint1
Ndc80
complex
CENP-T
H3
CENP-W
Hec1
Mis12 Complex
CENP-T
H3
CENP-W
Hec1
Ndc80
complex
Knl1/Zwint1
Knl1/Zwint1
CENP-T
H3
CENP-W
Hec1
Mis12 Complex
Hec1
CENP-T
H3
CENP-W
Ndc80
complex
Knl1/Zwint1

Figure 1-6. A schematic of how kinetochore affinity to microtubules is regulated by Aurora B and PP1. Under low tension (top), Aurora B can reach the outer kinetochore substrates including the N-terminal tail of Hec1, which contains 9 proposed Aurora B consensus sites. Upon stable bioriented attachment (bottom), sister kinetochores are under high tension, and are stretched apart, providing spatial separation of Aurora B from its outer kinetochore substrates. This provides a chance for kinetochore associated protein phosphatase 1 (PP1) to counteract Aurora B activity at the outer kinetochore and stabilize these attachments.

The Hec1 N-terminal tail contains 9 confirmed Aurora B phosphorylation sites that are phosphorylated early in mitosis (DeLuca et al., 2006). Addition of negative charges via phosphorylation disrupts electrostatic interactions between the positively charged N-terminus of Hec1 and the negatively charged microtubule lattice. Throughout mitotic progression, the Hec1 tail is gradually dephosphorylated, with the lowest levels occurring at the metaphase-to-anaphase transition (DeLuca et al., 2011). Precisely, how kinetochores transition from low to high affinity, while maintaining enough plasticity to diffuse along with growing K fibers is currently unknown.

Studies using purified kinetochore particles highlight the importance of changes in electrostatic affinity for the movement of kinetochores along the microtubule lattice and the maintenance of end-on attachments under load. *In vitro* studies using a Hec1 variant with alanine substitutions at all nine Aurora B phosphorylation sites (Hec1-9A) showed hyper-stable binding to the microtubule, with decreased motility along the microtubule lattice (Umbreit et al., 2012; Zaytsev et al., 2014). In contrast, purified Hec1 with nine phosphomimetic substitutions (Hec1-9E) was more likely to detach from the microtubule, suggesting that Hec1 phosphorylation regulates the binding of Hec1 to microtubules (Sarangapani et al., 2013; Umbreit et al., 2012).

In addition to harnessing microtubule-based forces for chromosome movement, kinetochore attachment can also affect microtubule plus-end turnover, which directly influences microtubule dynamics (DeLuca et al., 2005). Increased plus-end tubulin turnover on K fibers in cells expressing the phosphomimetic Hec1 variant suggests that low affinity interaction increases microtubule dynamics, exemplified by wide and faster

chromosome oscillations (Zaytsev et al., 2014). Conversely, K fibers in cells expressing a Hec1 variant with non-phosphorylatable alanine residues (Hec1-9A) at the phosphorylation sites show hyperstability even in conditions that normally destabilize microtubules. Cells expressing the non-phosphorylatable mutant also show decreased tubulin turnover at plus-ends, leading to significantly reduced chromosome oscillations (DeLuca et al., 2006). Hec1 affinity can be modified by adding phosphomimetic residues to the high affinity Hec1 variant (Hec1-9A). Interestingly, a Hec1 mutant containing one phosphomimetic site (Hec1-1D) recapitulated normal chromosome oscillations (DeLuca et al., 2011; Zaytsev et al., 2014). However, while normal oscillatory movement indicates normal regulation of microtubule dynamics necessary for chromosome alignment, cells expressing Hec1-1D are unable to restore chromosome alignment to levels observed in control cells (Zaytsev et al., 2014).

Spindle assembly checkpoint

The SAC monitors kinetochore attachment status to spindle microtubules and prevents cells from entering anaphase until all kinetochores are tethered to the spindle (Figure 1-7, 1.)(Hoyt et al., 1991; Li and Murray, 1991). Anaphase promoting complex (APC), an E3 ubiquitin ligase, targets proteins for degradation (Sudakin et al., 2001; Thornton and Toczyski, 2003). APC remains inactive by associating with an inhibitory complex called the mitotic checkpoint complex (MCC) when unattached kinetochores are present (Irniger et al., 1995; King et al., 1995; Sudakin et al., 1995). MCC association with the APC generates the ‘wait-anaphase’ signal by preventing the

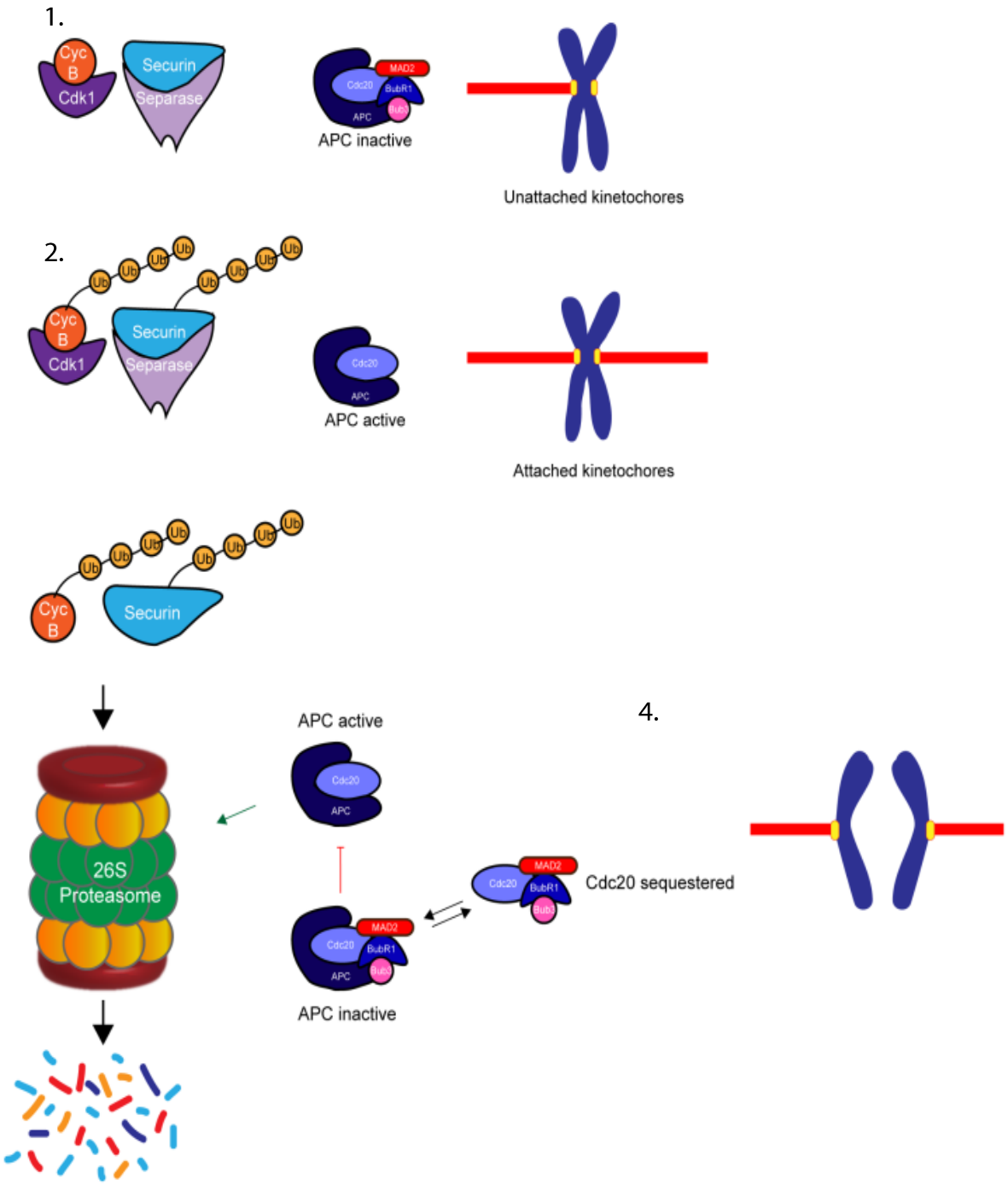
1.
Cyc B
Cdk1
Securin
Separase
MAD2
Cdc20
BubR1
Bub1
APC
APC inactive
Unattached kinetochores
2.
Ub
Cyc B
Cdk1
Securin
Separase
Cdc20
APC
APC active
Attached kinetochores
Cyc B
Securin
APC active
4.
26S Proteasome
Cdc20 sequestered
APC inactive

Figure 1-7. A schematic of how the spindle assembly checkpoint (SAC) prevents anaphase entry. 1.) When unattached kinetochores are present, the checkpoint proteins form a complex that inhibits a ubiquitin ligase APC, or anaphase promoting complex. 2.) When kinetochores are attached to spindle microtubules, the inhibitory complex is diminished, allowing active APC to ubiquitylate its target proteins, such as cyclin-B and securin. 3.) During metaphase, as kinetochores make contact with the spindle microtubules, inhibitors of APC assemble and disassemble. More unattached kinetochores result in more inhibitors of APC. As soon as the last unattached kinetochore binds to microtubules, degradation of cyclin-B and securin by the 26S proteasome is initiated. Securin inhibits the enzyme Separase, which cleaves cohesion that holds sister chromatids together. This allows the sister chromatids to separate (4.), and start moving towards the spindle poles.

degradation of Cyclin-B and Securin (Sudakin et al., 1995; Thornton and Toczyski, 2003). More specifically, Cdc20, the cofactor for APC, is sequestered by the MCC, which is comprised of proteins MAD2 (Mitotic arrest deficient 2), Bub3 (Budding uninhibited by benzimidazoles 3), and BubR1 (Bub related protein 1) (Fang et al., 1998a; Fang et al., 1998b; Hwang et al., 1998; Sudakin et al., 2001). MAD1 binds to unattached kinetochores where it recruits and activates soluble MAD2 for Cdc20 binding by inducing a conformational change in MAD2. MAD1 and MAD2 complexes are only displaced from kinetochores after end-on kinetochore microtubule attachments are established (Rieder et al., 1994). MAD1/MAD2 complexes are stripped from microtubule-attached kinetochores via a pathway that relies on dynein, a minus-end directed motor (Silva et al., 2014) upon microtubule binding. It has also been shown that the monopolar spindle 1 (Mps1) kinase recruits MAD1/MAD2 at the kinetochore (Jelluma et al., 2010). Mps1 removal from the kinetochore, in turn, can decrease MAD1/MAD2 kinetochore localization (Jelluma et al., 2010). It has also been speculated that microtubule binding sterically inhibits the dynamic binding of MAD1/MAD2 at the kinetochores, gradually diminishing the pool of MAD1/MAD2 that can remain bound at the kinetochore (Magidson et al., 2016; Magidson et al., 2015). The SAC detects the presence of kinetochores that are not coupled to the spindle microtubules (Chen et al., 1998; Rieder et al., 1994) but does not recognize all erroneous attachments. For example, monotelically attached sister kinetochore pairs fail to silence the SAC, whereas erroneous attachments involving syntelically or merotelically attached kinetochores are able to satisfy the SAC (Cimini et al., 2001).

Fortunately, the inherent dynamic instability of microtubules enhances the probability that they will detach from kinetochores. Sister kinetochore pairs that are not stably bioriented are under low tension also destabilize kinetochore-microtubule attachments through an Aurora B-dependent mechanism (Cimini et al., 2006; DeLuca et al., 2006), providing the opportunity for a correct attachment to be made by another microtubule. Thus, the tension created by bioriented attachments biases the stabilization of properly connected chromosome pairs (Akiyoshi et al., 2010)

Regulating K fiber dynamics

The mitotic spindle relies on dynamic microtubules to exert pushing and pulling forces to properly align chromosomes and to pull them apart. Microtubule associated proteins (MAPs), including kinesin family motor proteins, regulate the plus-end dynamics of spindle microtubules to promote chromosome alignment (Stumpff et al., 2008; Stumpff et al., 2012). Dynamic non-kinetochore microtubules contact chromosome arms and serve as the tracks for PEF-generating chromokinesins, such as Kid (kinesin-10). While PEFs push chromosome arms towards the midzone of the cell, depletion of chromokinesins has little impact on chromosome alignment during metaphase (Levesque and Compton, 2001; Stumpff et al., 2012). These data indicate that regulation of non-kinetochore microtubules does not play a significant role in chromosome organization at the midzone of the cell.

K fiber dynamics predominantly drive chromosome alignment during metaphase (McEwen et al., 1997; Skibbens et al., 1993) For K fiber dependent

chromosome alignment, biorientation is dispensable. For instance, cells that are forced to enter mitosis without replicating their genomes (mitosis with unreplicated genome, MUG) contain unpaired kinetochores that align at the spindle equator and satisfy the spindle assembly checkpoint (O'Connell et al., 2008). This suggests that regulation of K fiber dynamics is sufficient for chromosome alignment during metaphase. Members of the kinesin-8 family play a conserved role in the regulation of microtubule dynamics to promote chromosome alignment (Gupta et al., 2006; Mayr et al., 2007; Stumpff et al., 2008; Varga et al., 2006).

The mammalian kinesin-8 Kif18A (Figure 1-8) stably associates with the plus-ends of K fibers and directly attenuates their dynamics during metaphase (Du et al., 2010; Mayr et al., 2007; Stumpff et al., 2008). Cells depleted of endogenous Kif18A display wider and faster chromosome oscillations during metaphase, indicative of faster K fiber dynamics (Mayr et al., 2007; Stumpff et al., 2008). *In vitro* studies have shown that Kif18A is a highly processive, plus-end directed motor that can travel several microns along a microtubule track. Kif18A also displays a dwell time of 50+ seconds at the plus-ends of microtubules (Stumpff et al., 2011). This plus-end binding is critical for the motor to directly attenuate microtubule growth and shortening (Stumpff et al., 2011). Kif18A contains an additional microtubule binding site within the C-terminal tail that tethers the protein to the microtubule during processive movement. This activity allows the motor to travel distances along a microtubule equivalent to half of the spindle length *in vitro* and is required for Kif18A's accumulation at the plus-ends of K fibers in cells (Du et al., 2010; Stumpff et al., 2011; Stumpff et al., 2008). The C-

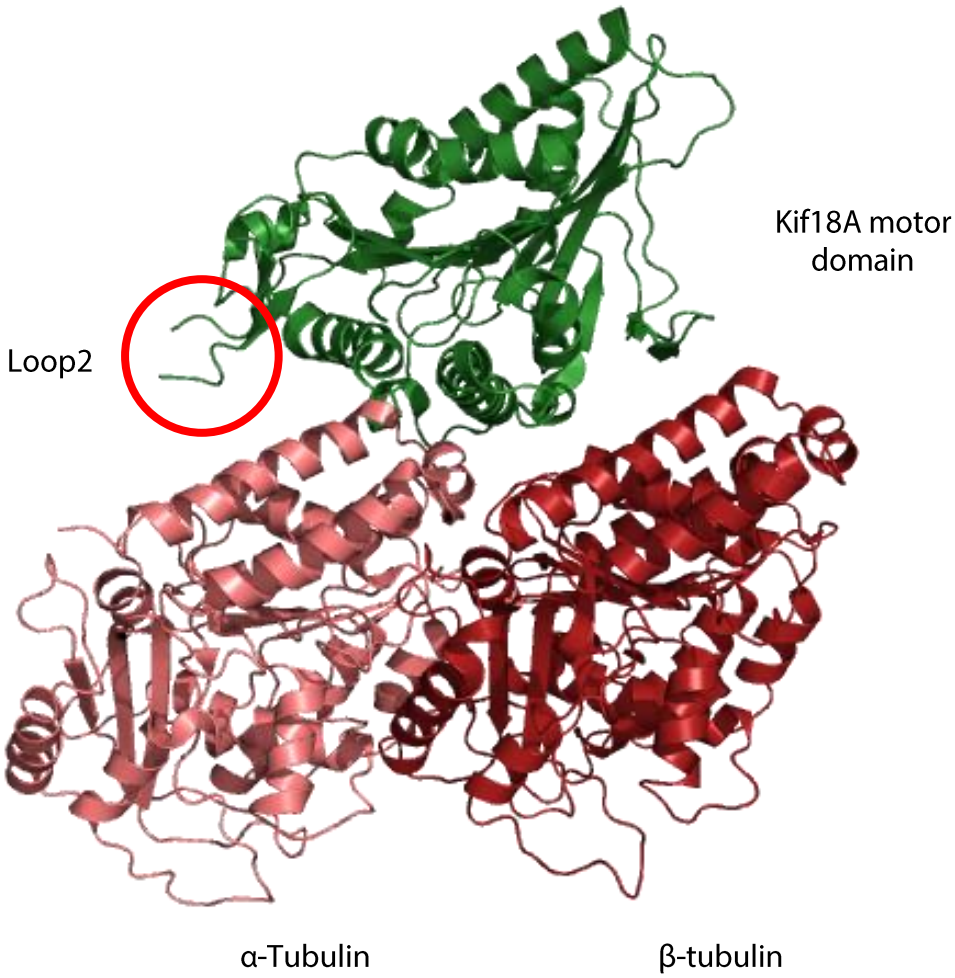

Figure 1-8. A model of Kif18A motor domain (green) docked onto a crystal structure of αβ-tubulin dimers (light pink, dark pink) using electron micrography data (PDB 5OGC). 4.8Å resolution. Loop2 region is partially displayed (red circle) and has been known to contact the α-tubulin subunit. Courtesy of Alex F. Thompson.

terminus is also partially responsible for Kif18A's plus-end binding, however, yet to be identified motor domain components are also required for stable association with microtubule ends (Stumpff et al., 2011).

Kif18A's undefined role in kinetochore-microtubule attachment

Interestingly, Kif18A depletion triggers a SAC-dependent mitotic arrest (Mayr et al., 2007; Zhu et al., 2005). As mentioned previously, an active spindle assembly checkpoint implies that unattached kinetochores are present (Rieder et al., 1994). However, it is not clear if the arrest when Kif18A is lost is due to an indirect effect of misregulated K fiber dynamics and chromosome alignment defects, or if Kif18A plays a more direct role in kinetochore-microtubule attachment. The profound effect of Kif18A depletion on chromosome alignment, coupled to its activation of the spindle assembly checkpoint, has led to the assumption that chromosome alignment is a prerequisite for proper mitotic progression. However, our lab has found that normal somatic cells, such as retinal pigment epithelial cells (RPE1) and mammary epithelial cells (MCF10A), and even certain cancer cell types (HCT116) do not arrest in mitosis when depleted of Kif18A but do exhibit a chromosome misalignment phenotype (Fonseca, 2018). These results argue against the notion that chromosome alignment is required for normal mitotic progression and provide a first line of evidence that Kif18A's function in chromosome alignment could be separate from its role in activating the spindle assembly checkpoint. What is the molecular basis for this additional attachment function?

Kinesin-8s' function in chromosome alignment is evolutionarily conserved in eukaryotic cell division (De Wever et al., 2014). While the C-termini of kinesin-8s have diverged over time, a binding motif for PP1, one of the key phosphatases that antagonize the activity of Aurora B kinase, has been conserved in this region. In fact, the fission yeast homolog of Kif18A, Klp5/Klp6 heterodimer requires PP1 binding for checkpoint silencing, although the role of motor bound PP1 remains unclear (Meadows et al., 2011). Recent studies have indicated that human Kif18A also directly interacts with PP1 through the conserved PP1 docking motif, suggesting this interaction may regulate mitotic progression and kinetochore affinity (De Wever et al., 2014; Hafner et al., 2014).

Chromosome organization and stable bioriented attachments are crucial steps towards maintaining genomic stability during cell division. Kif18A's requirement in both of these processes led us to hypothesize that Kif18A might be involved in coordinating chromosome attachment and alignment. Given the variable response to Kif18A depletion in the cell lines we have tested, we asked whether all cells require Kif18A to maintain stable kinetochore-microtubule attachments. If not, which ones do and why? What is the molecular basis of Kif18A-dependent attachment defects? Does Kif18A directly influence kinetochore affinity to the microtubule or does it play an indirect role through its known function in regulating microtubule dynamics? We know that microtubule plus-end binding is important for Kif18A's chromosome alignment function, but how does the motor stably associate with plus-ends? Furthermore, is

Kif18A-dependent chromosome alignment required for normal division and mammalian development?

In order to understand how Kif18A temporally coordinates chromosome alignment and the stabilization of kinetochore-microtubule attachments, we used quantitative cell biology approaches to evaluate mitotic chromosome attachment and alignment in established cell lines and primary murine cells. Chapter 2 describes a collaborative effort with Dr. Laura Reinholdt (The Jackson Laboratory) using cultured cells and mouse models to determine if Kif18A is required for kinetochore attachments in all cell types. This work also addresses the age old question of 'Is chromosome alignment required for cells to divide?' We found that primordial germ cells require Kif18A for attachment, which explains the germ cell depletion and infertility phenotypes displayed by Kif18A mutant mice. In contrast, Kif18A is necessary for chromosome alignment but not mitotic progression in primary embryonic fibroblasts. In Chapter 3, we describe the molecular basis of kinetochore attachment defects in Kif18A-depleted cells. More specifically, we tested several models that distinguished indirect from direct roles for Kif18A in promoting kinetochore-microtubule attachments. Our results indicate that Kif18A recruits PP1 to promote Hec1 dephosphorylation and increase the affinity of kinetochores for microtubules. The work described in Chapter 4 identified structural features that contribute to Kif18A's long dwell time at the plus-ends of microtubules. Kif18A has an elongated Loop2 (Figure 1-8), which is unique to a few different motor classes, including kinesin-8s and kinesin-13s that directly modify microtubule plus-ends. We show that Loop2 is

required for Kif18A's stable microtubule plus-end binding in cells and is thus crucial for chromosome alignment.

CHAPTER 2. KIF18A IS SPECIFICALLY REQUIRED FOR MITOTIC PROGRESSION DURING GERMLINE DEVELOPTMENT

Anne Czechanski[1], Haein Kim[2], Candice Byers[1], Ian Greenstein[1], Jason Stumpff[2*], Laura G. Reinholdt[1]*

1. The Jackson Laboratory, Genetic Resource Science, Bar Harbor, ME 04609;

2. Department of Molecular Physiology and Biophysics, University of Vermont, Burlington, VT 05405

*Equal contribution

Corresponding authors:

Laura G. Reinholdt, PhD
The Jackson Laboratory
600 Main Street
Bar Harbor, ME 04609 USA
Phone: 1 (207) 288-6693
e-mail: laura.reinholdt@jax.org

Jason Stumpff, PhD
Department of Molecular Physiology and Biophysics,
University of Vermont,
89 Beaumont Avenue
Burlington, Vermont 05405 USA
e-mail: jstumpff@uvm.edu

2.1 Abstract

Genome integrity in the developing germ line is strictly required for fecundity. In proliferating somatic cells and in germ cells, there are mitotic checkpoint mechanisms that ensure accurate chromosome segregation and euploidy. There is growing evidence of mitotic cell cycle components that are uniquely required in the germ line to ensure genome integrity. We previously showed that the primary phenotype of *germ cell deficient 2 (gcd2)* mutant mice is infertility due to germ cell depletion during embryogenesis. Here we show that the underlying mutation is a mis-sense mutation, R308K, in the motor domain of the kinesin-8 family member, KIF18A, a protein that is expressed in a variety of proliferative tissues and is a key regulator of chromosome alignment during mitosis. Despite the conservative nature of the mutation, we show that its functional consequences are equivalent to KIF18A deficiency in HeLa cells. We also show that somatic cells progress through mitosis, despite having chromosome alignment defects, while germ cells with similar chromosome alignment defects undergo mitotic arrest and apoptosis. Our data provide evidence for differential requirements for chromosome alignment in germ and somatic cells and show that Kif18a is one of a growing number of genes that are specifically required for cell cycle progression in proliferating germ cells.

2.2 Introduction

In mice, the development of germ cells begins with specification of primordial germ cells at the base of the allantois at embryonic day (E) 7.5. The newly established primordial germ cells then migrate through the dorsal mesentery and split into two laterally migrating groups that colonize the urogenital ridges between E10.5 – E12.5. During their migratory phase and during colonization of the emergent fetal gonads, primordial germ cells proliferate with an ~16h doubling time, expanding from a population of less than 100 cells to ~25,000 at E13.5 [1, 2]. Further expansion of the germ cell population occurs only in the male germ line with the proliferation of spermatogonial stem cells and spermatogonia in the testes resuming just after birth and continuing through the reproductive life of the male.

While meiosis is certainly the most well-recognized cell cycle specialization occurring in the germ line, there is also evidence for mitotic cell cycle specialization. This specialization is evident in the viable, yet infertile phenotypes of mice deficient for ubiquitously expressed mitotic and DNA repair genes. Among these is *Mad2l2* (*Rev7*), a sub-unit of the translesion repair DNA polymerase zeta and a component of the spindle assembly checkpoint. *Mad2l2* is uniquely required for cell cycle regulation soon after germ cell specification when primordial germ cells are programmed to briefly arrest in G2 and undergo epigenetic reprogramming[3, 4]. Similarly, the DNA repair proteins Fanconi anemia complementation group L and C (*FancL* and *FancC*), as well as minichromosome maintenance helicase 9 (*Mcm9*) are uniquely required for progression of the germ cell cycle [5-8]. However, unlike *Mad2l2*, these DNA repair

genes are also required for proliferation of germ cells during colonization of the genital ridge. The peptidylprolyl cis-trans isomerase gene, *Pin1*, which modulates the cell cycle by regulating cyclin E turnover is also specifically required in the developing germ line for cell cycle progression [9, 10]. *Pin1*, as a catalyst for conformational changes in phosphoproteins, was later shown to have key roles in cancer, ageing and Alzheimer's disease.

We previously reported that the recessive, ethylmethanosulfonate (EMS) induced mutation, *germ cell depletion 2* (gcd2) causes infertility in mice due to germ cell depletion during embryogenesis that is first evident in E11.5 embryos during colonization of the genital ridge. In adult mutant mice, there is gonad aplasia and infertility affecting both sexes with varying severity depending on inbred strain background. Here we report that the underlying mutation is a missense mutation in *Kif18a*. *Kif18a* is a member of the kinesin-8 subfamily of motor proteins and is broadly required for control of kinetochore microtubule dynamics and chromosome alignment during mitosis [11-13]. The *Kif18a*^{gcd2} mutation results in a conservative, arginine to lysine amino acid change at a highly conserved position in the motor domain of the protein. By expressing this mutation in HeLa cells, we show that despite its conservative nature, this mutation is sufficient to prevent the accumulation of KIF18A at the plus ends of kinetochore microtubules, leading to chromosome alignment defects and mitotic arrest. In contrast and consistent with the viable phenotype of *gcd2* mutant mice, primary somatic cells from *gcd2* mutant embryos do not arrest in mitosis despite having chromosome alignment defects and impaired growth *in vitro*. Finally, we found

that germ cells (and not somatic cells) from *gcd2* mutant fetal gonads exhibit cell cycle arrest and apoptosis, ultimately leading to germ cell depletion and infertility. Thus, it appears that *Kif18a,* a key regulator of chromosome alignment, is a new member of a growing number of mitotic proteins and DNA repair factors that are ubiquitously expressed but uniquely required for germ line development. Our data also show that while KIF18A mediated chromosome alignment is dispensable in the soma, it is uniquely required for germ line development.

2.3 Materials and methods

Ethics statement. All procedures involving mice were approved by The Jackson Laboratory's Institutional Animal Care and Use Committee and performed in accordance with the National Institutes of Health guidelines for the care and use of animals in research. The strains used for this study were CAST.129S1(B6)-*gcd2*/JcsMmjax (Mouse Mutant Resource and Research Center, stock # 034325-JAX), C57BL/6J (The Jackson Laboratory stock, #000664), C57BL/6J-$Kit^{W\text{-}v}$/J (The Jackson Laboratory, stock #000049) and B6.Cg-Kit^{W}/J (The Jackson Laboratory, stock #000164)

High-throughput targeted sequencing and validation. High molecular weight, total genomic DNA was extracted from *gcd2/gcd2* spleen by phenol chloroform extraction of enriched nuclei. DNA was fragmented (Covaris), end-repaired using T4 DNA polymerase, PNK and Taq DNA polymerase (New England Biolabs) and column

purified. Sequencing adapters were ligated (Roche) and the resulting fragments were size selected (300-350 bp) using agarose gel electrophoresis followed by gel extraction (Qiagen MinElute). The sample was amplified by PCR (Phusion enzyme, New England Biolabs) and then hybridized to a custom Agilent 1M feature array containing overlapping DNA probes representing the *gcd2* mapped interval (Chr2:108,786,520-109,929,176 bp (GRCm38/mm10)[14] for 65 hours according to the manufacturer's instructions (Agilent Technologies). The bar-coded, eluted samples were multiplexed with several other samples and sequenced 2 x 72 bp on an Illumina Genome Analyzer II. Approximately 6 million reads with an average read length of 68 bp were generated. A reference based (GRCm83/mm10) alignment was performed using the Burrows Wheeler Aligner (BWA) [15] and nucleotide variants were detected using SAM tools (mpileup)[16]. All resulting variants were annotated using a custom annotation tool and compared to known, strain specific SNPs from dbSNP as well as SNPs from the Sanger Mouse Genomes project [17]. Of 58 coding and/or splice site variants discovered in the data, 54 were known strain specific SNPs and 4 were novel.

HeLa cell culture, transfection, plasmids and fixation. HeLa cells were cultured in MEMα containing 10% FBS. For siRNA-mediated depletion, cells were treated with Silencer Validated siRNAs (Life Technologies) targeting Kif18A (GCUGGAUUUCAUAAGUGG) or Silencer Negative Control #1 complexed with RNAiMax (Life Technologies) following the manufacturer's instructions. A siRNA-resistant Kif18A clone was created by introducing silent mutations into the Kif18A

open reading frame via PCR mutagenesis (T84A, A87C, T90C and T93C). This product was cloned into a modified EGFP-C1 vector using Gateway cloning (Life Technologies). Point mutations were introduced into the siRNA-resistant EGFP-Kif18A clone using the Quickchange II site-directed mutagenesis kit (Stratagene) to create EGFP-Kif18A-R308K (G923A) and EGFP-Kif18A-R308A (A922G and G923C). All open reading frames were confirmed by DNA sequencing. For localization studies of EGFP-Kif18A clones, HeLa cells were transfected with plasmid DNA encoding siRNA-resistant EGFP-Kif18A, EGFP-Kif18A-R308K or EGFP-Kif18A-R308A 8 hours after siRNA treatment. Cells were fixed in 1% paraformaldehyde/ -20^{o}C methanol for 10 minutes 24 hours after DNA transfection. Cells were immunofluorescently labeled with the following primary and secondary antibodies: human anti-centromere (Antibodies Inc., 2.5 ug/mL), mouse anti-ɣ tubulin GTU-88 (Sigma, 0.5 µg/mL), goat anti-human Alexa Fluor 594 (Life Technologies, 2 µg/mL) and goat anti-mouse Alexa Flour 647 (Life Technologies, 2 µg/mL). Cells were imaged on an Eclipse Ti microscope (Nikon) equipped with a Clara CCD camera (Andor), Spectra X light engine (Lumencore), 100X 1.49 NA TIRF objective (Nikon) and NIS Elements software (Nikon). Optical sections were obtained every 200 nm through each mitotic spindle and maximum intensity projections of 10 optical sections at the center of each spindle are displayed. Kinetochore distributions were quantified as previously described [13, 18].

Western blot analyses. HeLa cells were lysed in RIPA buffer (50 mM Tris-HCl pH 7.4, 150 mM NaCl, 2 mM EDTA, 1% NP-40 and 0.1% SDS) 20 hours after DNA transfection and 28 hours after siRNA addition. Lysates were extracted on ice for 10 minutes. An equal volume of 2X Laemmli buffer was then added and lysates were boiled for 10 minutes. Lysates were separated by electrophoresis on 4-15% Tris-glycine polyacrylamide gels (BioRad) and transferred to PVDF membrane (BioRad). Membranes were blocked in TBS (Tris-buffered saline- 50 mM Tris-Cl pH 7.4 and 150 mM NaCl) containing 5% milk. Blocked membranes were probed with 1 µg/ml rabbit-anti-Kif18A antibodies (Bethyl Laboratories), 0.5 µg/ml mouse-anti-GAPDH antibodies (Millipore), DyLight 800 anti-rabbit IgG and DyLight 680 anti-mouse IgG antibodies (Thermo Scientific) diluted in TBS containing 5% milk and 0.1% Tween-20. Secondary antibody fluorescence was detected with an Odyssey CLx (LI-COR).

Mouse embryonic fibroblast (MEF) derivation. Mouse embryonic fibroblasts (MEFs) were derived from E12.5-E13.5 (embryonic day 12.5-13.5) embryos. Embryos were decapitated and eviscerated in sterile, PBS (Life Technologies, Invitrogen) on ice and then moved into ~3 ml of pre-warmed (37^{o}C) 0.05% Trypsin-EDTA (Life Technologies, Invitrogen), one embryo per well in a sterile 6 well culture dish. Each embryo was macerated with forceps and further dissociated by passing the resulting slurry through a 16-gauge needle. Following a 3 min. incubation, each tissue suspension was added to separate 15 ml conical tubes containing an equal volume of pre-warmed (37^{o}C) MEF medium (Dulbecco's Modified Eagle Medium (DMEM, high

glucose, no glutamine, no sodium pyruvate; Invitrogen) with 10% FBS (fetal bovine serum, ES grade, Lonza), 1X PenStrep (Invitrogen) and 2 mM GlutaMAX (Invitrogen). After allowing large tissue fragments to settle, each cell suspension was transferred to a new conical tube and centrifuged at 150xg for 5 min. The resulting pellets were resuspended in 1 ml of MEF media and then added to separate 60 mm, gelatinized tissue culture plates containing 3.5 ml of MEF media. Cultures were incubated at 37^{o}C, 5% CO_2 and were propagated by passaging 1:3 every 2-3 days. For growth curves, 9 independent MEF lines (3 +/+, 3 *Kif18a*^{gcd2}/+ and 3 *Kif18a*^{gcd2}/*Kif18a*^{gcd2} were plated in 7 triplicates (one per 24 hour point) on 12-well cell culture plates at a density of $2x10^5$ cells/ml. For counting, one triplicate set of cells from each genotype was trypsinized, washed once with PBS, and counted on an Auto-T4 Cellometer cell counter (Nexcellom). This was repeated with each triplicate every 24 hours over a period of seven days.

Live cell imaging. To maximize the number of cells in G_2/M, confluent MEF cultures were washed once with PBS and starvation medium (MEF medium without serum) was added. Cells were incubated in starvation medium at 37^{o}C, 5% CO_2 for 48 hours. Synchronized MEFs were cultured in glass bottom dishes (MatTek) in standard MEF media and then changed to CO_2-independent media with 10% FBS (Life Technologies) for imaging. Multiple fields of cells were imaged at 2-minute intervals by Differential Interference Contrast microscopy for up to 16 hours with a 40X lens on the temperature

controlled Eclipse-Ti system described above. Mitotic duration was calculated as the time from nuclear envelope breakdown to the onset of anaphase.

Mitotic profiling. Synchronized MEFs were trypsinized and plated at a density of $3x10^5$ cells/ml on glass coverslips treated with 0.1% gelatin in standard MEF media containing serum. After 24 hours, cells were fixed with 4% v/v paraformaldehyde in PBS. For sequential immunolabeling, cells were washed with PBS, permeabilized and blocked with 0.1% Triton X-100 and 5% FBS respectively. Primary and secondary antibody incubations were one hour at room temperature followed by 10 min. incubation in Hoechst 33342 trihydrochloride trihydrate (Life Technologies, Molecular Probes, H1399) to counterstain DNA. Primary antibodies were anti-α tubulin (Abcam Ab18251) and anti-centromere proteins (derived from CREST patients, Antibodies Inc., 15-234) and both were used for immunofluorescence at a dilution of 1:200. Coverslips were mounted on microscope slides overnight using Vectashield hard-set mounting medium (Vector Laboratories, H-1400), and imaged on a Leica SP5 confocal microscope or a Zeiss AxioImager epifluorescence microscope.

Flow Cytometry and Terminal Deoxynucleotidyl Transferase Nick-End Labeling (TUNEL) assays. *MEFs.* Confluent MEFs were trypsinized, washed in PBS, fixed with ice-cold 100% v/v methanol, and stored at -20°C. To prepare cells for flow cytometry, aliquots of $1x10^6$ cells/ml were washed with PBS containing 1% FBS, and blocked using BD Perm/Wash buffer (BD Bioscience) at room temperature for 15 min. All

subsequent washes were also with BD Perm/Wash. MEFs were incubated for one hour at room temperature in diluted antibodies. After immunolabeling, cells were washed and then stained in a solution containing 0.1% v/v Triton X-100, 0.2 mg/ml RNAse A (Life Technologies, Invitrogen), and 0.2 mg/ml propidium iodide (PI) (Life Technologies, Molecular Probes, P3566) in PBS for one hour. Cells were sorted on a FACSCalibur fluorescence-activated cell sorter (BD Biosciences), with voltage gating optimized for both Alexa Fluor-488 and propidium iodide.

To generate positive control samples, apoptosis was induced by culturing cells with 40 μM cisplatin for 16 hours. Media were collected and centrifuged for 5 minutes at 1,000 RPM to collect any non-adherent cells. Adherent cells were collected by trypsinization and added to the previously collected, non-adherent cells. Total cells were washed once with PBS, fixed with 4% paraformaldehyde on ice for 15 minutes and washed twice with PBS. Cells were resuspended in a minimal volume of PBS, added to 5 ml ice-cold 70% ethanol and stored overnight at -20°C. Aliquots of $1x10^6$ cells/ml were washed and stained using an APO-BrdU™ TUNEL Assay Kit (Life Technologies, Invitrogen, A23210) according to the manufacturer's instructions. An AlexaFluor 488 conjugated primary antibody against BrdU (Life Technologies A35126, 1:20) was used for detection. Samples were processed on a FACS Calibur fluorescence-activated cell sorter with voltage gating optimized for Alexa Fluor 488. All p values were calculated using unpaired, two sample Student's t-test.

Fetal gonads. Urogenital ridges (E11.5) and fetal gonads (E12.5) with accompanying mesonephroi were dissected from E11.5 or E12.5 embryos in 1X PBS. Tissues were rinsed in 1X PBS and incubated in 1X 0.05% trypsin-EDTA (Life Technologies 25300-120) at 37°C for 15 min. Trypsin was inactivated with DMEM supplemented with 20% FBS and the suspension was pipetted through a 40μm cell strainer. Cells were washed once with PBS, fixed with 4% paraformaldehyde on ice for 15 minutes and washed twice with PBS. Cells were resuspended in a minimal volume of PBS, added to 2 ml ice-cold 70% ethanol and stored overnight at -20°C. Cells were pelleted and resuspended in diluted primary antibody ((mouse anti-phospho-histone H3 (Ser10), clone 3H10 (Millipore, 05-806, 1/500), rabbit anti-DDX4/MVH (Abcam, 13840, 1/100)) for two hours at 37°C, washed 3x, and resuspended with diluted secondary antibody in the dark for one hour at 37°C. Cells were washed and then stained in a solution containing 1% FBS, and 2 μg/ml DAPI for 30 minutes at room temperature. Cells were sorted on a LSRII Fluorescence-activated cell sorter (BD Biosciences), with voltage gating optimized for Alexa Fluor-488, Alexa Fluor-647, and DAPI. For TUNEL labeling, fixed cells were stained using an APO-BrdU™ TUNEL Assay Kit (Life Technologies) according to the manufacturer's instructions using the kit controls. After the anti-BrdU incubation, cells were rinsed 2X in Perm/Wash and labeled with an antibody to mouse vasa homolog (MVH) as described above. Samples were processed on a LSRII fluorescence-activated cell sorter with voltage gating optimized for Alexa Fluor 488 and Alexa Fluor 647. All p values were calculated using unpaired, two sample Student's t-test.

RT-PCR

Tissues were dissected in PBS, immediately transferred to RNA*later* (Life Technologies) and stored at 4°C (up to 1 week) or -80°C (long term). Tissues were homogenized for 1 minute at 50 Hz using a TissueLyserLT (Qiagen) according to the manufacturer's instructions and RNA was extracted using an RNeasy Mini Kit (Qiagen). SuperScript III First Strand Synthesis System (Invitrogen) was used to generate cDNA for RT-PCR according to the manufactuer's instructions. Optimal cycle number and amount of cDNA was determined empirically for *Kif18a*. Primers and cycling conditions for *Actb* were according to the manufacturer's instructions. *Kif18a* primers flanked exons 10 – 13 with a product size of 736 bp and 0.5 µl of cDNA were added to each reaction. Primer sequences are provided in Supplemental Table 1.

Whole-mount *in situ* hybridization (WISH)

RNA probes for WISH were generated from cDNA clones obtained from Open Biosystems, (*Kif18a* clone ID 3499835, *Pou5f1 (Oct3/4)* clone ID 30019896). Restriction digests were performed (EcoR1 and XhoI for *Kif18a* and EcoRI and Eba1 for *Oct3/4*) to remove the 3' polyA and T7/Sp6 promoter sites. T7 and SP6 linkers were added and the resulting fragments used as template for *in vitro* transcription according to manufacturer's instructions (DIG RNA Labeling Mix, Roche). RNA probe sequences are provided in Supplemental Table 1. Embryos were harvested at E12.5 into 1X PBS and fetal gonads were removed. Tissues were fixed in 4% paraformaldehyde (PFA) overnight followed by a dehydration series in a methanol gradient (25%, 50%,

75%, 100% in PBS with 0.1% Tween-20, PBST) 5 minutes each with shaking at room temperature. WISH was carried out as previously described with optimization for fetal gonads[1]. Specifically each pair of E12.5 fetal gonads was digested in 0.5 ml of 10 µg/ml proteinase K for 9 minutes. The signal from the digoxigenin labeled probe was detected with NBT/BCIP substrate mix (Roche, #11681451001) followed by cold PBST washes, (3x5 min each) and the tissue was subsequently carried through a graded glycerol series to reduce background (25%, 50%, 80%). For imaging, fetal gonads were placed into 1X PBS and mounted on 1% agarose.

Immunohistochemistry

Testes from 6-8 dpp mice were dissected in PBS and fixed in 4% PFA overnight at 4C. Tissues were embedded in paraffin and sectioned at 5 µm thickness. Sections were deparaffinized and antigen retrieval was performed by immersing slides in 10mM sodium citrate, pH 6 and heating to 95°C for 30 min. Sections were then washed in 3 x 5 min in PBS followed by 2 x 5 min. washes with 50mM ammonium chloride. Sections were then blocked for 1 hour with PBS, 10% goat serum, 0.05% Triton X. Sections were incubated overnight at 4°C with one or more of the following antibodies, mouse anti-phospho-histone H3 (Ser10), clone 3H10 (Millipore, 05-806, 1:500), rabbit anti-DDX4/MVH (Abcam, ab 13840, 1:100), rabbit anti-MAD2 (Bethyl Laboratories, A300-301A, 1:200) and human anti-CREST used at dilution of 1:500. Sections were then washed 3 x 5 min. in PBST before addition of secondary antibodies. They were

then counterstained with 0.01% Sudan Black followed by DAPI and PBS washes. Sections were mounted in 80% glycerol for imaging with Zeiss AxioImager.Z2.

2.4 Results

Mice homozygous for the EMS (ethylmethanesulfonate) induced mutation, *gcd2 (germ cell depletion 2)* are infertile due to depletion of post-migratory germ cells at embryonic day (E) 11.5. Previously, we mapped the mutation to an ~1 Mb region on Chromosome 2 between 108,786,520-109,929,176 bp (GRCm38/mm10) containing 6 protein coding genes, including *Mettl15, Kif18A, Bdnf, Lin7c, Gm18939* and *Lgr4* [14].

To identify the underlying causative mutation, we used high-throughput, targeted sequencing of the entire 1.1 Mb interval on chromosome 2 (Chr2: 108,786,520-109,929,176) [19] and generated ~2M 76 bp, paired end reads from an affected *gcd2/gcd2* individual. When mapped to the reference genome, these data resulted in 85X median coverage across 97% of the target interval, including all coding sequence, introns, and conserved non-coding sequence and excluding 3% repetitive sequence. From the resulting alignment, a total of four novel variants were called and all were subsequently validated by Sanger sequencing of additional mutant, heterozygous and wild type samples from the *gcd2* colony, as well as CJ7 (129/SvImJ) ES cells, representing the genome in which the *gcd2* mutation was originally induced [20]. Of these 4 variants, 2 were heterozygous in the sequenced *gcd2/gcd2* sample and could not be validated by subsequent capillary sequencing. These were deemed sequencing or alignment artifacts. The third variant (Chr2: 109,908,059 G to T,

GRCm38, mm10) was found in *gcd2* samples, but was also found in the wild type, parental CJ7 ES cell line, as well as in DNA from the 129/SvImJ inbred strain. The fourth variant (Chr2: 109,296,645 (GRCm38, mm10), G to A in exon 7 of *Kif18a*) was found only in *gcd2* samples with 100% concordance to sample genotypes. Subsequent typing of the *gcd2* colony showed perfect linkage between this missense mutation and the phenotype (N~895), moreover allele specific PCR genotyping for this mutation was used to create two congenic lines (>N9) both of which retain the original phenotype after over 9 generations of backcrossing and selection for the mutation. Finally, consistent with the guanine alkylation activity of EMS, the *gcd2* mutation is a G to A transition. The predicted consequence of this mutation is a single, conservative amino acid change, R308K, occurring in a highly conserved amino acid within the kinesin motor domain (Fig. 1).

KIF18A is a microtubule attenuating kinesin motor that accumulates at the fast growing, plus ends of microtubules where it functions to regulate microtubule dynamics [21, 22]. During mitosis, this activity is required to restrict mitotic chromosome oscillations to the equator of the mitotic spindle during metaphase [13]. Studies of kinesin-1 motors indicate that the conserved arginine residue mutated in *Kif18a*^{gcd2} mice directly contacts beta-tubulin and is required for binding of kinesin to microtubules [23, 24]. Mutation of the equivalent arginine residue in human kinesin-1 to alanine (R278A) reduces the microtubule-stimulated ATPase activity of the motor by more than 15-fold [23]. To determine the consequences of mutating R308 on KIF18A function during mitosis, we expressed wild type KIF18A, KIF18A-R308K or KIF18A-

R308A fused with EGFP in HeLa cells depleted of endogenous KIF18A (Fig. 2A). Unlike the wild type protein, the mutant proteins did not accumulate at kinetochore microtubule plus ends and instead remained distributed along the length of the kinetochore microtubules (Fig. 2B). Moreover, HeLa cells expressing the mutant protein exhibited a significant increase in the distribution of kinetochores within the spindle (Fig 2. C-E), similar to that seen in cells depleted of wild type KIF18A [13]. Taken together, these data indicate that R308 is required for KIF18A's chromosome alignment function.

To investigate the consequences of the *Kif18a*^{gcd2} mutation in primary cells we derived mouse embryonic fibroblasts (MEFs) from mutant and littermate control E12.5-E13.5 embryos. Mutant MEFs grew slowly in culture (Fig. 3A) and had lower viability by dye exclusion (Fig. 3B). Since KIF18A-depleted HeLa cells arrest in mitosis, we surmised that the slow growth of mutant MEFs might be due to mitotic arrest. However, cell cycle analysis based on DNA content and labeling with phosphorylated histone H3 (a marker of late G2/M phase), revealed that unlike *Kif18a*^{R308K} expressing HeLa cells, mutant MEFs did not show evidence of mitotic arrest or increased apoptosis (Fig. 3C-E). To confirm that *Kif18a*^{gcd2} MEFs do not arrest in mitosis, we imaged live dividing cells via differential interference contrast microscopy (DIC). These studies revealed that wild type and *Kif18a*^{gcd2} MEFs progress from nuclear envelope breakdown to anaphase with comparable timing (Figure 4A-B).

In KIF18A depleted HeLa cells, impaired mitotic chromosome alignment is associated with activation of the spindle assembly checkpoint, mitotic arrest and

apoptosis[25]. Based on these data, we surmised that mutant *Kif18a*^{gcd2} MEFs progress through mitosis with normal chromosome alignment. To test this, we assessed chromosome distribution in mutant and wild type MEFs during mitosis. Surprisingly, mutant MEFs displayed a 7-fold increase in the ratio of preanaphase mitotic cells with unaligned versus aligned chromosomes (Fig. 5A-B). Consistent with these data, we also observed that chromosomes were not aligned in live *Kif18a*^{gcd2} MEFs prior to anaphase (Fig. 4A-B).

The mitotic phenotype of *Kif18a*^{gcd2} mutant MEFs notwithstanding, *Kif18a*^{gcd2} mutant mice are viable with respect to their wild type littermates. Both *Kif18a*^{gcd2} and *Kif18a*$^{-/-}$ animals are otherwise overtly normal with the exception of infertility due to germ cell depletion [14, 26]. It should be noted that while infertility is seen in both sexes of *Kif18a*^{gcd2} mice, male specific infertility and gonad aplasia was reported for *Kif18a*$^{-/-}$ mice and in these studies infertility was not attributed to germ cell depletion during embryogenesis [26]. We also previously showed that germ cell depletion in *Kif18a*^{gcd2} mutant mice is highly sensitive to strain background [14], which might underlie the male specific infertility that was previously reported for *Kif18a*$^{-/-}$ mice. The germ cell specific phenotype suggests that *Kif18a* is specifically expressed in the germ line and/or its expression is tightly regulated in the germ line. Data published by Liu *et al*. show that *Kif18a* RNA and protein are found in a variety of adult tissues in addition to the adult ovary and testes [26], and is particularly abundant in proliferative tissues. To expand this expression analysis to the developmental time point where functional *Kif18a* is required for fertility, we used and *in situ* hybridization to examine expression

in E11.5-12.5 fetal gonads [14]. As expected, we found that *Kif18a* is expressed in the fetal gonad at E11.5-12.5 and by comparing the expression pattern of *Kif18a* to a germ cell specific gene, *Pou5f1* (*Oct3/4*), we found that *Kif18a* does not exhibit a germ cell specific expression pattern (Fig. 6A). Using RT-PCR we found that *Kif18a* is expressed in both wild type and $Kif18a^{gcd2}$ mutant fetal gonads. Qualitatively, *Kif18a* expression was highest in the adult testes, which has the largest population of proliferating germ cells (Fig. 6B, lane 8). In contrast, *Kif18* expression was lowest in $Kif18a^{gcd2}$ and $Kit^{W/W\text{-}v}$ adult mutant ovaries and testes, which are devoid of proliferating germ cells (Fig. 6B, lanes 6, 7, 10). *Kif18a* expression is still detectable in the absence of proliferating germ cells, lending further support to the conclusion that *Kif18a* expression in the gonad is not restricted to the germ line. Unfortunately, commercially available KIF18A antibodies did not provide specific labeling in fetal gonads so the *in-situ* data could not be correlated with protein localization.

To determine the consequences of the $Kif18a^{gcd2}$ mutation on mitotic progression in germ cells, we performed cell cycle analysis on E12.5 fetal gonads, using an antibody to the germ cell specific mouse VASA homolog MVH/DDX4 to distinguish between germ cells (MVH positive) and somatic cells (MVH negative). There were more $Kif18a^{gcd2}$ mutant germ cells in G2/M when compared to germ cells from wild type littermate controls (Fig. 7A). There was also a corresponding reduction in the percentage of mutant germ cells in G1. A significantly higher percentage of $Kif18a^{gcd2}$ mutant germ cells were positive for phosphorylated histone H3 and TUNEL (Fig. 7B-C). Importantly, there were no significant differences in cell cycle distribution

or histone H3 phosphorylation in gonadal somatic cells (MVH negative) from mutant and wild type animals (Fig. 7B). Taken together these data provide evidence that mutant germ cells in the E12.5 fetal gonad exhibit mitotic arrest, which may ultimately lead to germ cell depletion and infertility. Since mutant gonads are not completely devoid of germ cells at birth [14], mitotic arrest appears to affect a specific population of germ cells.

To determine if *Kif18a*^{gcd2} mutant germ cells have underlying chromosome alignment defects, we used immunohistochemistry with antibodies recognizing alpha tubulin and the germ cell specific, GCNA (germ cell nuclear antigen) to examine mitotically dividing germ cells (spermatogonia) from testes at 6 days post partum. Aberrant spindle organization and defects in chromosome alignment were apparent in GCNA positive spermatogonial cells from pre-pubertal mutant testes (Fig. 7D). To determine if persistent unattached kinetochores underlie activation of the spindle checkpoint, we immunolabeled with an antibody against the checkpoint protein MAD2. MAD2 localization to kinetochores provides a signal that inhibits progression from metaphase to anaphase [27, 28]. We found that MAD2 is associated with kinetochores regardless of their position within the spindle in all (100%, N=40) mutant spermatogonia whereas MAD2 co-localization with kinetochores was more rare (30%, N=40) and more frequently associated with kinetochores of chromosomes off of the metaphase plate in wild type spermatogonia (Supplementary Figure 1). These data, combined with the observed increase in the fraction of mitotic germ cells within *gcd2*

embryos, are consistent with loss of KIF18A function leading to a germ cell specific mitotic arrest due to kinetochore-microtubule attachment defects.

2.5 Discussion

We found that the causative mutation underlying *gcd2* is a G to A (Chr2: 109,296,645 (GRCm38, mm10) transition in exon 7 of *Kif18a*; a mutation that results in a conservative amino acid change, R308K, in the motor domain of the protein. Recent crystal structure data show that the homologous arginine in the motor domain of kinesin-1 is a key residue in contact with β-tubulin when the motor is bound to microtubules [24]. Therefore, despite having similar properties (positively charged and polar), lysine is likely a poor functional substitute for arginine at this position. Consistent with this, expression of KIF18A-R308K in HeLa cells was functionally equivalent to KIF18A knockdown and to the more severe amino acid change, R308A, providing further evidence that this mis-sense mutation is a functionally null allele. Finally, the primary infertility phenotype of knockout *Kif18a* mice is nearly identical to the phenotype of *gcd2* mice [14, 26] with the exception that both male and female *gcd2* mutant mice are infertile, while only male infertility was reported in *Kif18a* knockout mice. Our previous data suggest that these differences are more likely due to differences in strain background rather than functional differences in the mutations per se (knockout allele vs. missense mutation) [14].

Unlike KIF18A-R308K expressing HeLa cells, mutant MEFs do not show evidence of G2 to M arrest or increased apoptosis, despite having chromosome

alignment defects, impaired growth and reduced viability. Moreover, progression through nuclear envelope breakdown to anaphase is comparable to wild type. Therefore, the impaired growth of mutant MEFs cannot be explained by delayed cell division. Impaired growth and reduced viability in the absence of spindle checkpoint activation and apoptosis could be due to the activation of alternative programmed cell death mechanisms like autophagy or necrosis; however additional work is necessary to decipher the mitotic consequences of KIF18A deficiency in primary MEFs. Certainly, the lack of spindle checkpoint activation in primary MEFs likely explains the viability of *Kif18a*^{gcd2} mutant embryos[14] and the viability of *Kif18a* null embryos [26]. However, we previously reported that homozygous, mutant *Kif18a*^{gcd2} mice are found in slightly reduced Mendelian ratios (~13-18% depending on the genetic background) at wean. Therefore, the mitotic phenotype of mutant MEFs may well have a subtle impact on the development of mutant embryos or survival prior to weaning (3 weeks). In adult mutant animals, the relatively subtle mitotic phenotype of somatic cells could sensitize or predispose proliferative tissues to environmental or genetic cell cycle perturbations. For example, loss of KIF18A function impairs tumorigenesis in induced colon cancer mouse models [29].

While *Kif18a* expression is not restricted to the germ cells, our data show that it is specifically required for chromosome alignment and mitotic progression in the germ cell lineage. Unlike somatic cells, mutant germ cells undergo mitotic arrest and apoptosis in the absence of functional KIF18A. These events are detectable as early as 11.5 dpc in the fetal gonad, but since mutant animals are born with a small germ cell

population, these events are seemingly stochastic. We examined MAD2 localization in spermatogonia from pre-pubertal testes and found persistent MAD2 localization to mutant kinetochores at metaphase, which is generally considered to be a marker of active spindle assembly checkpoint signaling due to kinetochore-microtubule attachment defects [27, 28, 30, 31]. Thus, these data are consistent with reduced kinetochore-microtubule attachment in germ cells lacking Kif18A function. However, more in depth profiling of other checkpoint proteins and directed studies of kinetochore function in isolated spermatogonia will be required to fully understand the underlying mechanism and timing of checkpoint activation in mutant spermatogonia and why Kif18A is required for mitotic progression in germ but not somatic cells.

Previous studies have demonstrated a similar germ cell specific sensitivity to mutations that disrupt the phospho-regulation of the enzyme separase, which cleaves the cohesin complexes linking sister chromosomes at the metaphase to anaphase transition [32]. Thus, somatic and germ cells appear to either have different thresholds for mitotic progression control or somatic cells possess mechanisms that impart functional redundancy in the absence of these mitotic regulators. Regardless, our data support the notion that regulation of the mitotic spindle is different in germline and somatic cells. This is consistent with the underappreciated concept of differential cell cycle regulation in germ and somatic cells. The infertility phenotype of mice deficient for peptidylprolyl cis-trans isomerase gene (*Pin1)* provides additional support for this concept. PIN1 is required for cyclin E turnover and PIN1 deficiency leads to germ cell deficiency due to a protracted cell cycle [10, 33]. Additional roles for PIN1 in ageing,

cancer, neurodegeneration, and bone density were later revealed by more extensive, specialized phenotyping of mutant mice; suggesting that additional roles for KIF18A may also exist outside the developing germ line but may require more specialized phenotyping in the context of additional environmental and/or genetic insults.

An alternative explanation for the germ cell specific cell cycle arrest observed in KIF18A deficient mice could be that KIF18A is required for aspects of germ cell development that are unrelated to chromosome alignment. Mammalian *Kif18a* was originally cloned from bone marrow stromal cells, where it was shown to associate with estrogen receptor (ER) alpha, implicating an expanded role for this kinesin in ER signaling [34, 35]. A downstream consequence of ER signaling is phosphorylation of AKT and KIF18A depleted cell lines and somatic tissues are deficient in the phosphorylated form of AKT [36]. During germ line development, ER signaling is required for expression of KITL in supporting somatic cells, ultimately leading to the phosphorylation of AKT kinase in the KIT expressing germ cells which in turn promotes germ cell survival. The balance of AKT phosphorylation in the developing germ line appears to be critical for regulated proliferation of germ cells and for inhibition of germ cell tumor formation via downstream activation of p53[37]. Whether AKT phosphorylation and/or signaling is disrupted during the development of germ cells in KIF18A deficient mice remains to be seen. However, supporting the notion of an additional role outside the developing germ line, our data indicate that *Kif18A* is not specifically expressed in germ cells during fetal gonad development. Therefore, future work will be focused on conditional ablation of KIF18A function in the germ line and

in the gonadal somatic cells as well as analysis of AKT signaling during germ line development in the absence of KIF18A. Since the consequences of mitotic error in germ cells can span generations, mitotic cell cycle specialization is likely the result of strong positive selection for genome integrity in the developing germ line.

2.6 References

1. Wilkinson, D.G. (1992). In Situ Hybridization: A Practical Approach, 2nd Edition, (Oxford University Press, USA).
2. Tam, P.P., and Snow, M.H. (1981). Proliferation and migration of primordial germ cells during compensatory growth in mouse embryos. J Embryol Exp Morphol *64*, 133-147.
3. Pirouz, M., Pilarski, S., and Kessel, M. (2013). A critical function of Mad2l2 in primordial germ cell development of mice. PLoS Genet *9*, e1003712.
4. Watanabe, N., Mii, S., Asai, N., Asai, M., Niimi, K., Ushida, K., Kato, T., Enomoto, A., Ishii, H., Takahashi, M., et al. (2013). The REV7 subunit of DNA polymerase zeta is essential for primordial germ cell maintenance in the mouse. J Biol Chem *288*, 10459-10471.
5. Hartford, S.A., Luo, Y., Southard, T.L., Min, I.M., Lis, J.T., and Schimenti, J.C. (2011). Minichromosome maintenance helicase paralog MCM9 is dispensible for DNA replication but functions in germ-line stem cells and tumor suppression. Proc Natl Acad Sci U S A *108*, 17702-17707.
6. Nadler, J.J., and Braun, R.E. (2000). Fanconi anemia complementation group C is required for proliferation of murine primordial germ cells. Genesis *27*, 117-123.
7. Lu, B., and Bishop, C.E. (2003). Late onset of spermatogenesis and gain of fertility in POG-deficient mice indicate that POG is not necessary for the proliferation of spermatogonia. Biol Reprod *69*, 161-168.
8. Agoulnik, A.I., Lu, B., Zhu, Q., Truong, C., Ty, M.T., Arango, N., Chada, K.K., and Bishop, C.E. (2002). A novel gene, Pog, is necessary for primordial germ cell proliferation in the mouse and underlies the germ cell deficient mutation, gcd. Hum Mol Genet *11*, 3047-3053.
9. Yeh, E.S., and Means, A.R. (2007). PIN1, the cell cycle and cancer. Nat Rev Cancer *7*, 381-388.

10. Yeh, E.S., Lew, B.O., and Means, A.R. (2006). The loss of PIN1 deregulates cyclin E and sensitizes mouse embryo fibroblasts to genomic instability. J Biol Chem *281*, 241-251.
11. Mayr, M.I., Hummer, S., Bormann, J., Gruner, T., Adio, S., Woehlke, G., and Mayer, T.U. (2007). The human kinesin Kif18A is a motile microtubule depolymerase essential for chromosome congression. Curr Biol *17*, 488-498.
12. Zhu, C., Zhao, J., Bibikova, M., Leverson, J.D., Bossy-Wetzel, E., Fan, J.B., Abraham, R.T., and Jiang, W. (2005). Functional analysis of human microtubule-based motor proteins, the kinesins and dyneins, in mitosis/cytokinesis using RNA interference. Molecular biology of the cell *16*, 3187-3199.
13. Stumpff, J., von Dassow, G., Wagenbach, M., Asbury, C., and Wordeman, L. (2008). The kinesin-8 motor Kif18A suppresses kinetochore movements to control mitotic chromosome alignment. Dev Cell *14*, 252-262.
14. Reinholdt, L.G., Munroe, R.J., Kamdar, S., and Schimenti, J.C. (2006). The mouse gcd2 mutation causes primordial germ cell depletion. Mech Dev *123*, 559-569.
15. Li, H., and Durbin, R. (2010). Fast and accurate long-read alignment with Burrows-Wheeler transform. Bioinformatics *26*, 589-595.
16. Li, H., Handsaker, B., Wysoker, A., Fennell, T., Ruan, J., Homer, N., Marth, G., Abecasis, G., and Durbin, R. (2009). The Sequence Alignment/Map format and SAMtools. Bioinformatics *25*, 2078-2079.
17. Keane, T.M., Goodstadt, L., Danecek, P., White, M.A., Wong, K., Yalcin, B., Heger, A., Agam, A., Slater, G., Goodson, M., et al. (2011). Mouse genomic variation and its effect on phenotypes and gene regulation. Nature *477*, 289-294.
18. Stumpff, J., Wagenbach, M., Franck, A., Asbury, C.L., and Wordeman, L. (2012). Kif18A and chromokinesins confine centromere movements via microtubule growth suppression and spatial control of kinetochore tension. Dev Cell *22*, 1017-1029.
19. D'Ascenzo, M., Meacham, C., Kitzman, J., Middle, C., Knight, J., Winer, R., Kukricar, M., Richmond, T., Albert, T.J., Czechanski, A., et al. (2009). Mutation

discovery in the mouse using genetically guided array capture and resequencing. Mammalian genome : official journal of the International Mammalian Genome Society *20*, 424-436.

20. Munroe, R.J., Bergstrom, R.A., Zheng, Q.Y., Libby, B., Smith, R., John, S.W., Schimenti, K.J., Browning, V.L., and Schimenti, J.C. (2000). Mouse mutants from chemically mutagenized embryonic stem cells. Nat Genet *24*, 318-321.
21. Stumpff, J., Du, Y., English, C.A., Maliga, Z., Wagenbach, M., Asbury, C.L., Wordeman, L., and Ohi, R. (2011). A tethering mechanism controls the processivity and kinetochore-microtubule plus-end enrichment of the kinesin-8 Kif18A. Mol Cell *43*, 764-775.
22. Du, Y., English, C.A., and Ohi, R. (2010). The kinesin-8 Kif18A dampens microtubule plus-end dynamics. Curr Biol *20*, 374-380.
23. Woehlke, G., Ruby, A.K., Hart, C.L., Ly, B., Hom-Booher, N., and Vale, R.D. (1997). Microtubule interaction site of the kinesin motor. Cell *90*, 207-216.
24. Gigant, B., Wang, W., Dreier, B., Jiang, Q., Pecqueur, L., Pluckthun, A., Wang, C., and Knossow, M. (2013). Structure of a kinesin-tubulin complex and implications for kinesin motility. Nat Struct Mol Biol *20*, 1001-1007.
25. Mayr, M.I., Hummer, S., Bormann, J., Gruner, T., Adio, S., Woehlke, G., and Mayer, T.U. (2007). The human kinesin Kif18A is a motile microtubule depolymerase essential for chromosome congression. Curr Biol *17*, 488-498.
26. Liu, X.S., Zhao, X.D., Wang, X., Yao, Y.X., Zhang, L.L., Shu, R.Z., Ren, W.H., Huang, Y., Huang, L., Gu, M.M., et al. (2010). Germinal Cell Aplasia in Kif18a Mutant Male Mice Due to Impaired Chromosome Congression and Dysregulated BubR1 and CENP-E. Genes Cancer *1*, 26-39.
27. Chen, R.H., Waters, J.C., Salmon, E.D., and Murray, A.W. (1996). Association of spindle assembly checkpoint component XMAD2 with unattached kinetochores. Science *274*, 242-246.
28. Li, Y., and Benezra, R. (1996). Identification of a human mitotic checkpoint gene: hsMAD2. Science *274*, 246-248.

29. Zhu, H., Xu, W., Zhang, H., Liu, J., Xu, H., Lu, S., Dang, S., Kuang, Y., Jin, X., and Wang, Z. (2013). Targeted deletion of Kif18a protects from colitis-associated colorectal (CAC) tumors in mice through impairing Akt phosphorylation. Biochemical and biophysical research communications *438*, 97-102.
30. Waters, J.C., Chen, R.H., Murray, A.W., Gorbsky, G.J., Salmon, E.D., and Nicklas, R.B. (1999). Mad2 binding by phosphorylated kinetochores links error detection and checkpoint action in mitosis. Curr Biol *9*, 649-652.
31. Waters, J.C., Chen, R.H., Murray, A.W., and Salmon, E.D. (1998). Localization of Mad2 to kinetochores depends on microtubule attachment, not tension. The Journal of cell biology *141*, 1181-1191.
32. Xu, J., Wang, M., Gao, X., Hu, B., Du, Y., Zhou, J., Tian, X., and Huang, X. (2011). Separase phosphosite mutation leads to genome instability and primordial germ cell depletion during oogenesis. PloS one *6*, e18763.
33. Atchison, F.W., Capel, B., and Means, A.R. (2003). Pin1 regulates the timing of mammalian primordial germ cell proliferation. Development *130*, 3579-3586.
34. Luboshits, G., and Benayahu, D. (2007). MS-KIF18A, a kinesin, is associated with estrogen receptor. J Cell Biochem *100*, 693-702.
35. Zusev, M., and Benayahu, D. (2009). The regulation of MS-KIF18A expression and cross talk with estrogen receptor. PLoS One *4*, e6407.
36. Nagahara, M., Nishida, N., Iwatsuki, M., Ishimaru, S., Mimori, K., Tanaka, F., Nakagawa, T., Sato, T., Sugihara, K., Hoon, D.S., et al. (2011). Kinesin 18A expression: clinical relevance to colorectal cancer progression. Int J Cancer *129*, 2543-2552.
37. Ewen, K.A., and Koopman, P. (2010). Mouse germ cell development: from specification to sex determination. Mol Cell Endocrinol *323*, 76-93.

2.7 Figures

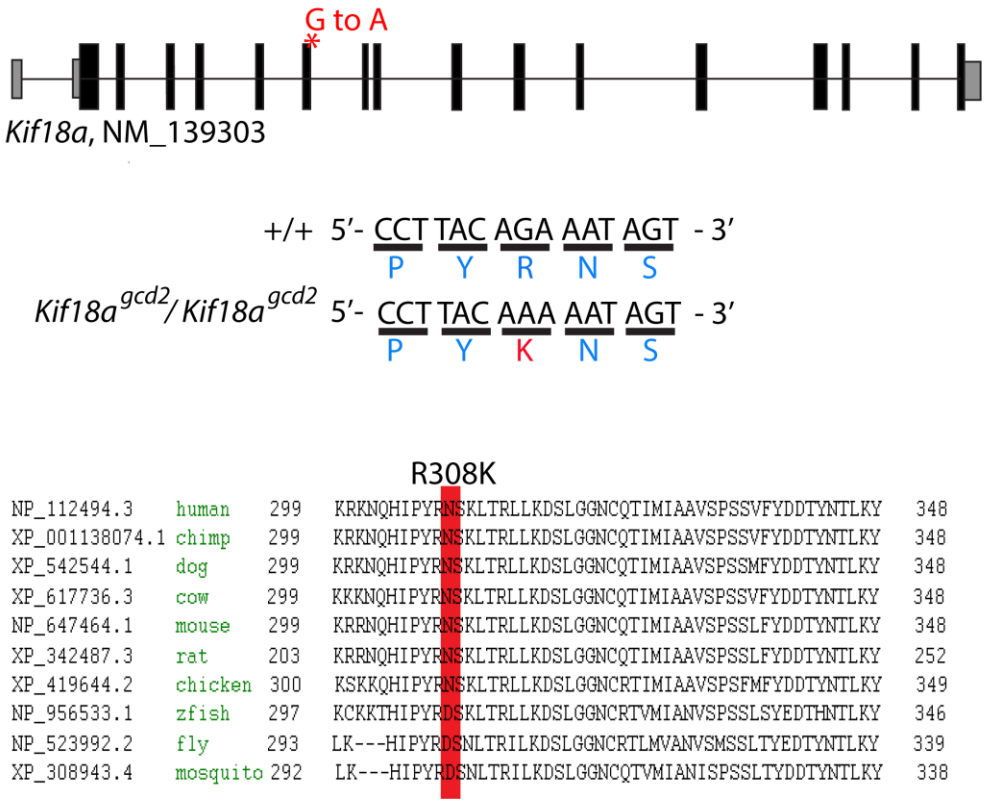

Figure 2-1. The *gcd2* mutation affects the highly conserved R308 residue within the KIF18A motor domain.

Gcd2 is a G to A transition in exon 7 of *Kif18a*. This is a missense mutation that changes an AGA codon to an AAA, leading to the single amino acid change, R308K. Arginine 308 is a highly conserved amino acid in the motor domain of the protein.

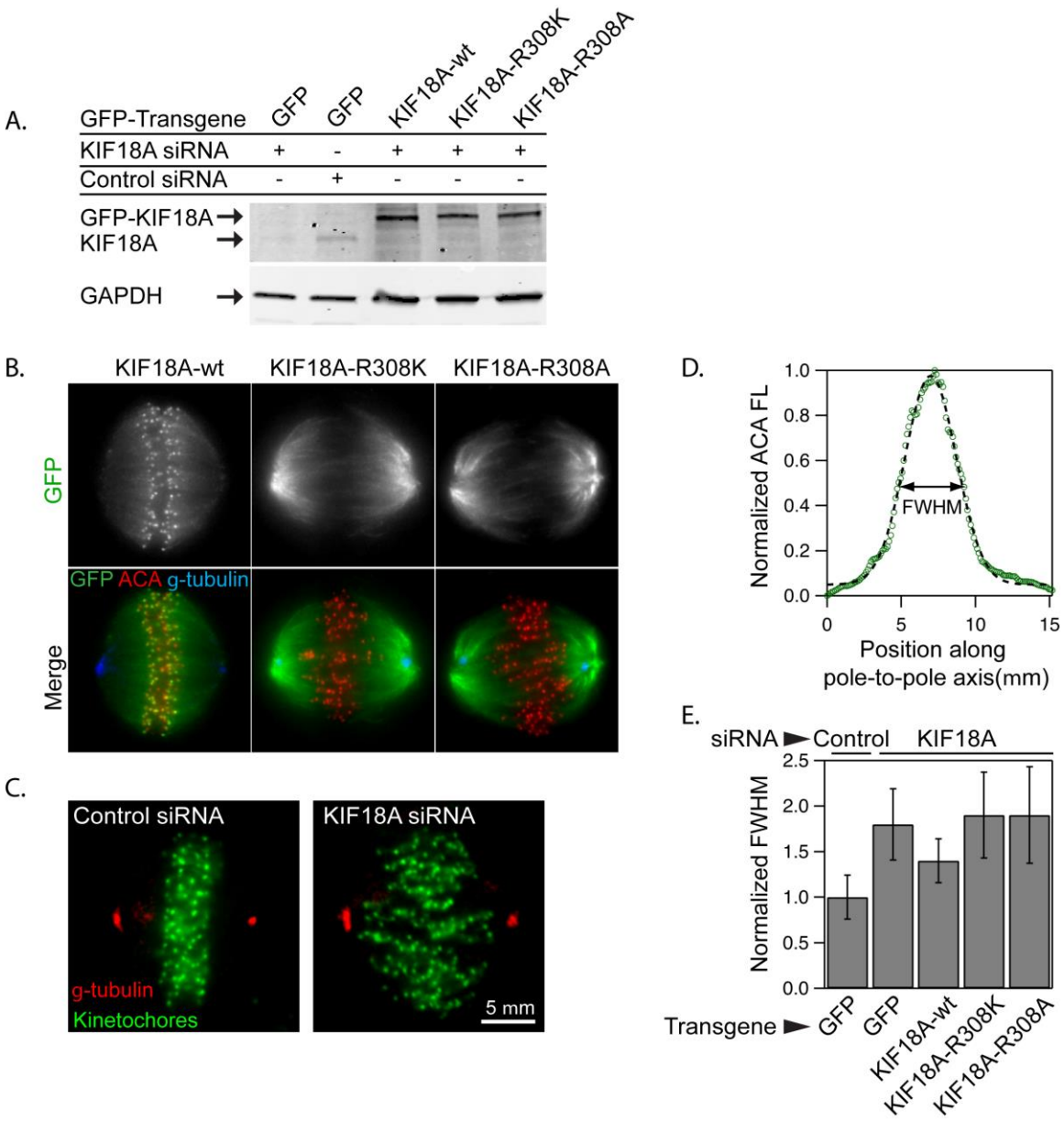

Figure 2-2. Mutations in R308 disrupt KIF18A's localization and chromosome alignment function.
(Contributed by HK)

HeLa cells were treated with siRNA oligonucleotides targeting endogenous KIF18A. Cells were rescued with GFP labeled wild type KIF18A or with the mutant GFP labeled KIF18A-R308K or KIF18A-R308A (A). Unlike KIF18A$^{WT\text{-}GFP}$, KIF18A$^{R308K\text{-}GFP}$ and KIF18A$^{R308A\text{-}GFP}$ (green) failed to concentrate near kinetochores (red) and instead were

distributed along the spindle between the centrosomes (ɣ-tubulin, blue) in KIF18A-depleted HeLa cells (B). To measure centromere alignment, the distribution of anti-centromere antigen fluorescence (ACA FL) along the normalized pole-to-pole axis was measured and the full width at half maximum (FWHM) was calculated for each condition. Representative images of control and Kif18A siRNA treated cells stained for ɣ-tubulin (red) and ACA (green) are shown (C). A plot of average ACA FL distribution (green circles) within a control cell is well fit by a single Gaussian function (dashed line) (D). Average FWHM measurements from HeLa cells treated with control or KIF18A siRNAs and expressing GFP or the indicated Kif18A constructs are plotted. Cells expressing KIF18A-R308 mutations displayed a similar increase in kinetochore distribution ($p > 0.05$), which were both significantly different from Kif18A-wt expressing cells ($p < 0.001$). The number of cells analyzed (N) is reported and error bars indicate SEM (E).

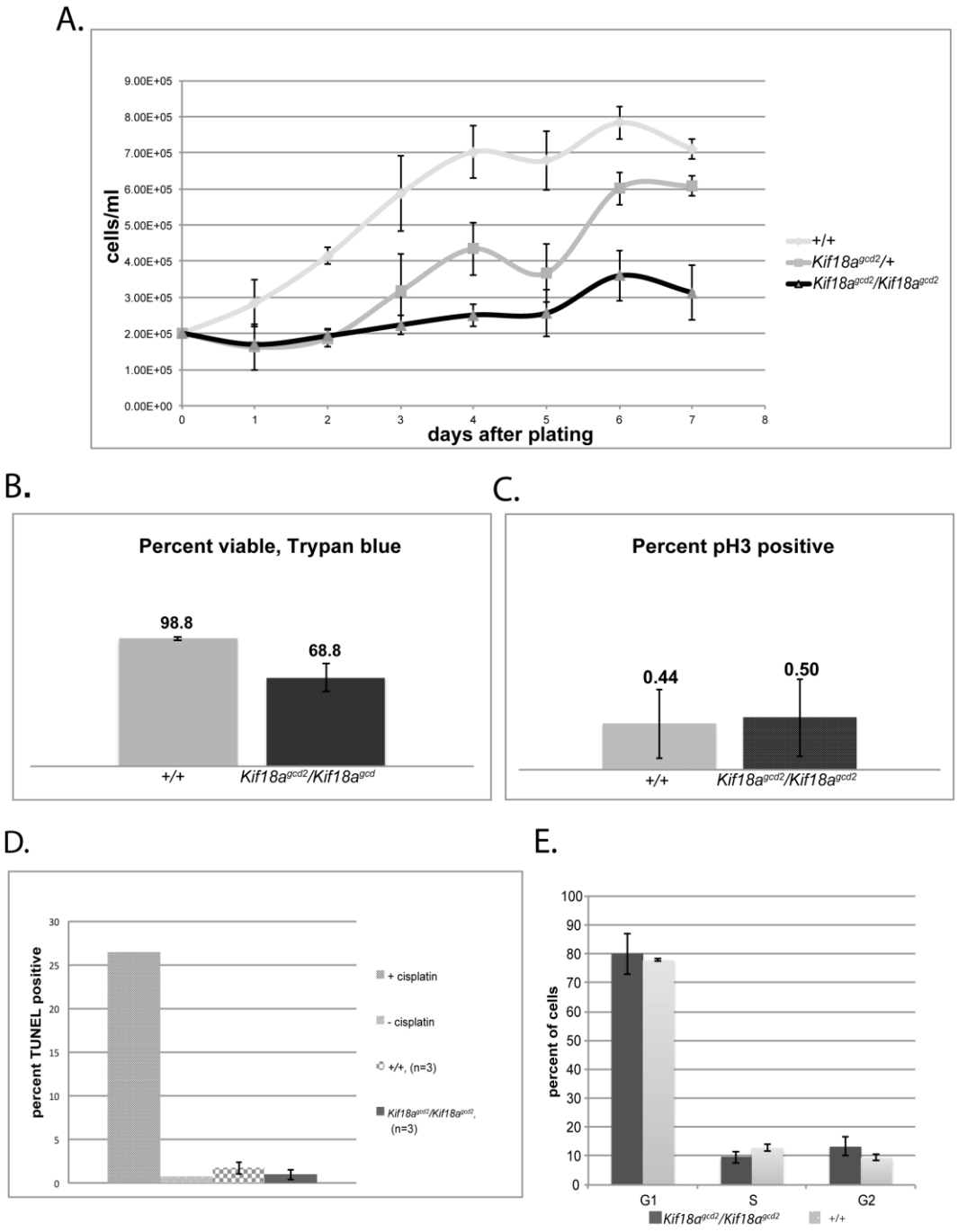

Figure 2-3. Primary *Kif18a*^{gcd2} embryonic fibroblasts do not display a cell cycle delay.

MEFs derived from mutant embryos were slow growing (A) and had reduced viability by trypan blue exclusion (B). There were no significant differences in histone H3 ser10 phosphorylation (C), in apoptosis related DNA fragmentation (TUNEL) (D) or cell

cycle staging by DNA content between mutant and wild type MEFs. All experiments were performed with three independently derived primary cell lines per genotype and technical replicates as described in the Methods.

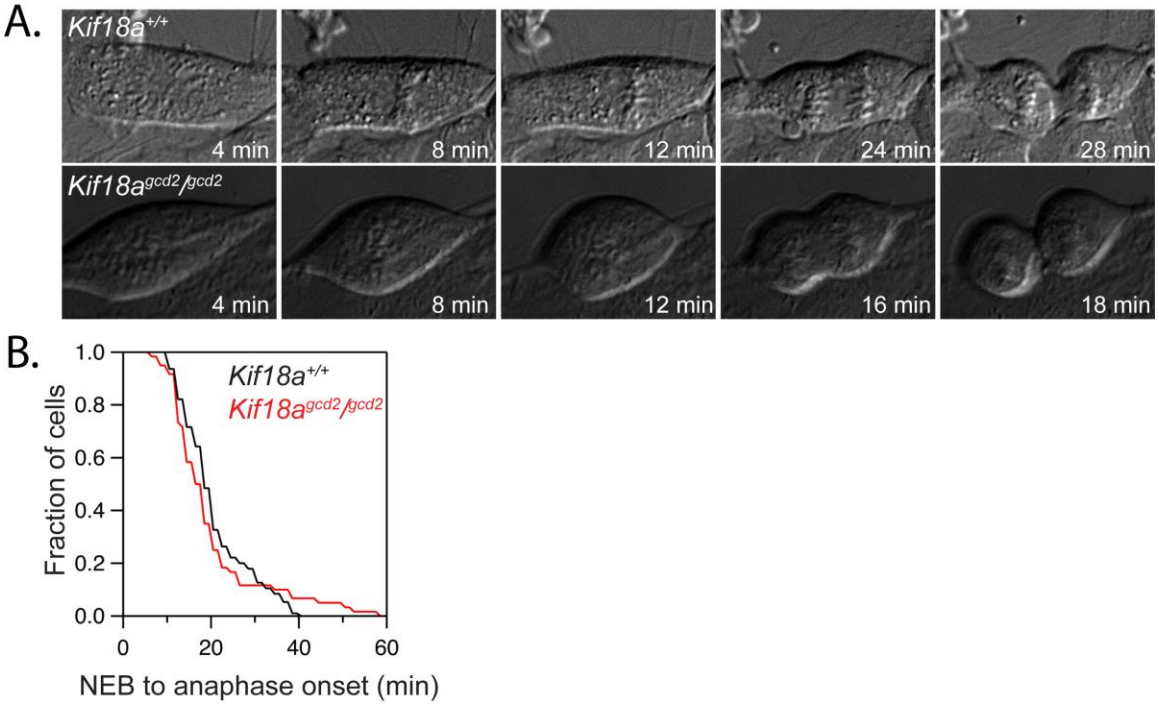

Figure 2-4. *Kif18a*^{gcd2} mutant and wild type MEFs progress through mitosis with similar timing. (Contributed by HK)

Mutant and control MEFs were imaged over a 16h period by differential interference contrast (A). Time from nuclear envelope breakdown to anaphase was recorded at 2-minute intervals and no significant difference was found between mutant and wild type MEFs ($p = 0.56$), n = 93 cells for *Kif18a*$^{+/+}$ and 58 cells for *Kif18a*$^{gcd2/gcd2}$ from 2 cell lines per genotype (B).

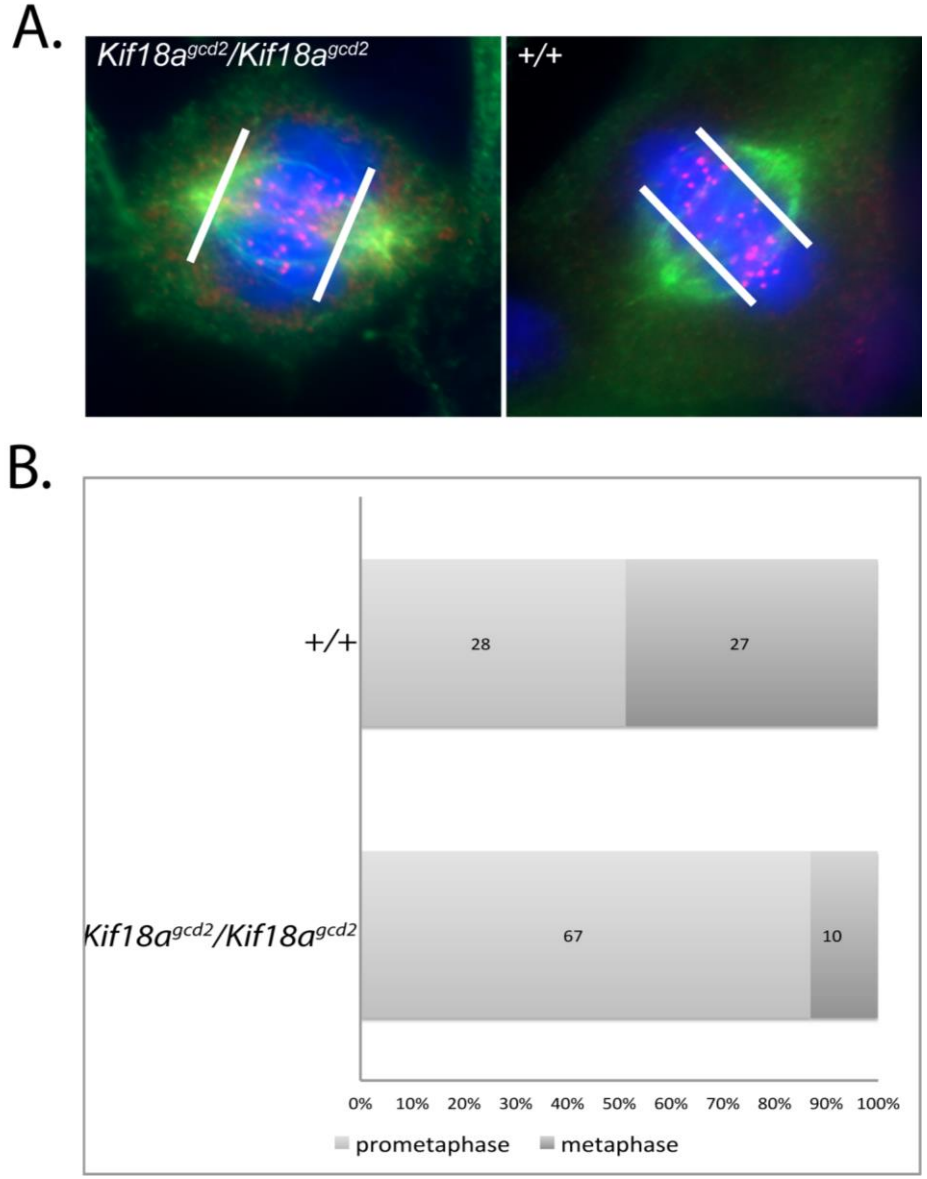

Figure 5. *Kif18a*^{gcd2} mutant MEFs exhibit chromosome alignment defects.

Mitotic profiling of *Kif18a*^{gcd2} mutant MEFs immunolabeled for tubulin (green) and CREST (red, centromeres) (A) revealed a high ratio of preanaphase mitotic cells with unaligned versus aligned chromosomes in mutant MEFs compared to wild type controls, n=3 cell lines per genotype, mean +/- s.d. is displayed (B).

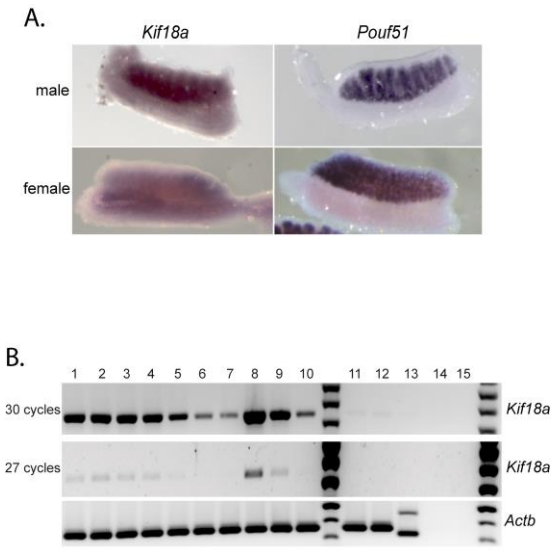

Figure 2-6. *Kif18a* is ubiquitously expressed in the fetal gonad.

In situ hybridization of *Kif18a* and the germ cell specific *Pou5f1* (*Oct3/4*) in wild type E12.5 ovaries and testes shows that *Kif18a* expression is not restricted to the germ line (A). RT-PCR shows that *Kif18a* is expressed in the fetal gonad, as well as the adult testes and ovary. *Kif18a* expression positively correlates with the presence of proliferating germ cells (high in the wild type testes and reduced in the germ cell deficient $Kit^{W/W\text{-}v}$ testes and ovaries). Lane 1, $Kif18a^{gcd2}/Kif18a^{gcd2}$ E11.5-12.5 fetal gonad; Lane 2, +/+ E11.5-12.5 fetal gonad; Lane 3, Kit+/+ E11.5-12.5 fetal gonad; Lane 4, $Kit^{W/W\text{-}v}$ E11.5-E12.5 fetal gonad; Lane 5, C57BL/6J adult ovary; Lane 6, $Kif18a^{gcd2}/Kif18a^{gcd2}$ adult ovary; Lane 7, $Kit^{W/W\text{-}v}$ adult ovary; Lane 8, C57BL/6J adult testes; Lane 9, $Kif18a^{gcd2}/Kif18a^{gcd2}$ adult testes; Lane 10, $Kit^{W/W\text{-}v}$ adult testes; Lane 11, C57BL/6J adult liver; Lane 12, C57BL/6J adult brain; Lane 13, DNA, no RNA, no reverse transcriptase; Lane 14, no reverse transcriptase; Lane 15, PCR water control, 100 bp ladder (B).

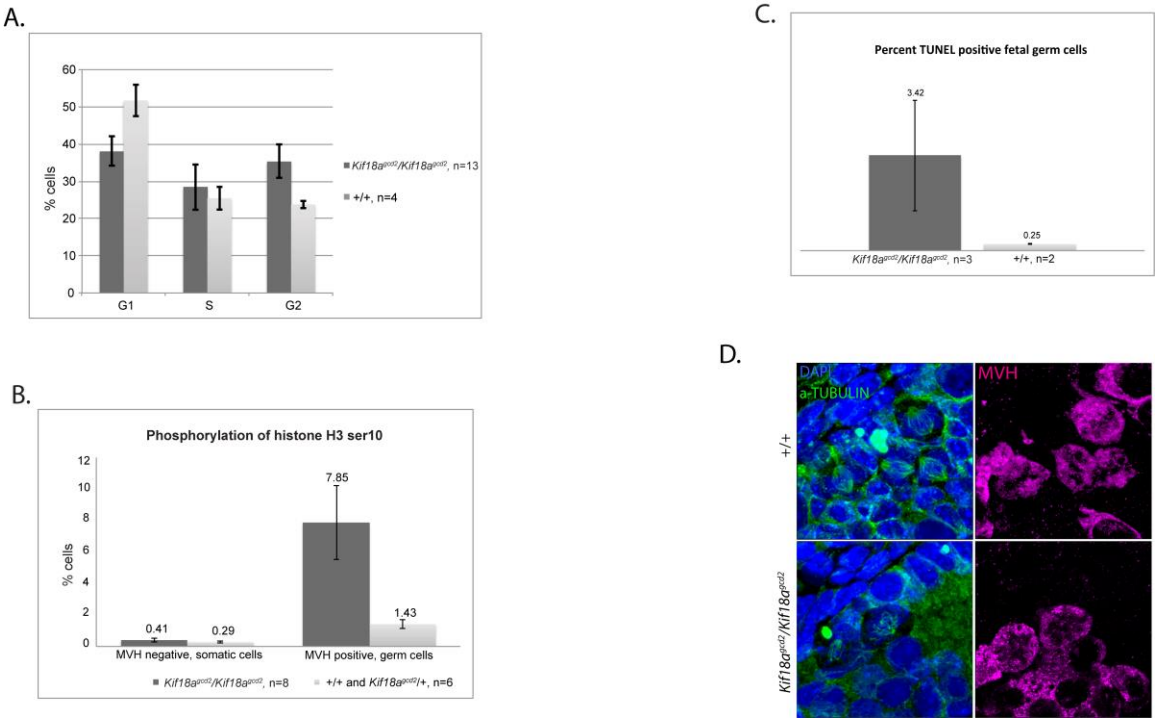

Figure 7. *Kif18a*^{gcd2} mutant germ cells arrest in mitosis with chromosome alignment defects.

Cell cycle analysis by DNA content revealed a significantly higher percentage of *Kif18a*^{gcd2} mutant germ cells in G2 compared to wild type (Student's t-test, p=0.006) and a correspondingly decreased percentage of cells in G1 (Student's t-test, p=0.002) (A). Phosphorylated histone H3 (B), and TUNEL labeling (C), both indicative of G2/M checkpoint activation were significantly increased in mutant germ cells (Student's t-test (pH3, germ cells), p=0.005; Student's t-test (pH3, somatic cells), p=0.02; Student's t-test (TUNEL, germ cells), p=0.05). In all cases, error bars represent standard deviation from the mean value from at least 3 age-matched, sibling biological replicates per genotype from multiple litters. For mutant genotypes, more biological replicates were required to obtain sufficient germ cells numbers for flow cytometry. Mitotically dividing spermatogonial cells (MVH positive) from pre-pubertal, mutant testes had poor spindle organization and showed defects in mitotic chromosome alignment (D).

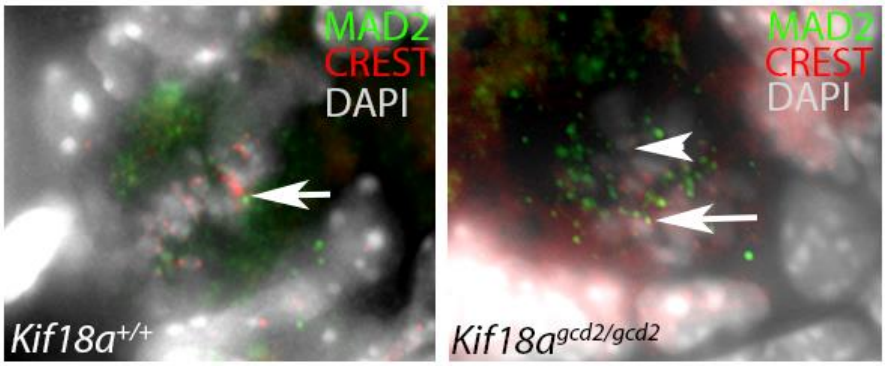

Figure 2-S1.

Immunolocalization of the cell cycle checkpoint protein, MAD2, in wild type, metaphase spermatogonia revealed few instances of MAD2 (green) co-localization with kinetochores (CREST, red) (30% (N=40)) (white arrow, *Kif18a*$^{+/+}$*).* In mutant mitotic spermatogonia, a mixed population of both MAD2 positive (white arrow, *Kif18a*$^{gcd2/gcd2}$) and MAD2 negative kinetochores (arrowhead, *Kif18a* $^{gcd2/gcd2}$) was observed in all cells (100%, N=40).

CHAPER 3: KIF18A PROMOTES HEC1 DEPHOSPHORYLATION TO COORDINATE CHROMOSOME ALIGNMENT WITH KINEOCHORE MICROTUBULE ATTACHMENTS

Haein Kim[1], and Jason Stumpff[1,2*]

[1]Department of Molecular Physiology and Biophysics, University of Vermont, Burlington, VT 05405, United States

[2]Lead Contact

*Correspondence to:

Jason Stumpff

Department of Molecular Physiology and Biophysics

University of Vermont

89 Beaumont Avenue

Burlington, VT 05405

802-656-7849 (phone)

802-656-0747 (fax)

jstumpff@uvm.edu

3.1. Abstract

Mitotic chromosomes are spatially confined at the spindle equator just prior to chromosome segregation through a process called chromosome alignment. Alignment requires temporal coordination of kinetochore microtubule attachment and dynamics. However, the molecular mechanisms that couple these activities are not understood. Kif18A (kinesin-8) suppresses the dynamics of kinetochore microtubules to promote chromosome alignment during metaphase. Loss of Kif18A function in HeLa and primordial germ cells leads to alignment defects accompanied by a spindle assembly checkpoint (SAC)-dependent mitotic arrest, suggesting the motor also plays a role in regulating kinetochore-microtubule attachments. We show here that Kif18A increases attachment by promoting dephosphorylation of the kinetochore protein Hec1, which provides the primary linkage between kinetochores and microtubules. This function requires a direct interaction between the Kif18A C-terminus and protein phosphatase-1 (PP1). However, the Kif18A-PP1 interaction is not required for chromosome alignment, indicating that regulation of kinetochore microtubule dynamics and attachments are separable Kif18A functions. Mitotic arrest in Kif18A-depleted cells is rescued by expression of a Hec1 variant that mimics a low-phosphorylation state, indicating that Kif18A-dependent Hec1 dephosphorylation is a key step for silencing the checkpoint and promoting mitotic progression. Our data support a model in which Kif18A provides positive feedback for kinetochore microtubule attachment by directly recruiting PP1 to dephosphorylate Hec1. We propose that this function works

synergistically with Kif18A's direct control of kinetochore microtubule dynamics to temporally coordinate chromosome alignment and attachment.

3.2. Introduction

Kinetochores, which form at the centromeric region of mitotic chromosomes, function to tether chromosomes to a subset of mitotic spindle microtubules known as kinetochore microtubules or K fibers. Proper regulation of K fiber dynamic instability and attachment is required for chromosome alignment at metaphase and the segregation of sister chromatids during anaphase [1-4]. K fiber attachments are stabilized as mitotic chromosomes align [5-7], but the mechanisms that temporally coordinate attachment and alignment are not understood.

End-on attachments between K fibers and kinetochores are primarily dependent on Hec1, a component of the NDC80 complex. Hec1 directly associates with microtubules through an electrostatic interaction that depends on its positively charged N-terminus [8, 9]. The Hec1 N-terminus contains nine Aurora B phosphorylation sites, which are phosphorylated in early mitosis [10-13]. Hec1 phosphorylation reduces the interaction between the kinetochore and the negatively charged microtubule surface, favoring K fiber detachment [2, 9, 14-16]. Hec1 is dephosphorylated as cells progress through mitosis, with the lowest levels occurring during late metaphase and anaphase [14]. These data indicate the affinity of kinetochores for microtubules increases as chromosomes align. Recruitment of protein phosphatase 1 (PP1) to kinetochores by proteins such as KNL1 [17, 18], and the SKA complex [19] has been shown to

antagonize Aurora B activity, however, the specific mechanism responsible for Hec1 dephosphorylation remains unclear.

Hec1 affinity for microtubules must be dynamically regulated, not only for proper biorientation of chromosomes, but also for normal chromosome alignment. Cells microinjected with antibodies that block Hec1 phosphorylation show hyperstable K fiber attachments, accompanied by alignment defects and decreased chromosome oscillations [2]. Similarly, cells expressing a Hec1 variant that prevents phosphorylation of the N-terminus are unable to align their chromosomes due to reduced K fiber dynamics [16, 20]. Conversely, in cells expressing a phosphomimetic Hec1 variant, with the 9 Aurora B sites in the N-terminus mutated to acid residues, kinetochores are uncoupled from K fibers and chromosomes fail to align [16, 20]. Furthermore, introduction of a single phosphomimetic residue to the non-phosphorylatable Hec1 variant (Hec1-1D) is sufficient to restore normal chromosome movement but not chromosome alignment [19, 20], suggesting that proper timing of Hec1 dephosphorylation is required for chromosome confinement to the metaphase plate. Consistent with this, PP1 accumulation at kinetochores increases as cells progress towards metaphase [21], coinciding with a decrease in phospho-Hec1 levels [14]. However, the mechanisms underlying temporal changes in Hec1 affinity and PP1 recruitment are not understood.

Kif18A (kinesin-8) is essential for chromosome alignment during metaphase and directly binds PP1 [4, 22-24]. This plus-end directed motor accumulates at the ends of K fibers and attenuates their dynamics as cells progress from prometaphase to metaphase. Reduced K fiber dynamics confines chromosome movements and promotes

metaphase plate formation [4]. In addition, Kif18A depletion in HeLa cells results in a spindle assembly checkpoint (SAC)-dependent metaphase arrest [4, 25, 26], which suggests a defect in kinetochore microtubule attachment. Similarly, loss of Kif18A function leads to a SAC-dependent mitotic arrest in primordial germ cells during murine embryogenesis [27]. Whether Kif18A has a direct or indirect role in promoting kinetochore microtubule attachments in these cells types is unclear. However, the fission yeast kinesin-8s Klp5 and Klp6 are required for SAC silencing through an unknown function that relies on direct interaction between the C-termini of the motors and PP1 [24]. Human Kif18A contains the conserved R/VxVxF/W PP1 binding motif found in Klp5 and Klp6 and directly binds PP1α/ɣ [22, 23]. The Kif18A-PP1 interaction has been proposed to antagonize phospho-inhibition of Kif18A by Cdk1, but a role for this interaction in promoting kinetochore microtubule attachments and the metaphase-to-anaphase transition has not been thoroughly explored.

In this study, we used a combination of quantitative immunofluorescence and live-cell imaging techniques to investigate the molecular basis of Kif18A's role in coordinating chromosome alignment with the metaphase-to-anaphase transition. We report that Kif18A-PP1 binding promotes Hec1 dephosphorylation and progression through mitosis. This mechanism, in combination with Kif18A's direct regulation of chromosome movement, coordinates chromosome alignment with the stabilization of K fiber attachments, promoting timely transition from metaphase-to-anaphase.

3.3. Results

3.3.1. Kif18A depletion increases Hec1 phosphorylation during metaphase

Observations that Kif18A is required for normal mitotic progression in HeLa and primordial germ cells suggest that the motor has a role in promoting or stabilizing kinetochore-microtubule attachments [26, 28]. To determine if Kif18A affects the phosphoregulation of Hec1, which is progressively dephosphorylated to increase the affinity of kinetochores for microtubules as chromosomes align, we analyzed Hec1 phosphorylation by immunofluorescence in HeLa cells treated with scrambled control (control KD) and Kif18A specific siRNAs (Kif18A KD), which we have extensively validated [4, 29, 30]. Previous work has shown that the signals from Hec1 antibodies against phosphorylated Ser8, Ser15, Ser44, and Ser55 decrease significantly between prometaphase and metaphase, with Ser44 and Ser55 showing the most dramatic changes [14]. Thus, we quantified the signal from a phospho-specific antibody against Hec1 Ser55 in metaphase arrested cells to determine if Kif18A is required for Hec1 dephosphorylation (Figure 1A). These studies revealed that Kif18A KD cells have a significantly higher level of phosphorylated Hec1 at metaphase kinetochores than control cells (Figure 1B). In contrast, total Hec1 levels were comparable between the two cell populations (Figure 1C). These data indicate that Kif18A is required to promote Hec1 dephosphorylation.

To determine if Kif18A dependent changes in phospho-Hec1 levels were due to the motor's previously identified interaction with PP1 [22, 23, 31], we quantified the effects of disrupting Kif18A-PP1 binding on Hec1 phospho-Ser55 levels. HeLa cells depleted of endogenous Kif18A were transfected with plasmids encoding GFP alone, GFP-tagged Kif18A full-length protein (GFP-Kif18AFL), or a GFP-Kif18A construct

containing two point mutations within the conserved PP1 binding site (GFP-Kif18A^{AVVVA}). These mutations have previously been shown to disrupt binding between kinesin-8 motors and PP1 [22-24]. Both GFP-Kif18A constructs localized to mitotic spindles and accumulated at K fiber plus-ends (Figure 2A). However, phospho-Ser55 levels were significantly lower in cells expressing GFP-Kif18AFL compared to those expressing similar levels of GFP-Kif18A^{AVVVA} (Figure 2B-C and Fig S1). Furthermore, phospho-Ser55 levels in GFP-Kif18A^{AVVVA} expressing cells were comparable to those measured in cells expressing GFP only (Figure 2B-C). These data indicate that Kif18A promotes Hec1 dephosphorylation through its interaction with PP1. This effect may not have been detected in a previous study due to utilization of a less sensitive measurement approach [23].

3.3.2. Loss of Kif18A function leads to an increased number of unattached kinetochores

One of the consequences of higher Hec1 phosphorylation during prometaphase is that kinetochores are more likely detach from microtubules, even when they are properly bioriented [14, 20, 28]. Since mutating the PP1 binding site in the Kif18A C-terminus increased phospho-Hec1 levels at kinetochores in metaphase, we investigated whether these changes correlate with metaphase kinetochore-microtubule attachment defects. We used the presence of the SAC protein MAD1 at kinetochores, determined by colocalization with anti-centromere associated (ACA) antibodies, as a readout for unattached kinetochores [32]. Previous work indicates that loss of Kif18A leads to an

increase in unattached kinetochores in asynchronously dividing HeLa cells [26]. We found that metaphase arrested Kif18A KD cells also display an increase in MAD1-positive kinetochores, indicating attachment errors persist to late metaphase in the absence of Kif18A (Figure S2A). The fraction of cells with at least one MAD1-positive kinetochore was similar in Kif18A KD cells expressing GFP-Kif18A^{AVVVA} (0.72 +/- 0.36, n = 42/58 cells) or GFP alone (0.8 +/- 0.4, n = 64/80 cells; Figure 3A-B). Control KD cells expressing GFP alone (0.23 +/- 0.12, n = 14/68 cells) had a lower fraction of cells with MAD1-positive kinetochores in comparison, as did cells expressing GFP-Kif18AFL (0.42 +/- 0.4, n = 22/50 cells; Figure 3A-B). Additionally, Kif18A KD cells expressing GFP-Kif18A^{AVVVA} have a similar number of MAD1-positive kinetochores per cell (3.9 +/- 4) as those expressing GFP (4.6 +/- 4) MAD1, while control KD cells expressing GFP (0.7 +/- 2) and Kif18A KD cells expressing GFP-Kif18AFL (1.6 +/- 3 per cell) both displayed significantly fewer MAD1-positive kinetochores per cell (Figure 3C). We found that cells with the highest levels of GFP-Kif18AFL expression had the fewest MAD1 positive kinetochores, but this trend was not true for GFP-Kif18A^{AVVVA} expressing cells (Figure S2B). Taken together, these data suggest that Kif18A-PP1 binding is necessary to maintain robust kinetochore-microtubule attachments and silence the SAC.

3.3.3. Kif18A is capable of accumulating at K fiber plus-ends and aligning chromosomes independent of PP1 binding

We observed that metaphase arrested Kif18A KD cells expressing GFP displayed chromosome alignment defects similar to those previously reported in Kif18A loss of function cells, while Kif18A KD cells expressing GFP-Kif18A^{AVVVA} had comparatively well aligned chromosomes. To quantify chromosome alignment, we measured kinetochore distribution across the pole-to-pole axis of the spindle in Kif18A KD cells expressing GFP or GFP-Kif18A constructs [29, 33] (Figure 4A-B). All values were normalized to the average kinetochore distribution measured in GFP expressing cells treated with control siRNAs for comparison. We found that chromosome alignment in cells expressing either GFP-Kif18A^{AVVVA} or GFP-Kif18AFL was comparable to that seen in control cells (Figure 4C). In contrast, the kinetochore distribution in Kif18A KD cells expressing GFP alone was significantly wider than the distribution in Control KD cells (Figure 4C). These data indicate that Kif18A's ability to align chromosomes, which depends on attenuation of microtubule dynamics, does not require PP1 binding. Consistent with this conclusion, we also find that GFP-Kif18A^{AVVVA} and GFP-Kif18AFL accumulated with similar kinetics at the plus-ends of K fibers treated with the microtubule-stabilizing drug taxol, indicating that the plus-end directed motility and stable plus-end binding of the two motors is comparable (Figure S3). Stable microtubule plus-end accumulation is required for Kif18A's function in suppressing microtubule dynamics, thus its role in chromosome alignment [33, 34]. Collectively, these data suggest that PP1-binding is not required for Kif18A's motility or chromosome alignment functions during metaphase.

3.3.4. Kif18A does not promote attachments by regulating chromosome positioning or kinetochore tension

It was previously reported that SAC proteins preferentially localized to unaligned kinetochores in Kif18A KD cells [26]. This raises the possibility that it is the unaligned chromosome population in these cells that has kinetochore microtubule attachment defects. Consistent with this idea, recent studies indicate that pole proximal kinetochores can be phosphorylated by Aurora A kinase, which has been shown to contribute to Hec1 phosphorylation [35, 36]. Therefore, we measured the location of MAD1 positive kinetochores relative to the center of the spindle in Kif18A KD cells expressing GFP-Kif18A constructs (Figure 5A). MAD-1-positive kinetochores were far from the midzone in Kif18A KD cells expressing GFP (2.59 +/- 1.54 μm) consistent with previous work [26] (Figure 5B). In contrast, MAD1-positive kinetochores in Kif18A KD cells expressing GFP-Kif18A^{AVVVA} were significantly closer to the midzone (1.36 μm +/- 0.96 μm) than those in Kif18A KD GFP cells and were positioned at comparable distances to those found in GFP-Kif18AFL (1.46 +/- 0.94 μm) and control KD GFP expressing cells (1.31 +/- 0.91 μm), which fully align their chromosomes (Figure 5B). These data indicate that chromosomes near the midzone require Kif18A-PP1 for attachment and that chromosome alignment is not sufficient for SAC inactivation.

Kif18A has also been implicated in regulating tension between kinetochores. Kif18A overexpression leads to hyperstretching between sister kinetochores, while depletion leads to a measurable decrease in interkinetochore distance (IKD) [4, 26].

Reduced kinetochore tension promotes Aurora B kinase-dependent phosphorylation of outer kinetochore substrates, such as Hec1 [37]. Thus, we measured the effect of GFP-Kif18A^{AVVVA} on IKD to determine if low tension could be contributing to the attachment defects observed in these cells. However, we found that the distances between sister kinetochores in Kif18A KD cells expressing GFP-Kif18A^{AVVVA} were comparable to those measured in control KD cells and Kif18A KD expressing GFP-Kif18AFL (Figure 5C-D). In contrast, Kif18A KD cells expressing GFP had significantly reduced IKDs compared to control KD cells (Figure 5D), consistent with previous reports [4, 26]. These results suggest that the attachment defects observed in GFP-Kif18A^{AVVVA} cells are not explained by reduced interkinetochore stretch.

3.3.5. A low phosphorylation mimetic Hec1 mutant is sufficient to promote progression through mitosis in Kif18A KD cells

To determine if the SAC-dependent arrest observed in Kif18A KD cells is caused by increased Hec1 phosphorylation, we asked if a Hec1 mutant that mimics low phosphorylation could rescue mitotic progression. Specifically, we analyzed the effects of a previously characterized Hec1 mutant, called Hec1-1D, which carries alanine substitutions in eight of the predicted Aurora B phosphorylation sites and a single phosphomimetic aspartic acid substituted for Ser55 [15, 16]. Expression of GFP Hec1-1D in cells depleted of endogenous Hec1 permits normal chromosome movement but does not fully rescue chromosome alignment [16]. We co-depleted HeLa cells of Kif18A and Hec1 using previously validated siRNAs [4, 14], and subsequently

transfected with plasmids encoding GFP-tagged wild type Hec1 (GFP-Hec1-WT), GFP-Hec1-1D, or GFP alone. The time from nuclear envelope breakdown to anaphase onset was measured using time-lapse DIC imaging in cells positive for GFP-Hec1 constructs (Figure 6A). The majority of Hec1 and Kif18A co-depleted cells expressing either GFP or GFP-Hec1-WT failed to divide during the time course of the movie or underwent apoptosis (Figure 6B). In contrast, the majority of GFP-Hec1-1D expressing cells completed division without chromosome alignment (Figure 6B). Thus, alleviating Hec1 phospho-regulation mitigates the mitotic arrest but not the chromosome alignment defects observed in Kif18A KD HeLa cells. These data suggest that a Kif18A-dependent increase in Hec1 affinity to microtubules silences the SAC and promotes the metaphase-to-anaphase transition independently of the motor's known role in regulating microtubule dynamics.

3.4. Discussion

Biorientation and chromosome alignment during cell division ensure maintenance of genomic stability. Temporally regulated changes in the affinity between kinetochores and microtubules help to promote and stabilize bioriented attachments. As biorientation occurs, K fiber dynamics are also dampened to confine chromosome movements at the spindle midzone and form the metaphase plate. Our work indicates that Kif18A possesses two separable functions, one relying on its ability to suppress microtubule dynamics and the second on its direct interaction with PP1, that together couple the stabilization of bioriented attachments with the alignment of chromosomes at the spindle equator [22, 23].

Our data strongly support a model in which Kif18A promotes Hec1 dephosphorylation by recruiting PP1 to the plus-ends of K fibers (Figure 7). Our data indicate that the majority of kinetochores are attached to K fibers and devoid of SAC proteins during metaphase in the absence of Kif18A activity, suggesting that the motor is not necessary for initial end-on attachments during prometaphase (Figure 7A). This is also consistent with previous studies indicating that Kif18A's motility to K fiber plus-ends, which is relatively slow (~75-100 nm/sec), is contingent on the presence of a stable kinetochore microtubule track (Figure 7B) [34, 38] . As kinetochores become attached, Kif18A accumulates at K fiber plus-ends, where it confines chromosome movements and promotes the complete dephosphorylation of Hec1. We propose that Kif18A's dual functions provide positive feedback for K fiber attachment while the motor simultaneously dampens K fiber dynamics to align chromosomes during metaphase (Figure 7C-D). These combined activities facilitate temporal coordination between attachment and alignment.

Recent findings show that Hec1 has different binding configurations on polymerizing and depolymerizing microtubules, and that Hec1 phosphorylation only affects microtubule association on polymerizing microtubules [39]. These data suggest that Hec1 dephosphorylation primarily increases the affinity of kinetochores for polymerizing K fibers. Kif18A's behavior on growing and shortening microtubules is consistent with a role for the motor in specifically promoting the attachment of polymerizing K fibers. For example, Kif18A localizes asymmetrically on sister K fibers in mitotic cells [4]. Furthermore, purified Kif18A accumulates on growing

microtubules but dissociates from shortening microtubules *in vitro* [34]. Taken together, these data imply that Kif18A may accumulate preferentially on growing K fibers, where it could promote Hec1 dephosphorylation. Switching to a phosphorylation-independent binding state during depolymerization circumvents the need for constant suppression of Aurora B activity near its outer kinetochore substrates for stabilizing and maintaining attachments.

Our data also address two alternative models for Kif18A's role in promoting kinetochore microtubule attachment. We considered that Kif18A could indirectly promote Hec1 dephosphorylation by increasing tension at kinetochores, displacing Hec1 from the inner-centromere localized Aurora B kinase [37]. Consistent with this model, Kif18A accumulation at the plus-ends of K fibers enhances inter-kinetochore stretch [4, 26]. However, we found that cells expressing GFP-Kif18A^{AVVVA} displayed normal inter-kinetochore stretch but abnormally high Hec1 phosphorylation and MAD1 levels, suggesting Kif18A-dependent regulation of kinetochore tension does not explain its role in promoting Hec1 dephosphorylation or kinetochore microtubule attachment.

We also considered the possibility that Kif18A's function in chromosome alignment excludes chromosomes from the spindle poles, preventing Aurora A kinase from phosphorylating Hec1. Pole proximal chromosomes are often improperly attached, and cells rely on Aurora A kinase activity to destabilize erroneous attachments [35, 36]. Some chromosome pairs in Kif18A depleted cells are significantly displaced from the metaphase plate. Thus, these misaligned pairs could be subject to regulation by Aurora A, explaining the observed increase in Hec1

phosphorylation. However, our data indicate that Kif18A KD cells expressing GFP-Kif18A^{AVVVA} have aligned chromosomes with increased phospho-Hec1 levels. Furthermore, primary embryonic fibroblasts isolated from *Kif18a* mutant mice divide with normal kinetics despite chromosome alignment defects [27]. These data collectively indicate that Kif18A's chromosome alignment and attachment functions are independent of each other. While these alternative models are not mutually exclusive with Kif18A's recruitment of PP1 to kinetochores, our data strongly support PP1-dependent dephosphorylation of Hec1 as the primary mechanism for Kif18A's role in enhancing kinetochore-microtubule attachments.

Existing evidence suggests that a role for kinesin-PP1 coupling of chromosome alignment and attachment is conserved in eukaryotes. We have shown that murine primordial germ cells require Kif18A activity for kinetochore microtubule attachment, chromosome alignment, and completion of mitosis. However, while somatic cells from *Kif18a* mutant embryos also display chromosome alignment defects, they progress through mitosis with normal timing. These data are consistent with a role for Kif18A in coordinating chromosome alignment and attachment in at least some cell types during mammalian development and suggest that other mechanisms are able to compensate for the loss of Kif18A's attachment function in others [18, 19, 40-42]. The fission yeast kinesin-8 motors Klp5/Klp6 are also required for chromosome alignment [42, 43] and interact with PP1 to silence the SAC [24]. The mechanism for checkpoint silencing in this case has not been identified, but Klp5/6 mutants are synthetically lethal with mutations in dam1 [44], suggesting a role for the heterodimeric Klp5/6 motor in

kintetochore microtubule attachment. Furthermore, recent work from Suzuki *et al*. (accompanying paper) indicates that an interaction between Cin-8 (kinesin-5) and PP1 is required for kintetochore microtubule attachment in budding yeast. Interestingly, it is Cin-8, rather than the budding yeast kinesin-8 motor Kip3, that plays a more prominent role in regulating kinetochore microtubule dynamics and chromosome alignment in S. cerevisiae, suggesting Cin-8 may function to coordinate alignment and attachment [45].

In summary, our study indicates that the kinesin-8 motor Kif18A recruits PP1 and directly regulates microtubule dynamics to couple the attachment and alignment of mitotic chromosomes. Hec1 is a critical substrate of Kif18A associated PP1, and Kif18A-dependent dephosphorylation of Hec1 is required for cells to progress from metaphase into anaphase. In contrast, Kif18A-dependent chromosome alignment is not a prerequisite for satisfying the SAC. Thus, chromosome alignment and attachment are separable processes. Mechanisms that temporally coordinate these functions are likely necessary to prevent chromosome segregation errors.

3.5. Materials and Methods

Plasmids and siRNAs

A Kif18A PP1 binding mutant (GFP-Kif18A^{AVVVA}) was generated by mutating residues K612 and W616 via site-directed mutagenesis, resulting in K612A and W616A (forward sequence 5'-TCGAACATTTGGTAGAGAGGAAAGCAGTGGTAGTTGCGGCTGACCAAACTGCCGAAC-3') using siRNA-resistant GFP-Kif18AFL as a template, described previously in Stumpff *et al*, 2008. Cells were treated with previously validated control

(Silencer Negative Control #1, Life Technologies), Kif18A (5'-GCUGGAUUUCAUAAAGUGG -3', Life Technologies, [4, 29, 33], and Hec1 siRNAs (5′-CCCUGGGUCGUGUCAGGAA-3', Qiagen, [14].

Cell culture and transfections

HeLa cells were cultured in 5% CO_2 at 37^{o}C in MEM-alpha (Life Technologies) with 10% fetal bovine serum (FBS, Gibco) and 1% antibiotics (Pen/Strep, Gibco). For siRNA transfections, 5.0 x 10^5 cells were plated on 60mm^2 dishes and grown overnight. 300 pmols of siRNA per 60mm^2 dish (control and Kif18A) were incubated with Lipofectamine RNAiMAX transfection reagent (Thermo Scientific) in Opti-Mem reduced serum media as per manufacturer's instructions, and added to cells for 8 hours. Cells were trypsinized, collected and pelleted. 5.0 x 10^5 cells were electroporated with 3.5 µg of plasmid DNA (GFP only (pmax-GFP^{TM}, Lonza, Germany), GFP-Kif18AFL, or GFP-Kif18A^{AVVVA}, GFP-Hec1-WT, GFP-Hec1-1D, or 2.0µµg of mCherry-PP1ɣ, mCherry-CENP-B) using the Lonza 4D nucleofector system. Electroporated cells were seeded onto 12 mm^2 glass coverslips (Electron Microscopy Sciences, Hatfield, PA) or Poly L-lysine treated glass bottom imaging dishes (MatTek) and allowed to incubate for approximately 18-24 hrs after transfection. Cells were treated with 20 µM MG132 for 3 hours to enrich for metaphase cells in fixed cell assays.

Immunofluorescence

Cells were fixed on 12 mm^2 glass coverslips (EMS) for 10 minutes in -20º C methanol and 1% paraformaldehyde on ice, and washed twice in TBS for 5 minutes. Coverslips were incubated with 20% boiled goat serum diluted in antibody-diluting buffer (Abdil, 1x TBS, 2% goat serum albumin, 0.2% sodium azide) for 1 hr at ambient temperature, then washed twice with TBS for 5 min. Coverslips were incubated with human anti-centromeric protein A (ACA) serum (Antibodies Incorporated, Davis, CA) at 2.5 µg/mL overnight at 4^oC, mouse anti ɣ-tubulin at 1.0 µg/mL (Sigma-Aldrich, St. Louis, MO), mouse anti-α-tubulin at 1 µg/mL (Sigma-Aldrich), mouse anti-ɣ-tubulin at 1 µg/mL (Life technologies) at ambient temperature for 1 hr, mouse anti-MAD1 at 3.6 µg/mL at 4^o C overnight. Cells used to detect total Hec1 and phospho-serine 55 Hec1 were pretreated with PHEM extraction buffer (60mM PIPES, 25mM HEPES, 10mM EGTA, 4mM $MgCl_2$ (PHEM), 0.5% Triton-X, pH 6.9, 1x Halt protease and phosphatase inhibitor cocktail (Thermo Fisher) 100 µM Microcystin-LR (Sigma-Aldrich) for 5 minutes at 37^o C before fixing with 4% paraformaledehyde in 1x PHEM buffer for 15 minutes at ambient temperature. Cells were washed twice with 1x PHEM buffer for 5 min, then incubated at 4^o C overnight with 3.44 µg/mL mouse anti-Hec1 (GeneTex) and 2.57 µg/mL rabbit anti-Hec1 Phospho-Ser55 (GeneTex). Coverslips were mounted onto glass slides with Prolong gold anti-fade mounting medium with 4′,6-Diamidine-2′-phenylindole dihydrochloride (Prolong Gold with DAPI, Life Sciences).

Microscopy

Fixed and live cell imaging was performed using a Nikon Ti-E inverted microscope controlled by NIS Elements software (Nikon Instruments, Melville, NY) with APO 100x/1.49 numerical aperture (NA) and Plan APO 60x/1.42 NA oil immersion objectives (Nikon Instruments), Spectra-X light engine (Lumencore, Beaverton, OR), and Clara cooled charge-coupled device (CCD) camera or iXon X3 DU-897 EMCCD camera (Andor, South Windsor, CT). Some fixed cell imaging was also performed using a Nikon TE2000-E2 inverted microscope controlled by NIS elements software (Nikon Instruments) with a Plan Apo 60X/1.42 NA oil immersion objective, EXFO X-CITE 120 illuminator, Uniblitz shutters, and a Photometrics Cool-SNAP HQ2 14-bit camera.

Live imaging of mitotic division

Cells co-depleted of Kif18A and Hec1 were electroporated with GFP-Hec1-WT or GFP-Hec1-1D plasmid DNA (kind gifts from Dr. Jennifer DeLuca, Zaytsev, et al., 2014) 8 hrs after siRNA incubation, then plated onto 35 mm^2 glass bottom filming dishes (MatTek) and imaged approximately 30 hours post-electroporation. Cell culture media was changed to CO_2-independent media containing 10% FBS and 1% antibiotics (Pen/Strep) prior to imaging. DIC images were taken every 2 minutes, with GFP images taken once every 40 frames concurrently to minimize phototoxicity. Only cells that were positive for GFP-Hec1 constructs were analyzed. For analyses of dividing

cells, only cells that entered mitosis during the movie and displayed one of the following behaviors were included: (1) completed division during the movie, (2) underwent apoptosis (counted as did not divide), or (3) were in mitosis for at least two hours and were still in mitosis at the end of the movie (counted as did not divide).

Chromosome alignment analyses

After fixation, single focal plane images were taken of mitotic cells with both spindle poles in the same plane of focus. The images were rotated to ensure that the spindle pole axis was horizontal, and a line was drawn between the two poles. The Plot Profile command in ImageJ was used to measure the distribution of ACA-labeled kinetochore fluorescence within a region of interest (ROI) defined by the length of the spindle with a set height of 17.5 μm (Stumpff 2012, Kim 2014). Plots of normalized average ACA fluorescence in each pixel column as a function of distance along the normalized spindle pole axis were analyzed by Gaussian fits using Igor Pro (Wavemetrics). The full width at half maximum intensity for the Gaussian fit was used as a metric for chromosome alignment in that cell.

To measure the position of MAD1-positive kinetochores relative to the spindle midzone, an ellipse was drawn to encompass the mitotic cell. Major and minor axes were determined by the ellipse draw command in NIS elements, with major axes drawn parallel to the spindle pole axis. The midzone was determined as the point that bisects the major axis. Distances were measured from the midzone to MAD1-positive

kinetochores with fluorescence intensity greater than 1.5 times the background fluorescence.

Total Hec1 and phospho-Hec1 Ser55 fluorescence quantification

A maximum intensity projection of 5 optical sections taken at 200 nm intervals was used to quantify total Hec1 and phospho-Hec1 Ser55 fluorescence. Hec1 foci were used to define regions of interest (ROIs) at individual kinetochores where both total and phospho-Hec1 Ser55 fluorescence were measured. Only ROIs that did not overlap with a neighboring kinetochore were analyzed. All fluorescence measurements were normalized to the mean control fluorescence level in each channel.

Motor accumulation measurements

Kif18A-depleted cells co-transfected with GFP rescue constructs (GFP, GFP-Kif18AFL, or GFP-Kif18A^{AVVVA}) and mCherry-CENPB were plated on 35 mm^2 glass bottom filming dishes and imaged approximately 30 hours post-transfection. Cell culture media was changed to CO_2-independent media containing 10% FBS and 1% antibiotics (Pen/Strep) prior to imaging. To determine motor accumulation after taxol addition, an equal volume of 20 μM taxol diluted in CO_2-independent media was added to each dish to achieve a final concentration of 10 μM taxol. Four frames were collected at 5 sec intervals prior to taxol addition. Following taxol addition, images were taken at 5 sec intervals for 5 minutes. To quantify the relative rate of motor accumulation to K fiber plus-ends, GFP fluorescence was fit to a Gaussian across the spindle pole axis at every frame of the movie. The full width at half maximum

(FWHM) of GFP fluorescence was measured and plotted as a function of time to obtain a relative rate of accumulation, reported as a rate of decreasing FWHM over time.

ACKNOWLEDGEMENTS

Support for this work comes from NIH GM121491 (to JS), Susan G Komen grant CCR16377648 (to JS), and an Institutional Research Grant 14-196-01 from the American Cancer Society. The authors wish to thank Cindy Fonseca for technical assistance, Guy Kennedy for microscope support, and Dr. Jennifer DeLuca for reagents. We also thank Dr. Laura Reinholdt, Dr. Heidi Malaby, Alex Thompson, Leslie Sepaniac, Cindy Fonseca, Dr. Jamie Stern, and Victoria DeVault for insightful comments and suggestions.

3.6 References

1. Lampson, M.A., Renduchitala, K., Khodjakov, A., and Kapoor, T.M. (2004). Correcting improper chromosome-spindle attachments during cell division. Nature cell biology *6*, 232-237.
2. DeLuca, J.G., Gall, W.E., Ciferri, C., Cimini, D., Musacchio, A., and Salmon, E.D. (2006). Kinetochore microtubule dynamics and attachment stability are regulated by Hec1. Cell *127*, 969-982.
3. Rieder, C.L., Schultz, A., Cole, R., and Sluder, G. (1994). Anaphase onset in vertebrate somatic cells is controlled by a checkpoint that monitors sister kinetochore attachment to the spindle. The Journal of cell biology *127*, 1301-1310.
4. Stumpff, J., von Dassow, G., Wagenbach, M., Asbury, C., and Wordeman, L. (2008). The kinesin-8 motor Kif18A suppresses kinetochore movements to control mitotic chromosome alignment. Developmental cell *14*, 252-262.
5. Cassimeris, L., Rieder, C.L., Rupp, G., and Salmon, E.D. (1990). Stability of microtubule attachment to metaphase kinetochores in PtK1 cells. Journal of cell science *96 (Pt 1)*, 9-15.
6. McEwen, B.F., Heagle, A.B., Cassels, G.O., Buttle, K.F., and Rieder, C.L. (1997). Kinetochore fiber maturation in PtK1 cells and its implications for the mechanisms of chromosome congression and anaphase onset. The Journal of cell biology *137*, 1567-1580.
7. Jaqaman, K., King, E.M., Amaro, A.C., Winter, J.R., Dorn, J.F., Elliott, H.L., McHedlishvili, N., McClelland, S.E., Porter, I.M., Posch, M., et al. (2010). Kinetochore alignment within the metaphase plate is regulated by centromere stiffness and microtubule depolymerases. The Journal of cell biology *188*, 665-679.
8. DeLuca, J.G., Dong, Y., Hergert, P., Strauss, J., Hickey, J.M., Salmon, E.D., and McEwen, B.F. (2005). Hec1 and nuf2 are core components of the kinetochore

outer plate essential for organizing microtubule attachment sites. Molecular biology of the cell *16*, 519-531.

9. Cheeseman, I.M., Chappie, J.S., Wilson-Kubalek, E.M., and Desai, A. (2006). The conserved KMN network constitutes the core microtubule-binding site of the kinetochore. Cell *127*, 983-997.
10. Biggins, S., Severin, F.F., Bhalla, N., Sassoon, I., Hyman, A.A., and Murray, A.W. (1999). The conserved protein kinase Ipl1 regulates microtubule binding to kinetochores in budding yeast. Genes & development *13*, 532-544.
11. Cimini, D., Wan, X., Hirel, C.B., and Salmon, E.D. (2006). Aurora kinase promotes turnover of kinetochore microtubules to reduce chromosome segregation errors. Current biology : CB *16*, 1711-1718.
12. Kelly, A.E., and Funabiki, H. (2009). Correcting aberrant kinetochore microtubule attachments: an Aurora B-centric view. Current opinion in cell biology *21*, 51-58.
13. Sarangapani, K.K., Akiyoshi, B., Duggan, N.M., Biggins, S., and Asbury, C.L. (2013). Phosphoregulation promotes release of kinetochores from dynamic microtubules via multiple mechanisms. Proceedings of the National Academy of Sciences of the United States of America *110*, 7282-7287.
14. DeLuca, K.F., Lens, S.M., and DeLuca, J.G. (2011). Temporal changes in Hec1 phosphorylation control kinetochore-microtubule attachment stability during mitosis. Journal of cell science *124*, 622-634.
15. Zaytsev, A.V., and Grishchuk, E.L. (2015). Basic mechanism for biorientation of mitotic chromosomes is provided by the kinetochore geometry and indiscriminate turnover of kinetochore microtubules. Molecular biology of the cell *26*, 3985-3998.
16. Zaytsev, A.V., Sundin, L.J., DeLuca, K.F., Grishchuk, E.L., and DeLuca, J.G. (2014). Accurate phosphoregulation of kinetochore-microtubule affinity requires unconstrained molecular interactions. The Journal of cell biology *206*, 45-59.
17. Liu, D., Vleugel, M., Backer, C.B., Hori, T., Fukagawa, T., Cheeseman, I.M., and Lampson, M.A. (2010). Regulated targeting of protein phosphatase 1 to the outer

kinetochore by KNL1 opposes Aurora B kinase. The Journal of cell biology *188*, 809-820.

18. Foley, E.A., Maldonado, M., and Kapoor, T.M. (2011). Formation of stable attachments between kinetochores and microtubules depends on the B56-PP2A phosphatase. Nature cell biology *13*, 1265-1271.
19. Sivakumar, S., Janczyk, P.L., Qu, Q., Brautigam, C.A., Stukenberg, P.T., Yu, H., and Gorbsky, G.J. (2016). The human SKA complex drives the metaphase-anaphase cell cycle transition by recruiting protein phosphatase 1 to kinetochores. eLife *5*.
20. Umbreit, N.T., Gestaut, D.R., Tien, J.F., Vollmar, B.S., Gonen, T., Asbury, C.L., and Davis, T.N. (2012). The Ndc80 kinetochore complex directly modulates microtubule dynamics. Proceedings of the National Academy of Sciences of the United States of America *109*, 16113-16118.
21. Trinkle-Mulcahy, L., Andersen, J., Lam, Y.W., Moorhead, G., Mann, M., and Lamond, A.I. (2006). Repo-Man recruits PP1 gamma to chromatin and is essential for cell viability. The Journal of cell biology *172*, 679-692.
22. De Wever, V., Nasa, I., Chamousset, D., Lloyd, D., Nimick, M., Xu, H., Trinkle-Mulcahy, L., and Moorhead, G.B. (2014). The human mitotic kinesin KIF18A binds protein phosphatase 1 (PP1) through a highly conserved docking motif. Biochemical and biophysical research communications.
23. Hafner, J., Mayr, M.I., Mockel, M.M., and Mayer, T.U. (2014). Pre-anaphase chromosome oscillations are regulated by the antagonistic activities of Cdk1 and PP1 on Kif18A. Nature communications *5*, 4397.
24. Meadows, J.C., Shepperd, L.A., Vanoosthuyse, V., Lancaster, T.C., Sochaj, A.M., Buttrick, G.J., Hardwick, K.G., and Millar, J.B. (2011). Spindle checkpoint silencing requires association of PP1 to both Spc7 and kinesin-8 motors. Developmental cell *20*, 739-750.
25. Zhu, C., Zhao, J., Bibikova, M., Leverson, J.D., Bossy-Wetzel, E., Fan, J.B., Abraham, R.T., and Jiang, W. (2005). Functional analysis of human microtubule-

based motor proteins, the kinesins and dyneins, in mitosis/cytokinesis using RNA interference. Molecular biology of the cell *16*, 3187-3199.

26. Mayr, M.I., Hummer, S., Bormann, J., Gruner, T., Adio, S., Woehlke, G., and Mayer, T.U. (2007). The human kinesin Kif18A is a motile microtubule depolymerase essential for chromosome congression. Current biology : CB *17*, 488-498.
27. Czechanski, A., Kim, H., Byers, C., Greenstein, I., Stumpff, J., and Reinholdt, L.G. (2015). Kif18a is specifically required for mitotic progression during germ line development. Developmental biology.
28. Czechanski, A., Kim, H., Byers, C., Greenstein, I., Stumpff, J., and Reinholdt, L.G. (2015). Kif18a is specifically required for mitotic progression during germ line development. Developmental biology *402*, 253-262.
29. Stumpff, J., Wagenbach, M., Franck, A., Asbury, C.L., and Wordeman, L. (2012). Kif18A and chromokinesins confine centromere movements via microtubule growth suppression and spatial control of kinetochore tension. Developmental cell *22*, 1017-1029.
30. Kim, H., Fonseca, C., and Stumpff, J. (2014). A unique kinesin-8 surface loop provides specificity for chromosome alignment. Molecular biology of the cell *25*, 3319-3329.
31. Weaver, L.N., Ems-McClung, S.C., Stout, J.R., LeBlanc, C., Shaw, S.L., Gardner, M.K., and Walczak, C.E. (2011). Kif18A uses a microtubule binding site in the tail for plus-end localization and spindle length regulation. Current biology : CB *21*, 1500-1506.
32. Magidson, V., He, J., Ault, J.G., O'Connell, C.B., Yang, N., Tikhonenko, I., McEwen, B.F., Sui, H., and Khodjakov, A. (2016). Unattached kinetochores rather than intrakinetochore tension arrest mitosis in taxol-treated cells. The Journal of cell biology *212*, 307-319.
33. Kim, H., Fonseca, C., and Stumpff, J. (2014). A unique kinesin-8 surface loop provides specificity for chromosome alignment. Molecular biology of the cell.

34. Stumpff, J., Du, Y., English, C.A., Maliga, Z., Wagenbach, M., Asbury, C.L., Wordeman, L., and Ohi, R. (2011). A tethering mechanism controls the processivity and kinetochore-microtubule plus-end enrichment of the kinesin-8 Kif18A. Molecular cell *43*, 764-775.

35. Chmatal, L., Yang, K., Schultz, R.M., and Lampson, M.A. (2015). Spatial Regulation of Kinetochore Microtubule Attachments by Destabilization at Spindle Poles in Meiosis I. Current biology : CB *25*, 1835-1841.

36. Ye, A.A., Deretic, J., Hoel, C.M., Hinman, A.W., Cimini, D., Welburn, J.P., and Maresca, T.J. (2015). Aurora A Kinase Contributes to a Pole-Based Error Correction Pathway. Current biology : CB *25*, 1842-1851.

37. Liu, D., Vader, G., Vromans, M.J., Lampson, M.A., and Lens, S.M. (2009). Sensing chromosome bi-orientation by spatial separation of aurora B kinase from kinetochore substrates. Science *323*, 1350-1353.

38. Mayr, M.I., Storch, M., Howard, J., and Mayer, T.U. (2011). A non-motor microtubule binding site is essential for the high processivity and mitotic function of kinesin-8 Kif18A. PloS one *6*, e27471.

39. Long, A.F., Udy, D.B., and Dumont, S. (2017). Hec1 Tail Phosphorylation Differentially Regulates Mammalian Kinetochore Coupling to Polymerizing and Depolymerizing Microtubules. Current biology : CB *27*, 1692-1699 e1693.

40. Lampson, M.A., and Kapoor, T.M. (2005). The human mitotic checkpoint protein BubR1 regulates chromosome-spindle attachments. Nature cell biology *7*, 93-98.

41. Wei, R., Ngo, B., Wu, G., and Lee, W.H. (2011). Phosphorylation of the Ndc80 complex protein, HEC1, by Nek2 kinase modulates chromosome alignment and signaling of the spindle assembly checkpoint. Molecular biology of the cell *22*, 3584-3594.

42. West, R.R., Malmstrom, T., and McIntosh, J.R. (2002). Kinesins klp5(+) and klp6(+) are required for normal chromosome movement in mitosis. Journal of cell science *115*, 931-940.

43. Garcia, M.A., Koonrugsa, N., and Toda, T. (2002). Two kinesin-like Kin I family proteins in fission yeast regulate the establishment of metaphase and the onset of anaphase A. Current biology : CB *12*, 610-621.

44. Sanchez-Perez, I., Renwick, S.J., Crawley, K., Karig, I., Buck, V., Meadows, J.C., Franco-Sanchez, A., Fleig, U., Toda, T., and Millar, J.B. (2005). The DASH complex and Klp5/Klp6 kinesin coordinate bipolar chromosome attachment in fission yeast. The EMBO journal *24*, 2931-2943.

45. Gardner, M.K., Bouck, D.C., Paliulis, L.V., Meehl, J.B., O'Toole, E.T., Haase, J., Soubry, A., Joglekar, A.P., Winey, M., Salmon, E.D., et al. (2008). Chromosome congression by Kinesin-5 motor-mediated disassembly of longer kinetochore microtubules. Cell *135*, 894-906.

3.7 Figures

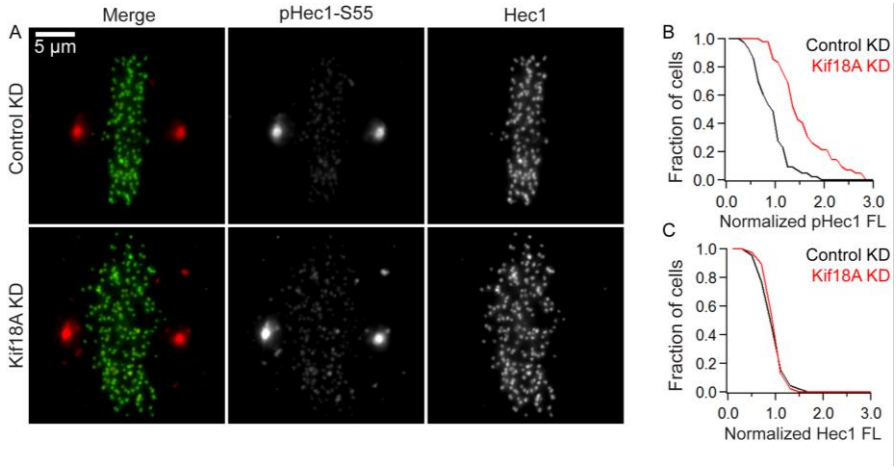

Figure 3-1. Kif18A-depleted HeLa cells show a significant increase in phospho-Hec1 levels at kinetochores.

A. Immunofluorescence microscopy images of cells labeled with total Hec1 (green) and phospho-Hec1 Ser55 (pHec1-S55, red) antibodies. Cells were treated with control (Control KD) or Kif18A siRNAs (Kif18A KD), then arrested in late metaphase with MG132 for 3 hours and fixed. B-C. Quantification of phospho-Ser55 (B) and total Hec1 fluorescence (C) at kinetochores in Control KD and Kif18A KD cells normalized to average Control KD levels. Data are from 3 independent experiments: n = 43 cells, 2100 kinetochores for Control KD, n = 42 cells, 2000 kinetochores for Kif18A KD, A student's t-test was used to compare normalized fluorescence intensities ($p < 0.0001$, phospho-Ser55 fluorescence and $p > 0.05$, total Hec1 fluorescence).

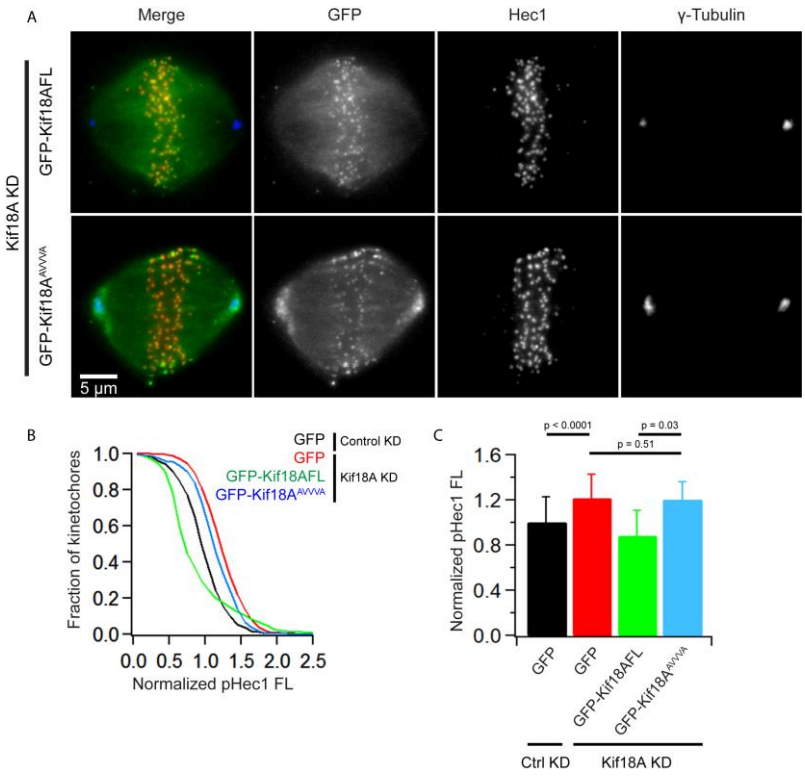

Figure 3-2 PP1 binding is required for Kif18A-dependent changes in Hec1 phosphorylation.

A. Representative images of Kif18A KD cells expressing GFP-Kif18AFL and GFP-Kif18A^{AVVVA}. **B-C.** Cells were treated with control (Control KD) or Kif18A siRNA (Kif18A KD) and transfected with the indicated GFP or GFP-Kif18A constructs. Cells were arrested in MG132 for 3 hours, then incubated with Hec1 phospho-Ser55 and total Hec1 antibodies and imaged. **B**. Plot of phospho-Ser55 Hec1 (pHec1) fluorescence intensity at kinetochores normalized to control phospho-Ser55 levels. **C**. Plot of mean normalized phospho-Ser55 Hec1 fluorescence for the indicated conditions. Error bars represent std dev. Means were compared using a student's t-test. Data are from 3 independent experiments: n = 26 cells, 858 kinetochores (KTs), (Control KD, GFP only), n = 21 cells, 1188 KTs (Kif18A KD, GFP only), n = 13 cells, 705 KTs (Kif18A KD, GFP-Kif18AFL), n = 12 cells, 597 KTs (Kif18A KD, GFP-Kif18A^{AVVVA}).

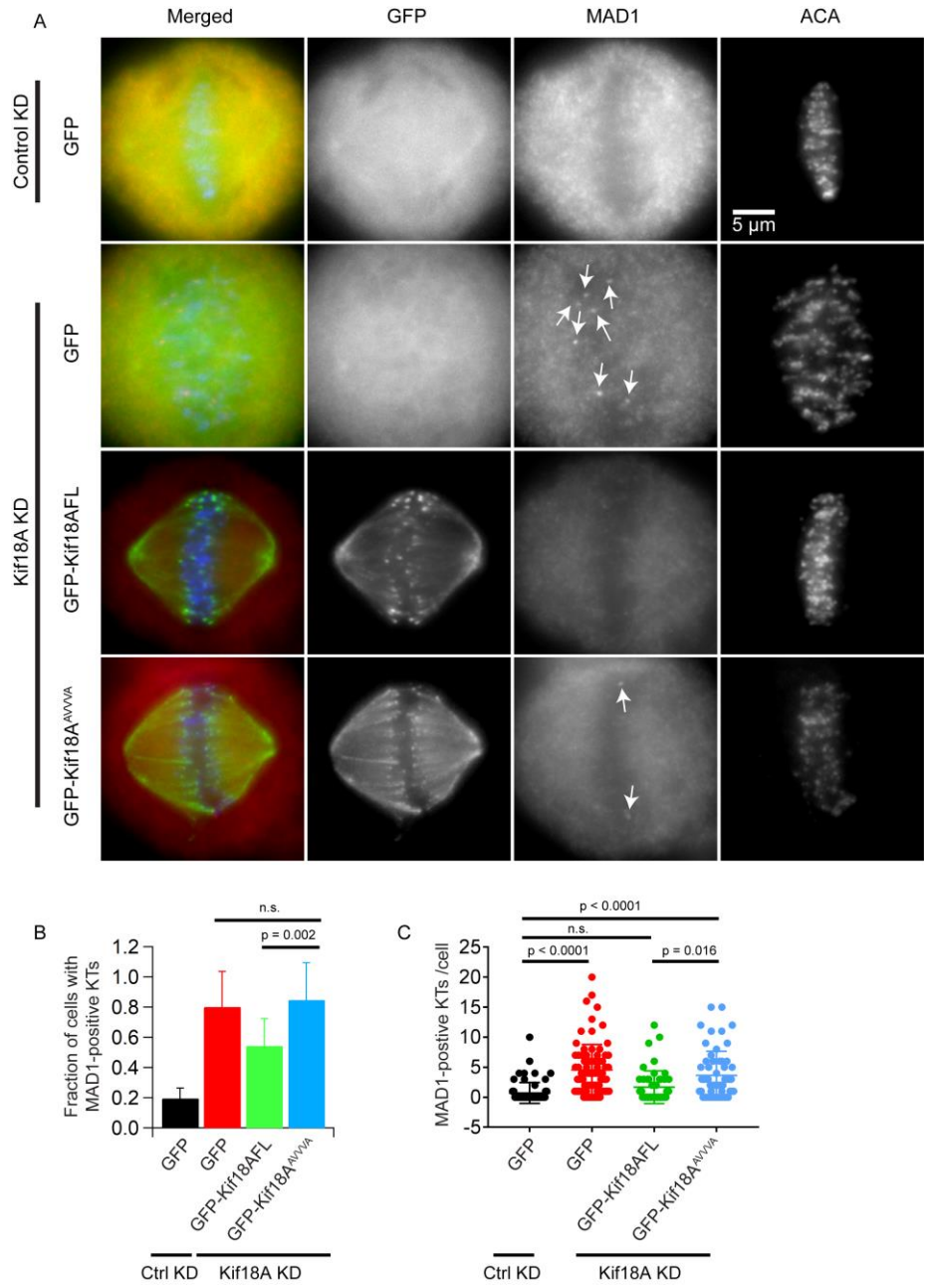

Figure 3-3. Metaphase cells expressing Kif18A^{AVVVA} display an increase in kinetochore-localized MAD1 on aligned kinetochores.

A. Representative immunofluorescence images of Control KD or Kif18A KD HeLa cells expressing the indicated GFP constructs and immunofluorescently labeled for MAD1 and kinetochores (ACA). Arrows indicate MAD1-positive kinetochore. **B.** Bar graph displaying the fraction of cells with at least 1 MAD1-positive kinetochore (KT) for the indicated conditions. Data were compared using a chi-squared analysis. **C.** Scatter plot

showing the number of MAD1-positive kinetochores per GFP-positive cell. Data were compared via a one-way ANOVA and Tukey's multiple comparisons test. Data are from 3 independent experiments: n = 68 cells (Control KD, GFP only), n = 80 cells (Kif18A KD, GFP only), n = 50 cells (Kif18A KD, GFP-Kif18AFL), n = 58 cells (Kif18A KD, GFP-Kif18A^{AVVVA}).

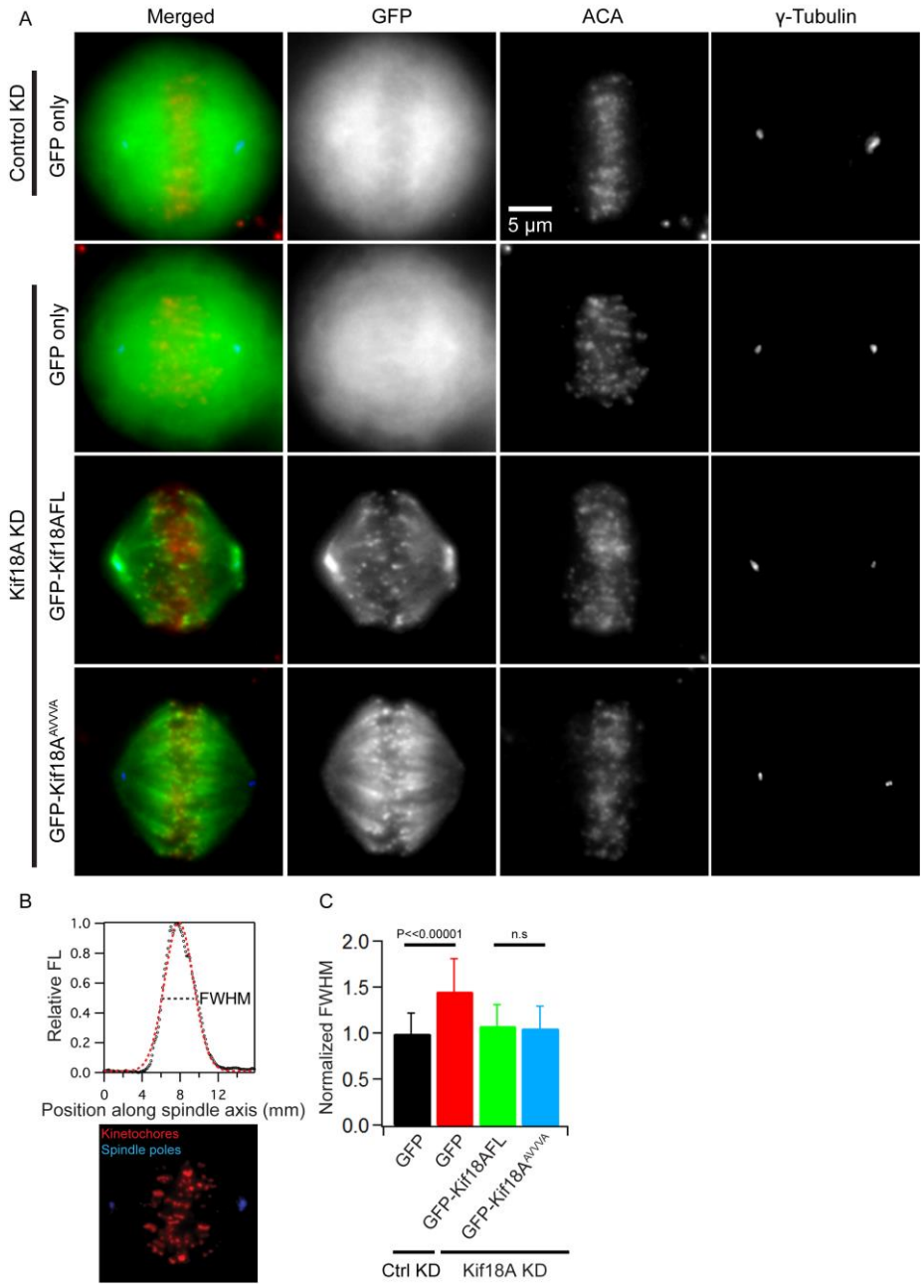

Figure 3-4. Kif18A is capable of aligning chromosomes independently of PP1 binding.

A. Representative images of cells expressing GFP, GFP-Kif18AFL, or GFP-Kif18A^{AVVVA} variants immunoflourescently labeled for kinetochores (ACA) and centrosomes (γ-tubulin). Cells were treated with control (Control KD) or Kif18A siRNAs (Kif18A KD) and transfected with the indicated GFP constructs. **B.** Schematic of the method used to quantify kinetochore fluorescence distribution along the pole-to-pole axis

of the spindle. Kinetochore fluorescence was fit to a Gaussian, and full width at half maximum (FWHM) was determined as a measure of chromosome alignment (dashed line in plot). **C.** A bar graph displaying normalized FWHM means for kinetochore fluorescence distributions from the indicated cell populations. Data were compared using a student's t-test.

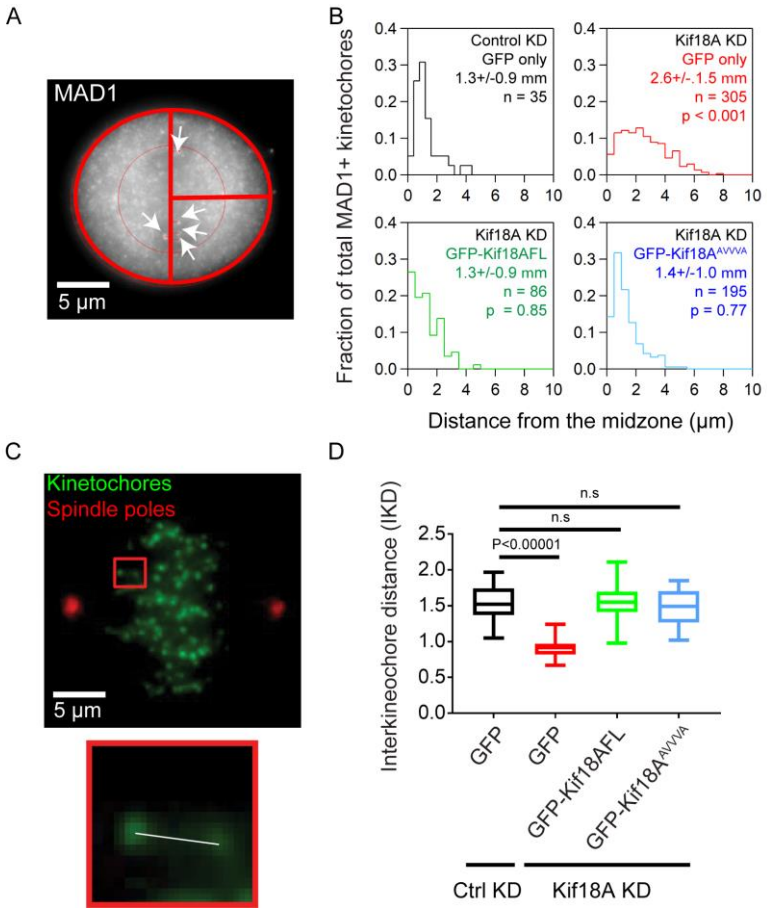

Figure 3-5. Kif18A does not promote attachments by regulating chromosome positioning or kinetochore tension.

A. Representative image depicting the positions of MAD1-positive kinetochores (arrows) relative to the spindle midzone (vertical red line). **B.** Histograms displaying distances of MAD1 positive (MAD1+) kinetochores from the midzone for each condition listed. Mean +/- s.d. is indicated for each condition, n = number of kinetochores from >14 cells and 3 independent experiments. Data were compared using a one-way ANOVA with Dunnett's multiple comparison test. Reported p-values represent comparison to Control KD + GFP condition. **C.** Mitotic cell immunofluorescently labeled for kinetochores (ACA) and spindle poles (γ-tubulin). Interkinetochore distance (IKD) was determined by measuring the distance between the centroids of sister kinetochores in the same focal plane (white line in inset). **D.** Box and whisker plot displaying the average IKD for the indicated experimental conditions. Data are from 3 independent experiments: n = 28 cells, 368 kTs

(Control KD, GFP only), n = 55 cells, 531 kTs Kif18A KD, GFP only), n = 20 cells, 156 kTs (Kif18A KD, GFP-Kif18AFL), n = 21 cells, 176 kTs (Kif18A KD, GFP-Kif18A^{AVVVA}). Data were compared using a student's t-test.

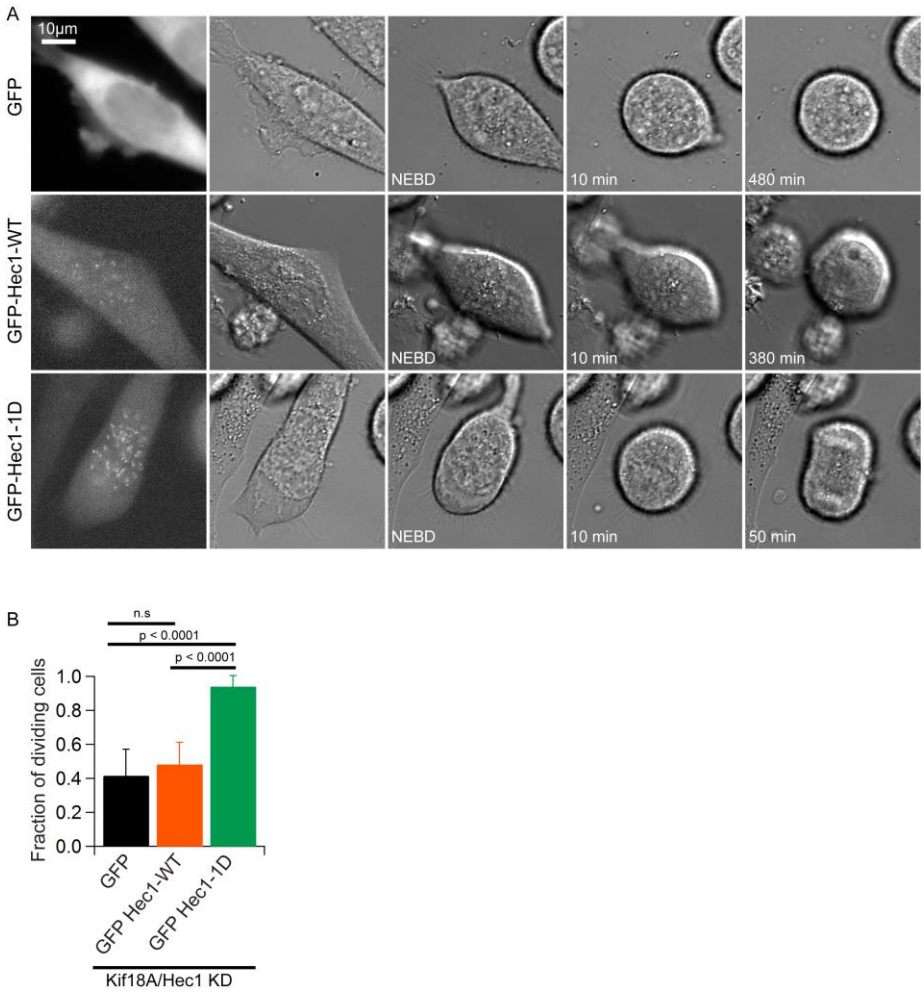

Figure 3-6. A Hec1 mutant that mimics low phosphorylation rescues the mitotic arrest caused by loss of Kif18A function.

A. Still frames from time-lapse DIC imaging used to measure division in HeLa cells co-depleted of Hec1 and Kif18A and expressing GFP, GFP-Hec1-WT, or a GFP-tagged Hec1 mutant that mimics phosphorylation at a single site (GFP Hec1-1D). Mitotic division was defined as progress from nuclear envelope breakdown (NEBD) to anaphase onset. **B.** Bar graph representing the fraction of cells that divide in each condition. Data are from 3 independent experiments: n = 153 (GFP only), n = 79 (GFP Hec1-WT), and n = 70 (GFP Hec1-1D). Data were compared using chi-squared analyses.

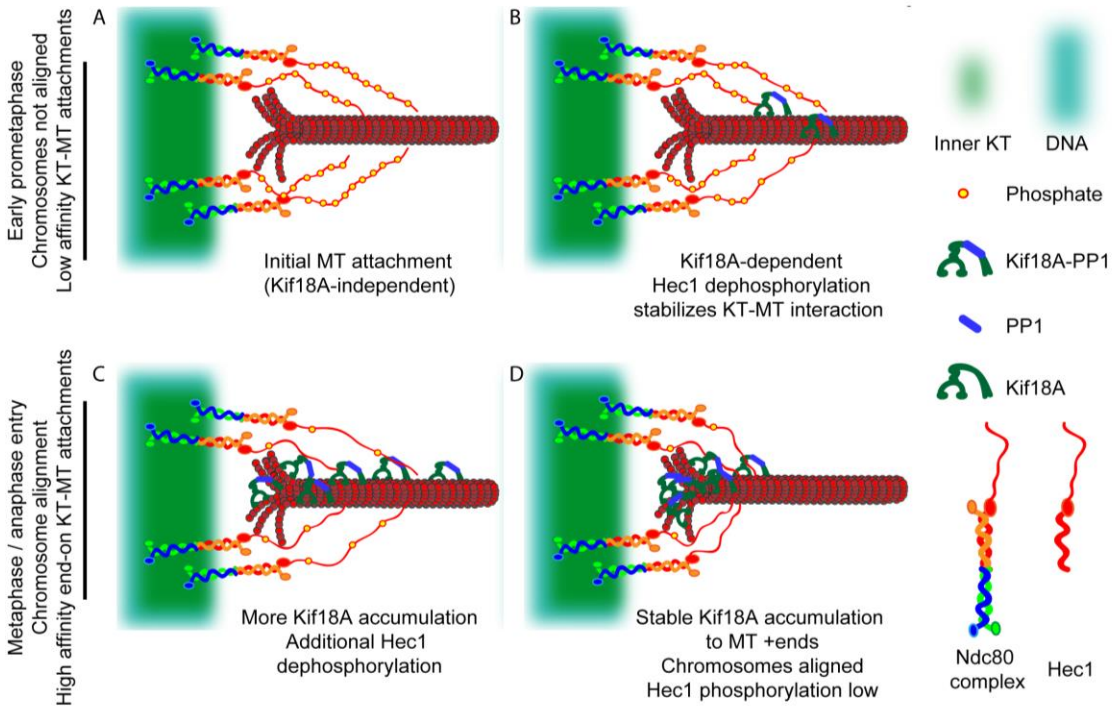

Figure 3-7. Model for Kif18A-dependent temporal coordination of chromosome alignment with stabilization of kinetochore microtubule attachments.

A. During early prometaphase, microtubules (MTs) come in contact with the N-terminal tail of Hec1 in a Kif18A-independent manner. Phosphorylation of the Hec1 N-terminus is relatively high (yellow circles). **B.** Initial kinetochore microtubule (KT-MT) attachments (Kif18A-independent) provide stable tracks for Kif18A and Kif18A associated PP1 (Kif18A-PP1) to translocate to microtubule plus-ends. Kif18A-PP1 dependent Hec1 dephosphorylation reinforces KT-MT attachments. **C.** Kif18A-PP1 accumulation at KT-MT plus-ends dampens MT dynamics and confines chromosome movements to the spindle equator. In parallel, additional Kif18A-PP1 continues to dephosphorylate Hec1, providing positive feedback for KT-MT attachments. **D.** As K fibers mature, more Kif18A motors accumulate at K fiber plus-ends, promoting complete chromosome alignment and further enhancing stabilization of end-on attachments to silence the SAC and promote anaphase entry.

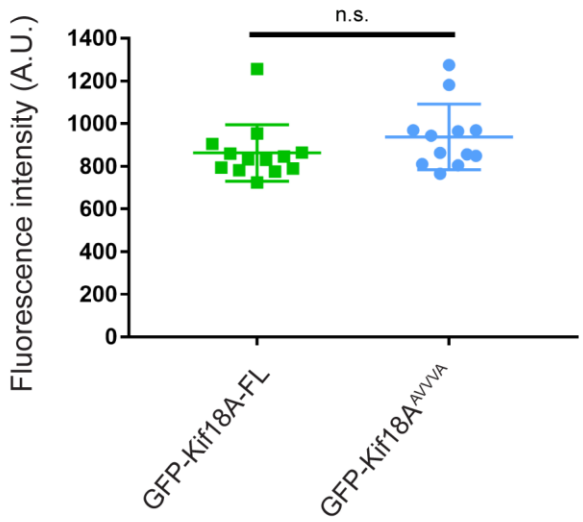

Figure 3-S1, related to Figure 2. Cells analyzed expressed comparable levels of GFP-Kif18A constructs.

Plot of average GFP fluorescence intensity measured in cells expressing GFP-Kif18AFL and GFP-Kif18A^{AVVVA}. Data were compared using a student's t-test ($p = 0.14$). $n = 13$ cells (GFP-Kif18AFL), $n = 12$ cells (GFP-Kif18A^{AVVVA}).

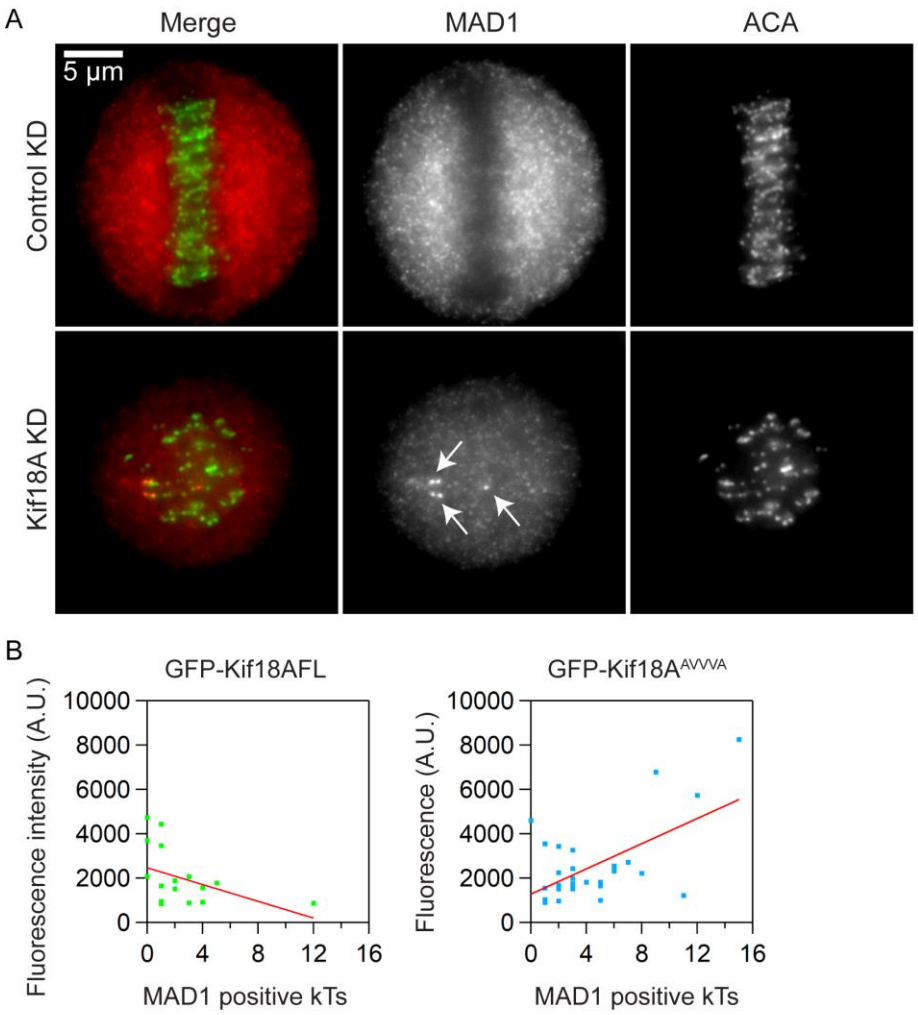

Figure 3-S2, related to Figure 3. Metaphase Kif18A KD display MAD-1 positive kinetochores.

A. Representative images of metaphase-arrested cells immunofluorescently labeled for kinetochores (ACA) and MAD1 following treatment with the indicated siRNAs. Kif18A KD cells exhibit MAD1-positive kinetochores (arrows). **B.** Plots of GFP-fluorescence intensity as a function of MAD1-positive kinetochore number measured in Kif18A KD cells expressing GFP-Kif18AFL and GFP-Kif18A^{AVVVA}. n = 17 cells (GFP-Kif18AFL) and 29 cells (GFP-Kif18A^{AVVVA}).

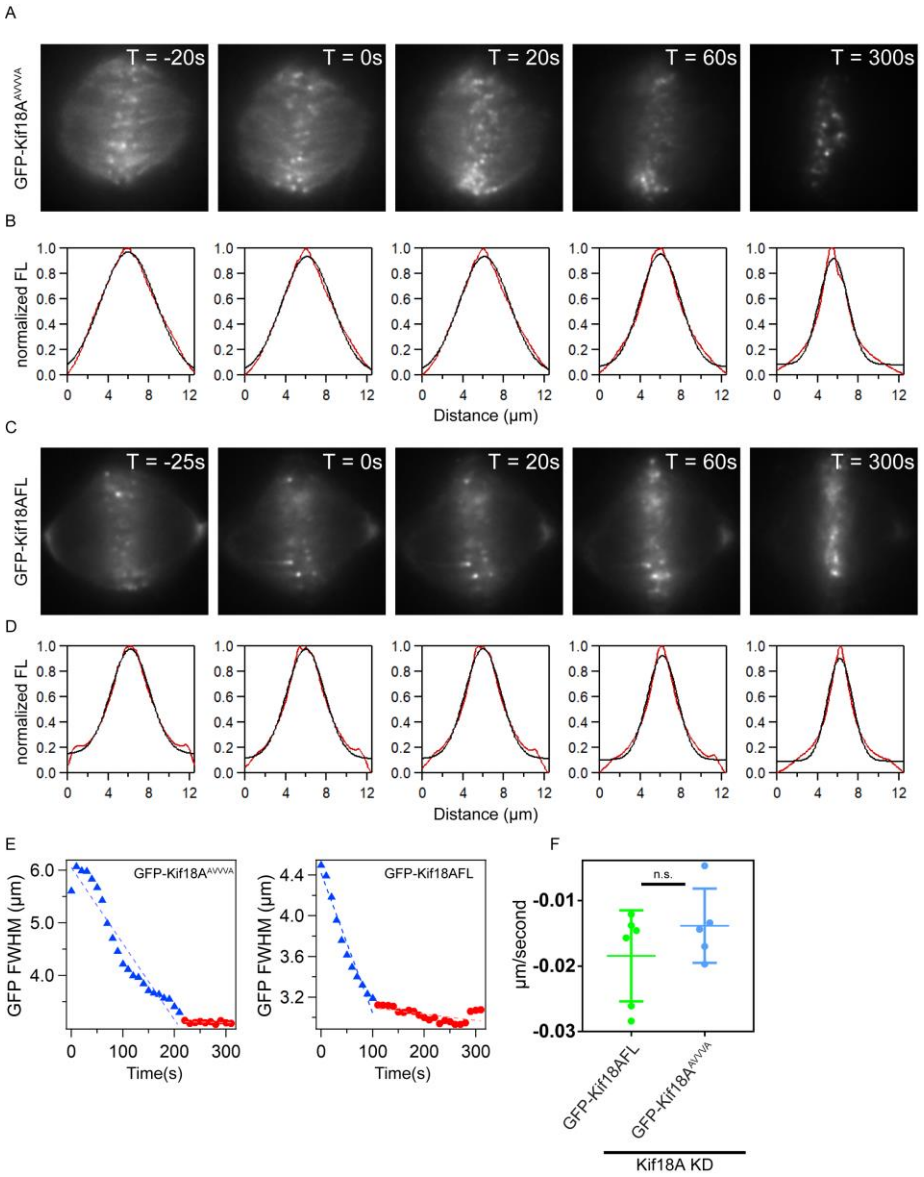

Figure 3-S3, related to Figure 4. GFP-Kif18A^{AVVVA} and GFP-Kif18AFL accumulate at K fiber ends at similar rates.

A and C. Selected still frames from time-lapse fluorescence imaging of Kif18A KD cells expressing GFP-Kif18A^{AVVVA} (A) or GFP-Kif18AFL (C) before and after taxol addition. **B and D.** Plots of normalized GFP fluorescence (red lines) fitted to a Gaussian (black lines) for each frame shown in A and C. The FWHM of each Gaussian fit was determined as a measure of GFP-Kif18A distribution. **E.** Representative graphs of FWHM as a function of time from cells expressing GFP-Kif18A^{AVVVA} (left) and GFP-Kif18AFL (right). Blue triangles indicate time points during which FWHM is decreasing due to

motor accumulation at kinetochore plus-ends. Red squares indicate time points after motor accumulation has plateaued and FWHM changes are minimal. **F.** Scatter plot displaying rates of GFP-Kif18A^{AVVVA} and GFP-Kif18AFL accumulation following taxol addition, based on the rate of FWHM decrease. n = 5 cells, -0.014 +/-0.0056 µm/s (Kif18A KD, GFP-Kif18A^{AVVVA}), and n = 6 cells, -0.018 +/- 0.0069 µm/s (Kif18A KD, GFP-Kif18AFL). Data were compared using a student's t-test.

CHAPTER 4: A UNIQUE KINESIN-8 SURFACE LOOP PROVIDES SPECIFICITY FOR CHROMOSOME ALIGNMENT

Haein Kim[§], Cindy Fonseca[§] and Jason Stumpff[§*]

[§] Department of Molecular Physiology and Biophysics, University of Vermont, Burlington, Vermont.

[*]Correspondence to:

Jason Stumpff

Department of Molecular Physiology and Biophysics

University of Vermont

89 Beaumont Avenue

Burlington, VT 05405

802-656-7849 (phone)

802-656-0747 (fax)

jstumpff@uvm.edu

Running Title: Kif18A loop2 controls congression

4.1. Abstract

Microtubule length control is essential for the assembly and function of the mitotic spindle. Kinesin-like motor proteins that directly attenuate microtubule dynamics make key contributions to this control, but the specificity of these motors for different subpopulations of spindle microtubules is not understood. Kif18A (kinesin-8) localizes to the plus-ends of the relatively slow growing kinetochore fibers (K-fibers) and attenuates their dynamics, while Kif4A (kinesin-4) localizes to mitotic chromatin and suppresses the growth of highly dynamic, non-kinetochore microtubules. While Kif18A and Kif4A similarly suppress microtubule growth *in vitro*, it remains unclear whether microtubule-attenuating motors control the lengths of K-fibers and non-kinetochore microtubules through a common mechanism. To address this question, we engineered chimeric kinesins that contain the Kif4A, Kif18B (kinesin-8) or Kif5B (kinesin-1) motor domain fused to the C-terminal tail of Kif18A. Each of these chimeric kinesins localizes to K-fibers, however, K-fiber length control requires an activity specific to kinesin-8s. Mutational studies of Kif18A indicate that this control depends on both its C-terminus and a unique, positively charged surface loop, called loop2, within the motor domain. These data support a model in which microtubule-attenuating kinesins are molecularly "tuned" to control the dynamics of specific subsets of spindle microtubules.

4.2. Introduction

During cell division, microtubule length control is critical for mitotic spindle positioning, spatial control of chromosome movements and cytokinesis. However, it

remains unclear how cells regulate the lengths of the different subpopulations of spindle microtubules necessary for these functions. For example, astral and non-kinetochore microtubules, which interact with the cell cortex and apply pushing forces to chromosome arms, display short half lives as well as fast polymerization and depolymerization rates (Zhai *et al.*, 1995; Tirnauer *et al.*, 2002; Stumpff *et al.*, 2012). In contrast, the microtubules that bind to kinetochores, specialized protein structures that assemble at the centromeric regions of mitotic chromosomes, display relatively long half-lives with slower polymerization and depolymerization rates (Rieder and Salmon, 1994; Zhai *et al.*, 1995). These kinetochore fibers (K-fibers) consist of 10-45 microtubules, and changes in their length facilitate the movement and alignment of chromosomes within the spindle (Rieder and Salmon, 1998). Whether cells use specialized or generalized mechanisms to control the lengths of dynamically diverse spindle microtubules is not understood.

Molecular motors of the kinesin-4 (Kif4A), kinesin-8 (Kif18A and Kif18B) and kinesin-13 (Kif2A, Kif2B and MCAK) families play key roles in regulating spindle microtubule length to facilitate cell division in vertebrates (Kline-Smith and Walczak, 2002; Castoldi and Vernos, 2006; Manning *et al.*, 2007; Mayr *et al.*, 2007; Stumpff *et al.*, 2008; Stout *et al.*, 2011). The kinesin-13 motors function by inducing microtubule depolymerization, whereas Kif4A and Kif18A directly attenuate microtubule dynamic instability (Desai *et al.*, 1999; Bringmann *et al.*, 2004; Bieling *et al.*, 2010; Du *et al.*, 2010; Stumpff *et al.*, 2011; Stumpff *et al.*, 2012). While individual kinesin-13 motors localize to and regulate both K-fibers and non-kinetochore microtubules, Kif4A,

Kif18A and Kif18B display specificity for particular microtubule subsets (Kline-Smith and Walczak, 2002; Moore *et al.*, 2005; Lee *et al.*, 2010; Stout *et al.*, 2011; Tanenbaum *et al.*, 2011; Stumpff *et al.*, 2012; Wandke *et al.*, 2012). Prior to anaphase, Kif4A localizes to mitotic chromatin where it suppresses the lengths and growth rates of non-kinetochore microtubules (Lee *et al.*, 2001; Stumpff *et al.*, 2012; Wandke *et al.*, 2012). In contrast, Kif18A localizes to and attenuates the dynamics of K-fibers, while Kif18B primarily localizes to and regulates the lengths of astral microtubules (Mayr *et al.*, 2007; Stumpff *et al.*, 2008; Lee *et al.*, 2010; Stout *et al.*, 2011; Tanenbaum *et al.*, 2011).

While the biochemical activity of Kif18B has not been determined, Kif18A and Kif4A similarly attenuate microtubule dynamics but display different motile behaviors. Kif18A and Kif4A are plus-end directed motors that accumulate at microtubule ends, where they suppress both polymerization and depolymerization (Bringmann *et al.*, 2004; Bieling *et al.*, 2010; Stumpff *et al.*, 2012; Subramanian *et al.*, 2013). Kif4A translocates along microtubules at a relatively fast velocity where it forms a steady state concentration at microtubule ends, indicating that individual Kif4A molecules readily dissociate from the microtubule tip (Bringmann *et al.*, 2004; Bieling *et al.*, 2010; Subramanian *et al.*, 2013). In contrast, Kif18A is a slow, highly processive motor that stably associates with microtubule ends both in reconstituted systems and in mitotic cells (Du *et al.*, 2010; Mayr *et al.*, 2011; Stumpff *et al.*, 2011). Stable microtubule end association is significantly reduced for Kif18A mutants lacking the C-terminal tail. The tail contains microtubule-binding domains that function to enhance the association of

the protein with microtubules (Mayr *et al.*, 2011; Stumpff *et al.*, 2011; Su *et al.*, 2011; Weaver *et al.*, 2011). However, Kif18A truncation mutants still display some capacity to stably associate with microtubule ends, suggesting that regions within the Kif18A motor domain also contribute to microtubule tip binding (Stumpff *et al.*, 2011). These differences in motor activity raise the question of whether Kif18A and Kif4A control microtubule lengths through a common mechanism or contain unique molecular attributes that facilitate their regulation of particular microtubule subsets.

To address this question, we tested the ability of the Kif4A, Kif18B, and Kif5B (kinesin-1) motor domains to functionally substitute for Kif18A during mitotic chromosome alignment. The kinesin-8 motor Kif18B, but not Kif4A or Kif5B, was capable of controlling K-fiber lengths to facilitate chromosome alignment, indicating that Kif4A and human kinesin-8 motors control microtubule lengths through distinct mechanisms. Furthermore, a positively charged surface loop within the motor domains of kinesin-8s, called loop2, is required for stable association with K-fiber ends, chromosome alignment and spindle length control. These data support a model in which unique molecular structures within the motor domains of microtubule attenuating kinesins facilitate their specific control of K-fiber versus non-kinetochore microtubule dynamics.

4.3. Results

4.3.1. The Kif18A tail is not sufficient to facilitate accumulation of plus-end directed motors at K-fiber ends

The Kif18A C-terminal tail is necessary for the motor's accumulation at K-fiber plus-ends (Stumpff *et al.,* 2011). To determine if the Kif18A tail is sufficient to facilitate the concentration of other plus-end directed kinesins at K-fiber ends, we engineered chimeric kinesins consisting of the motor and neck-linker domains of Kif18B (kinesin-8), Kif4A (kinesin-4) and Kif5B (kinesin-1) fused to the Kif18A C-terminus (Figure 1A). Chimeric kinesins were expressed as EGFP-fusion proteins in HeLa cells depleted of endogenous Kif18A and cells with similar GFP fluorescence levels were evaluated (Figure S1). Kif18A siRNA treated cells expressed 9.8 +/- 1.3% of the Kif18A detected by Western blot in control treated cells (Figure 1A). While all of the chimeras localized to K-fibers, only wild type Kif18A and the Kif18B-18A chimera efficiently concentrated at K-fiber ends (Figure 1 C-D). Interestingly, the Kif4A-18A chimera displayed accumulation at the ends of K-fibers on the spindle periphery but not at the ends of those on the spindle interior. In contrast, the Kif5B-18A chimera was uniformly distributed on the spindle (Figure 1 C-D). These data indicate that the Kif18A-tail can target plus-end directed kinesins to K-fibers, however, an element common to the kinesin-8 motors Kif18A and Kif18B is additionally required for efficient accumulation at K-fiber ends.

4.3.2. A kinesin-8 motor domain specific activity facilitates stable binding of motors at K-fiber ends

Given the ability of purified Kif4A to form a steady state accumulation at the ends of stable microtubules, the accumulation of Kif4A-18A specifically at the ends of peripheral K-fibers could be explained if peripheral and interior K-fibers display

differences in their dynamic instability (Subramanian *et al.*, 2013). Consistent with this, previous studies have demonstrated a significant reduction in the oscillatory movements of kinetochores, which are closely coupled to K-fiber dynamic instability, on the periphery compared to those in the interior of the spindle (Canman *et al.*, 2002; Cimini *et al.*, 2004; Stumpff *et al.*, 2008). Thus, we hypothesized that peripheral K-fibers provide a stable track that allows a steady state accumulation of Kif4A-18A. To test this idea, we briefly treated Kif18A-depleted HeLa cells expressing GFP-tagged chimeric kinesins with the microtubule-stabilizing drug taxol (10 μM) and then analyzed kinesin localization. Similar to the previously observed behavior of Kif18A-FL in taxol-treated cells, the concentration of each of the chimeric kinesins at the ends of K-fibers was increased following taxol addition (Figure 2 A-B) (Stumpff *et al.*, 2011). GFP-chimera signal accumulated to K-fiber ends within 60-90 seconds of taxol addition (Figure 2C). Importantly, this rapid accumulation is consistent with efficient plus-end directed movement of active motors to microtubule ends.

While the localization of these chimeras was similar in taxol-treated cells, it was not clear if their behavior at K-fiber ends was comparable. To address this question, a fluorescence recovery after photobleaching (FRAP) assay was used to examine the kinetics of chimeric kinesins at K-fiber ends in taxol-treated cells. For these experiments, a small region of interest containing GFP-kinesin was photobleached near an mRFP-CENP-B labeled centromere and fluorescence recovery was visualized at 2-second intervals (Figure 3A). Wild type Kif18A and the Kif18B-18A chimera displayed only a small mobile fraction at K-fiber ends under these conditions,

consistent with previous studies of Kif18A turnover (Stumpff 2011) (Figure 3B and Table 1). In contrast, the Kif4A-18A and Kif5B-18A chimeras displayed significantly higher mobile fractions at K-fiber ends (Figure 3B and Table 1). A Kif18A truncation mutant (Kif18A-770), which lacks the microtubule-binding regions at the C-terminal end of the tail, accumulates at K-fibers ends specifically in taxol-treated cells (Figure S2). Kif18A-770 displays an increase in the mobile fraction at K-fiber ends but does not fully recover (Figure 3B, Figure S2 and Table 1). These data indicate that Kif18A's stable association at K-fiber ends requires both the C-terminal tail and a kinesin-8 motor specific element that is shared between Kif18A and Kif18B. Furthermore, the behavior of Kif4A-18A and Kif5B-18A at the ends of taxol-stabilized K-fibers is consistent with these motors forming a steady state accumulation, similar to that observed for purified Kif4A (Subramanian *et al.*, 2013).

The rates of fluorescence recovery in FRAP experiments, measured as the halftime to max recovery ($t_{1/2}$) or the percent of recovery after 30 seconds, also differed among the kinesins tested. The three kinesin-8 motor containing constructs displayed relatively slow rates of recovery compared to the Kif4A-18A and Kif5B-18A chimeras (Figure 3B and Table 1). The rates of recovery correlate with the previously reported plus-end directed velocities measured for single molecules of full-length kinesin-8 (75-199 nm/s for Kif18A), tailless Kif18A (210-299 nm/s), kinesin-4 (800 nm/s for Xklp1) and Kif5B (780 nm/s for Kif5B-560), consistent with fluorescence recovery being facilitated by directional movement of motors into the bleached region (Lakamper *et al.*, 2003; Bieling *et al.*, 2010; Mayr *et al.*, 2011; Stumpff *et al.*, 2011).

4.3.3. Kif18A loop2 is required for its accumulation and stable binding at K-fiber ends

To understand the molecular basis of the differences in K-fiber end association displayed by kinesin-8 motors compared to Kif4A and Kif5B, we compared the sequences of these proteins to look for candidate structures in the kinesin-8s that might explain their ability to stably bind microtubule ends. This analysis revealed that Kif18A and Kif18B contain an extended loop2 region compared to Kif4A and Kif5B (Figure 4A). Kif18A loop2 contains six lysine residues, four of which are conserved in Kif18B (Figure 4A). Structural studies indicate that this positively charged extension in Kif18A directly contacts the negatively charged surface of α-tubulin (Peters *et al.*, 2010). Furthermore, a similar loop2 structure is necessary for the microtubule depolymerization activity of kinesin-13 motors (Ogawa *et al.*, 2004; Shipley *et al.*, 2004). To test if this unique surface loop contributes to kinesin-8 specific K-fiber end-binding activity, we engineered Kif18A mutants that contain a truncated loop2 (Kif18A-L2Δ) or alanine substitutions at each of the six lysine residues in loop2 (Kif18A-L2-K6A) (Figure 4A).

When expressed in mitotic cells depleted of endogenous Kif18A, neither Kif18A-L2Δ nor Kif18A-L2-K6A efficiently accumulated at K-fiber plus-ends (Figure 4 B-C). However, both loop2 mutants accumulated at K-fiber ends in cells briefly treated with 10 μM taxol (Figure 5 A-B). The accumulation of Kif18A-L2-K6A occurred with similar kinetics to those displayed by the chimeric kinesins tested in this study, however, the Kif18A-L2Δ mutant accumulated more slowly and to a lesser

extent, primarily on peripheral K-fibers (Figure 5C). FRAP studies revealed that both loop2 mutants displayed an increased mobile fraction at K-fiber ends in taxol-treated cells compared to wild type Kif18A (Figure 5D and Table 1). These data indicate that loop2 is necessary for Kif18A's stable association with K-fiber ends.

To determine if loop2 and the C-terminal tail of Kif18A are sufficient for the stable association of plus-end directed motors with K-fiber ends, we inserted the loop2 region of Kif18A into the Kif4A-18A chimera (Kif4A-L2-18A) (Figure 4A). Kif4A-L2-18A failed to accumulate at K-fiber ends in cells with dynamic microtubules (Figure 4 C-D) but did concentrate efficiently at ends in taxol-treated cells (Figure 5 A-C). In FRAP assays, Kif4A-L2-18A displayed a significantly reduced mobile fraction and a slower recovery rate compared to the Kif4A-18A chimera (Figure 5E and Table 1). While the rate of recovery and mobile fraction for Kif4A-L2-18A were also significantly different than those measured for Kif18A-FL, they were comparable to the values obtained from FRAP analyses of Kif18B-18A. These data indicate that Kif18A's loop2 and C-terminal tail underlie the majority of the stable microtubule-end binding activity displayed by the two kinesin-8 motors.

4.3.4. The Kif4A motor domain cannot functionally substitute for Kif18A to control chromosome alignment and spindle length

To determine whether loop2 is required for Kif18A's regulation of K-fiber lengths during mitosis, we assayed the ability of our chimeric kinesins and loop2 mutants to facilitate chromosome alignment and regulate spindle length in cells depleted of endogenous Kif18A. Cells depleted of Kif18A were transfected with GFP-

tagged kinesins and then treated approximately 18 hours later with MG132 (20 μM), which prevents anaphase entry (Figure 6A). Cells were then fixed and immunofluorescently stained with antibodies against centromeric (ACA) and centrosomal (γ-tubulin) proteins. Under these conditions, the majority of cells transfected with scrambled control siRNAs and a GFP control plasmid had well-aligned kinetochores. In contrast, cells transfected with Kif18A siRNAs and a GFP control plasmid displayed unaligned kinetochores (Figure 6A).

Chromosome alignment was quantified in cells with similar GFP expression levels (Figure S1) by measuring the distribution of ACA fluorescence along the pole-to-pole axis and computing the full-width at half max of a Gaussian fit to the distribution (Figure 6B). Spindle length was measured as the distance between the two centrosomes. Kif18A-FL and the Kif18B-18A chimeras were able to facilitate chromosome alignment and reduce spindle length in the absence of endogenous Kif18A (Figure 6 C-D). In contrast, the Kif4A-18A, Kif4A-L2-18A and Kif5B-18A chimeras were not capable of aligning chromosomes or reducing spindle length compared to GFP expressing cells depleted of Kif18A (Figure 6 C-D). Similarly, the Kif18A-L2**Δ**and Kif18A-L2-K6A mutants failed to align chromosomes or reduce spindle length in the absence of endogenous Kif18A (Figure 6 C-D). These data indicate that loop2 provides an essential activity for Kif18A's function in regulating K-fiber lengths to align mitotic chromosomes. However, the inability of Kif4A-L2-18A to rescue chromosome alignment and spindle length in Kif18A-depleted cells suggests that these regions are not sufficient for Kif18A's mitotic functions.

4.4 Discussion

The molecular control of microtubule dynamics is essential for diverse cellular processes such as division, migration and morphogenesis. While microtubules are intrinsically dynamic, their growth and shortening are modulated in cells by polymerizers, depolymerizers and attenuators. This regulation is complex within structures that are comprised of closely packed microtubule subpopulations with dramatically different dynamic properties, such as the mitotic spindle. The data presented here indicate that the Kif4A and Kif18A motor domains are not functionally equivalent for spindle microtubule length control and likely attenuate microtubule dynamics through distinct mechanisms. Furthermore, Kif18A's specific ability to control K-fiber lengths requires a unique, positively charged loop2 region common to kinesin-8 motors. This implies that the differential control of K-fibers and non-kinetochore microtubules relies in part on the specialized activities of microtubule-attenuating kinesins.

Kif4A controls the lengths and dynamics of non-kinetochore microtubules within the spindle to regulate polar ejection forces and spindle length (Stumpff *et al.*, 2012; Wandke *et al.*, 2012). While Kif4A displays a similar attenuation of microtubule dynamics to Kif18A, it does not have an extended loop2 region or stably associate with microtubule ends (Bringmann *et al.*, 2004; Bieling *et al.*, 2010; Stumpff *et al.*, 2012; Subramanian *et al.*, 2013). Consistent with loop2 and stable end binding being required for K-fiber length control, the Kif4A-18A chimera was unable to regulate chromosome alignment or spindle length. These data suggest that Kif4A and Kif18A attenuate

microtubule dynamics through distinct mechanisms. We speculate that Kif4A's fast velocity facilitates its steady state accumulation at the ends of fast growing non-kinetochore microtubules within the spindle. This concentration of motor could in turn inhibit the addition and loss of tubulin. Assuming that a threshold of motor accumulation is necessary to attenuate microtubule dynamics, such a mechanism could efficiently control the lengths of individual microtubules, but stable association with microtubule tips, as exhibited by the Kif18A and Kif18B motor domains, may be required to reach the motor concentrations necessary to attenuate the dynamics of the 15-20 microtubules in a HeLa cell K-fiber (McEwen *et al.*, 2001).

Kif18A controls K-fiber lengths to spatially confine the movements of mitotic chromosomes to the spindle equator (Stumpff *et al.*, 2008; Stumpff *et al.*, 2012). This function depends on Kif18A's highly processive plus-end directed motility, stable association with microtubule ends and direct suppression of microtubule dynamics (Mayr *et al.*, 2011; Stumpff *et al.*, 2011). Microtubule-binding regions found in the C-terminal tails of kinesin-8s promote targeting of these motors to the ends of microtubules by increasing motor processivity (Mayr *et al.*, 2011; Stumpff *et al.*, 2011; Su *et al.*, 2011; Weaver *et al.*, 2011). However, Kif18A's tail does not account for all of the motor's microtubule end specific functions. For example, the ability of a Kif18A-truncation mutant lacking the tail to dwell at microtubule ends and suppress their dynamics is attenuated but not ablated, indicating that these properties are intrinsic to the Kif18A motor domain (Stumpff *et al.*, 2011). Our data indicate that the loop2 region of kinesin-8s underlies these unique motor activities.

The contribution of Kif18A's loop2 to its function in controlling K-fiber lengths is particularly intriguing because an analogous region is required for kinesin-13-dependent microtubule depolymerization. Kinesin-13 loop2 forms an anti-parallel β-sheet structure that ends with a KVD-finger, which is essential for microtubule depolymerization activity but not microtubule binding (Ogawa *et al.*, 2004; Shipley *et al.*, 2004). These data suggest that kinesin-13 loop2 has a microtubule-end specific function. Consistent with this, loop2 is necessary for kinesin-13s to induce curvature between α-tubulin and β-tubulin subunits, an activity predicted to facilitate microtubule disassembly (Desai *et al.*, 1999; Moores *et al.*, 2002; Tan *et al.*, 2008; Asenjo *et al.*, 2013).

Our data suggest that, similar to kinesin-13 loop2, Kif18A's loop2 promotes microtubule tip association and functions in the regulation of K-fiber dynamics. However, in contrast to kinesin-13s, loop2 in Kif18A is longer, conformationally dynamic and lacks a KVD finger (Peters *et al.*, 2010). Cryo-electron microscopy studies indicate that the positively charged Kif18A loop2 directly associates with the negatively charged surface of α-tubulin (Peters *et al.*, 2010). We speculate that the structural differences between the loop2 regions of kinesin-13s and Kif18A could explain the different effects of these motors on microtubule dynamics. Kif18A's loop2 could analogously modify the conformation of tubulin at microtubule tips in such a way that it inhibits loss or gain of tubulin dimers from the end rather than inducing terminal tubulin removal. Furthermore, stable association with microtubule tips may perturb the ability of other microtubule regulators to access microtubule ends. Our analyses of the

Kif4A-L2-18A chimera indicate that while loop2 and the Kif18A tail facilitate Kif4A's stable association with K-fiber ends, they are not sufficient for K-fiber length control. Thus, other yet to be identified differences between the structure and activity of the Kif4A and Kif18A motors likely contribute to the functional specificity of these kinesins.

Kif18B controls the lengths of astral microtubules during mitosis, but whether it functions as a microtubule attenuator or depolymerizer is unresolved (Stout *et al.*, 2011; Tanenbaum *et al.*, 2011). The similarity between the loop2 regions of Kif18A and Kif18B and the ability of the Kif18B-18A chimera to functionally substitute for Kif18A during chromosome alignment in our studies suggest that Kif18B attenuates microtubule dynamic instability similar to Kif18A. This implies that differentially localized kinesin-8s may use similar mechanisms to regulate distinct subsets of spindle microtubules. While all kinesin-8 motors appear to have an extended loop2, the depolymerizing kinesin-8, Kip3p, has a longer (38 amino acid) and divergent loop2 compared to Kif18A and Kif18B (Gupta *et al.*, 2006; Varga *et al.*, 2006; Peters *et al.*, 2010). Perhaps differences in the interactions of kinesin-8 loop2 structures with tubulin at the ends of microtubules can explain the diversity of effects on microtubule dynamics observed for kinesin-8 family members (Gupta *et al.*, 2006; Varga *et al.*, 2006; Du *et al.*, 2010; Stumpff *et al.*, 2011; Erent *et al.*, 2012; Niwa *et al.*, 2012).

4.5 Materials and Methods

Plasmids and siRNAs

Chimeric kinesins were constructed from the codons indicated in Figure 1A and Figure 4A by overlap extension PCR. Site-directed mutagenesis was used to make Kif18A-L2Δ and to introduce silent mutations within the motor domains of Kif18A-FL and all Kif18A mutants to facilitate siRNA resistance (forward primer sequence 5'-CGTCCGGAAAACACTAAAGAAAAAGCAGCaGGcTTcCAcAAAGTGGTTCATG TTGTGG-3'). The Kif18A-L2-K6A construct was synthesized (Life Technologies). Construction of mRFP-CENP-B was previously described (Stumpff *et al.*, 2008). The scrambled control (Silencer Negative Control #1, Life Technologies) and validated Silencer Kif18A siRNAs (5'-GCUGGAUUUCAUAAAGUGG -3', Life Technologies) used were also described previously (Stumpff *et al.*, 2008; Stumpff *et al.*, 2012).

Cell culture and transfections

HeLa cells were cultured at 37º C and 5% CO_2 in MEM-alpha medium (Life Technologies) containing 10% FBS (Life Technologies) plus antibiotics. For siRNA transfections, 5-6.5 x 10^5 cells were plated in 60 mm^2 dishes. Approximately 16 hours later, cells were treated with 300 pmol siRNA complexed with 12 µl RNAiMax (Life Technologies) following the manufacturer's instructions. After 8 hours, cells were trypsinized, pooled and transfected with plasmid DNA using a Nucleofector 4D system (Lonza). Electroporated cells were then plated on 12 mm glass coverslips (Electron Microscopy Supplies) for fixed cell assays or poly-L-lysine coated 35 mm^2 glass-bottom dishes (MatTek) for live cell studies. Cells were treated with 10 µM taxol or 20

μM MG132 5 minutes or 2 hours prior to fixation, respectively, where indicated in the text.

Western Blot analysis

Cells were lysed in RIPA buffer (50 mM Tris-HCl pH 7.4, 150 mM NaCl, 2 mM EDTA, 1% NP-40 and 0.1% SDS) 20 hours after DNA transfection and 28 hours after siRNA addition. Lysates were extracted on ice for 10 minutes. An equal volume of 2X Laemmli buffer was then added and lysates were boiled for 10 minutes. Recombinant Kif18A-GFP was purified as previously described (Stumpff *et al.*, 2011). Lysates and purified proteins were separated by electrophoresis on 4-15% Tris-glycine polyacrylamide gels (BioRad) and transferred to PVDF membrane (BioRad). Membranes were blocked in Odyssey blocking buffer (1:1 ratio of TBS (Tris-buffered saline- 50 mM Tris-Cl pH 7.4 and 150 mM NaCl) and Odyssey blocking reagent (Li-COR)). Blocked membranes were probed with 1 μg/ml rabbit-anti-Kif18A antibodies (Bethyl Laboratories), 4 μg/ml of rabbit-anti-GFP antibodies (Life Technologies), or 0.5 μg/ml mouse-anti-GAPDH antibodies (Millipore) diluted in Odyssey blocking buffer with 0.1% Tween-20. Secondary DyLight 800 anti-rabbit IgG and DyLight 680 anti-mouse IgG antibodies (Thermo Scientific) were diluted to 0.03 μg/ml in Odyssey blocking buffer with 0.1% Tween-20 and 0.01% SDS. Secondary antibody fluorescence was detected with an Odyssey CLx (LI-COR). Kif18A knockdown was quantified from 3 independent experiments by densitometry using ImageJ software (NIH). The amount of Kif18A remaining in each Kif18A siRNA treated lysate was

determined by comparing the Kif18A band density to that in the matched control lysate and correcting for protein load relative to the GAPDH signal.

Immunofluorescence microscopy

Cells were fixed on coverslips for 10 minutes in 1% paraformaldehyde (Electron Microscopy Sciences)/ -20º C methanol, washed in 1X TBS and blocked in 20% goat serum in antibody diluting solution (1X TBS, 2% BSA, 0.1% Azide, 0.1% Triton-X 100) for 1 hour. Cells were labeled with the following primary antibodies: 2.5 µg/ml human anti-centromere serum (Antibodies incorporated), 1 µg/ml mouse anti-α-tubulin (Sigma-Aldrich) and 1 µg/ml mouse anti-γ-tubulin (Sigma-Aldrich). Cells were labeled with goat anti-human-Alexa Fluor 594 or goat anti-mouse-Alexa Fluor 647 secondary antibodies at 1 µg/ml (Life Technologies). Coverslips were mounted on glass slides in Prolong Gold antifade reagent plus DAPI (Life Technologies). Cells were imaged on a Nikon Ti-E inverted microscope controlled by NIS Elements software (Nikon) with APO 100X 1.49 NA and Plan APO 60X 1.42 NA oil immersion objectives (Nikon), Spectra-X light engine (Lumencore) and Clara cooled-CCD camera (Andor). Optical sections were collected at 200 nm intervals through each spindle. Representative images are max intensity projections of 5 optical slices centered on the pole-to-pole axis. Brightness and contrast were adjusted using Photoshop CS6 (Adobe). Two-dimensional linear protein mapping was performed within single focal planes using the linescan tool in NIS Elements.

FRAP studies

Kif18A-depleted HeLa cells transfected with mRFP-CENP-B and GFP-tagged kinesin constructs were switched into CO_2-independent media containing 10% FBS (Life Technologies) just prior to imaging. For analyses of kinesin redistribution after taxol addition, mitotic cells were imaged for 20 seconds at 10-second intervals and then an equal volume of 37ºC CO_2-independent media containing taxol was added so the final taxol concentration was 10 µM. Cells were then imaged at 10-second intervals for 10 minutes. For FRAP assays, GFP expressing cells were imaged at 2 second intervals for 10 seconds prior to bleaching, GFP foci near mRFP-CENP-B foci were then photobleached using a point-focused 405 nm laser and GFP imaging was continued at 2-second intervals. GFP fluorescence was quantified in the bleached zone before and after laser activation using NIS Elements software. Fluorescence data were analyzed and plotted using Igor Pro (Wavemetrics) and statistical comparisons were performed using a Student's two-tailed t-test. Fluorescence intensities were normalized such that the pre-bleach value is set to one and the post-bleach value is zero. Imaging was performed on the Nikon Ti-E inverted microscope described above, but images were captured with an iXon X3 EMCCD camera (Andor) to minimize exposure times and photobleaching.

Quantification of chromosome alignment

Single focal plane images of MG132 arrested cells where both centrosomes were in the same focal plane were captured and rotated such that the pole-to-pole axis was

horizontal. The Plot Profile command in ImageJ (NIH) was used to measure the distribution of ACA fluorescence within a rectangular region of interest (ROI) with a length defined by the distance between the centrosomes and a set height of 17.5 μm. The average normalized ACA fluorescence in each pixel column within the ROI was plotted as a function of position along the pole-to-pole axis and fit with a Gaussian in Igor Pro (Wavemetrics). The full-width at half max of the Gaussian was calculated as a metric for chromosome alignment in a single cell. Statistical comparisons were performed using a Student's two-tailed t-test.

ACKNOWLEDGEMENTS

We thank Ryoma Ohi for anti-Kif18A antibodies. David Warshaw and Christopher Berger provided insightful suggestions and critical feedback on the manuscript. This work was supported by a Leukemia and Lymphoma Society Special Fellow Award (3652-11), Basil O'Connor Research Starter Scholar Award (#5-FY14-33) and a Vermont Cancer Center/ LCCRO Program Award to J.S.

4.6 References

1. Stumpff, J., Wagenbach, M., Franck, A., Asbury, C.L., and Wordeman, L. (2012). Kif18A and chromokinesins confine centromere movements via microtubule growth suppression and spatial control of kinetochore tension. Dev Cell *22*, 1017-1029.

2. Tirnauer, J.S., Canman, J.C., Salmon, E.D., and Mitchison, T.J. (2002). EB1 targets to kinetochores with attached, polymerizing microtubules. Mol Biol Cell *13*, 4308-4316.

3. Zhai, Y., Kronebusch, P.J., and Borisy, G.G. (1995). Kinetochore microtubule dynamics and the metaphase-anaphase transition. J Cell Biol *131*, 721-734.

4. Rieder, C.L., and Salmon, E.D. (1994). Motile kinetochores and polar ejection forces dictate chromosome position on the vertebrate mitotic spindle. J Cell Biol *124*, 223-233.

5. Rieder, C.L., and Salmon, E.D. (1998). The vertebrate cell kinetochore and its roles during mitosis. Trends Cell Biol *8*, 310-318.

6. Castoldi, M., and Vernos, I. (2006). Chromokinesin Xklp1 contributes to the regulation of microtubule density and organization during spindle assembly. Mol Biol Cell *17*, 1451-1460.

7. Kline-Smith, S.L., and Walczak, C.E. (2002). The microtubule-destabilizing kinesin XKCM1 regulates microtubule dynamic instability in cells. Mol Biol Cell *13*, 2718-2731.

8. Manning, A.L., Ganem, N.J., Bakhoum, S.F., Wagenbach, M., Wordeman, L., and Compton, D.A. (2007). The kinesin-13 proteins Kif2a, Kif2b, and Kif2c/MCAK have distinct roles during mitosis in human cells. Mol Biol Cell *18*, 2970-2979.

9. Mayr, M.I., Hummer, S., Bormann, J., Gruner, T., Adio, S., Woehlke, G., and Mayer, T.U. (2007). The human kinesin Kif18A is a motile microtubule depolymerase essential for chromosome congression. Curr Biol *17*, 488-498.

10. Stout, J.R., Yount, A.L., Powers, J.A., Leblanc, C., Ems-McClung, S.C., and Walczak, C.E. (2011). Kif18B interacts with EB1 and controls astral microtubule length during mitosis. Mol Biol Cell *22*, 3070-3080.

11. Stumpff, J., von Dassow, G., Wagenbach, M., Asbury, C., and Wordeman, L. (2008). The kinesin-8 motor Kif18A suppresses kinetochore movements to control mitotic chromosome alignment. Developmental cell *14*, 252-262.

12. Bieling, P., Telley, I.A., and Surrey, T. (2010). A Minimal Midzone Protein Module Controls Formation and Length of Antiparallel Microtubule Overlaps. Cell *142*, 420-432.

13. Bringmann, H., Skiniotis, G., Spilker, A., Kandels-Lewis, S., Vernos, I., and Surrey, T. (2004). A kinesin-like motor inhibits microtubule dynamic instability. Science *303*, 1519-1522.

14. Desai, A., Verma, S., Mitchison, T.J., and Walczak, C.E. (1999). Kin I kinesins are microtubule-destabilizing enzymes. Cell *96*, 69-78.

15. Du, Y., English, C.A., and Ohi, R. (2010). The kinesin-8 Kif18A dampens microtubule plus-end dynamics. Current biology : CB *20*, 374-380.

16. Stumpff, J., Du, Y., English, C.A., Maliga, Z., Wagenbach, M., Asbury, C.L., Wordeman, L., and Ohi, R. (2011). A tethering mechanism controls the processivity and kinetochore-microtubule plus-end enrichment of the kinesin-8 Kif18A. Molecular cell *43*, 764-775.

17. Lee, Y.M., Kim, E., Park, M., Moon, E., Ahn, S.M., Kim, W., Hwang, K.B., Kim, Y.K., Choi, W., and Kim, W. (2010). Cell cycle-regulated expression and subcellular localization of a kinesin-8 member human KIF18B. Gene *466*, 16-25.

18. Moore, A.T., Rankin, K.E., von Dassow, G., Peris, L., Wagenbach, M., Ovechkina, Y., Andrieux, A., Job, D., and Wordeman, L. (2005). MCAK associates with the tips of polymerizing microtubules. J Cell Biol *169*, 391-397.

19. Tanenbaum, M.E., Macurek, L., van der Vaart, B., Galli, M., Akhmanova, A., and Medema, R.H. (2011). A complex of Kif18b and MCAK promotes microtubule depolymerization and is negatively regulated by Aurora kinases. Curr Biol *21*, 1356-1365.

20. Wandke, C., Barisic, M., Sigl, R., Rauch, V., Wolf, F., Amaro, A.C., Tan, C.H., Pereira, A.J., Kutay, U., Maiato, H., et al. (2012). Human chromokinesins promote chromosome congression and spindle microtubule dynamics during mitosis. J Cell Biol *198*, 847-863.

21. Lee, Y.M., Lee, S., Lee, E., Shin, H., Hahn, H., Choi, W., and Kim, W. (2001). Human kinesin superfamily member 4 is dominantly localized in the nuclear matrix and is associated with chromosomes during mitosis. Biochem J *360*, 549-556.

22. Subramanian, R., Ti, S.C., Tan, L., Darst, S.A., and Kapoor, T.M. (2013). Marking and measuring single microtubules by PRC1 and kinesin-4. Cell *154*, 377-390.

23. Mayr, M.I., Storch, M., Howard, J., and Mayer, T.U. (2011). A non-motor microtubule binding site is essential for the high processivity and mitotic function of kinesin-8 Kif18A. PloS one *6*, e27471.

24. Su, X., Qiu, W., Gupta, M.L., Jr., Pereira-Leal, J.B., Reck-Peterson, S.L., and Pellman, D. (2011). Mechanisms underlying the dual-mode regulation of microtubule dynamics by Kip3/kinesin-8. Molecular cell *43*, 751-763.

25. Weaver, L.N., Ems-McClung, S.C., Stout, J.R., LeBlanc, C., Shaw, S.L., Gardner, M.K., and Walczak, C.E. (2011). Kif18A uses a microtubule binding site in the tail for plus-end localization and spindle length regulation. Current biology : CB *21*, 1500-1506.

26. Canman, J.C., Salmon, E.D., and Fang, G. (2002). Inducing precocious anaphase in cultured mammalian cells. Cell Motil Cytoskeleton *52*, 61-65.

27. Cimini, D., Cameron, L.A., and Salmon, E.D. (2004). Anaphase spindle mechanics prevent mis-segregation of merotelically oriented chromosomes. Curr Biol *14*, 2149-2155.

28. Lakamper, S., Kallipolitou, A., Woehlke, G., Schliwa, M., and Meyhofer, E. (2003). Single fungal kinesin motor molecules move processively along microtubules. Biophys J *84*, 1833-1843.

29. Peters, C., Brejc, K., Belmont, L., Bodey, A.J., Lee, Y., Yu, M., Guo, J., Sakowicz, R., Hartman, J., and Moores, C.A. (2010). Insight into the molecular mechanism of the multitasking kinesin-8 motor. EMBO J *29*, 3437-3447.

30. Ogawa, T., Nitta, R., Okada, Y., and Hirokawa, N. (2004). A common mechanism for microtubule destabilizers-M type kinesins stabilize curling of the protofilament using the class-specific neck and loops. Cell *116*, 591-602.

31. Shipley, K., Hekmat-Nejad, M., Turner, J., Moores, C., Anderson, R., Milligan, R., Sakowicz, R., and Fletterick, R. (2004). Structure of a kinesin microtubule depolymerization machine. EMBO J *23*, 1422-1432.

32. McEwen, B.F., Chan, G.K., Zubrowski, B., Savoian, M.S., Sauer, M.T., and Yen, T.J. (2001). CENP-E is essential for reliable bioriented spindle attachment, but chromosome alignment can be achieved via redundant mechanisms in mammalian cells. Mol Biol Cell *12*, 2776-2789.

33. Asenjo, A.B., Chatterjee, C., Tan, D., DePaoli, V., Rice, W.J., Diaz-Avalos, R., Silvestry, M., and Sosa, H. (2013). Structural model for tubulin recognition and deformation by kinesin-13 microtubule depolymerases. Cell reports *3*, 759-768.

34. Moores, C.A., Yu, M., Guo, J., Beraud, C., Sakowicz, R., and Milligan, R.A. (2002). A mechanism for microtubule depolymerization by KinI kinesins. Mol Cell *9*, 903-909.

35. Tan, D., Rice, W.J., and Sosa, H. (2008). Structure of the kinesin13-microtubule ring complex. Structure *16*, 1732-1739.

36. Gupta, M.L., Jr., Carvalho, P., Roof, D.M., and Pellman, D. (2006). Plus end-specific depolymerase activity of Kip3, a kinesin-8 protein, explains its role in positioning the yeast mitotic spindle. Nat Cell Biol *8*, 913-923.

37. Varga, V., Helenius, J., Tanaka, K., Hyman, A.A., Tanaka, T.U., and Howard, J. (2006). Yeast kinesin-8 depolymerizes microtubules in a length-dependent manner. Nat Cell Biol *8*, 957-962.

38. Erent, M., Drummond, D.R., and Cross, R.A. (2012). S. pombe kinesins-8 promote both nucleation and catastrophe of microtubules. PloS one *7*, e30738.

39. Niwa, S., Nakajima, K., Miki, H., Minato, Y., Wang, D., and Hirokawa, N. (2012). KIF19A Is a Microtubule-Depolymerizing Kinesin for Ciliary Length Control. Dev Cell *23*, 1167-1175.

4.7 Figures

GFP-Kinesin	$t_{1/2}$ (s)	Mobile Fraction (%)	Fraction recovered 30 sec after bleach (%)	n (# cells)
Kif18A-FL	45.0 ± 20.0	18.6 ± 8.8	6.6 ± 4.0	8
Kif18B-18A	19.5 ± 5.0**	20.9 ± 8.2	12.2 ± 4.9	4
Kif4A-18A	10.4 ± 3.3**	43.2 ± 21.5**	40.4 ± 20.7**	9
Kif5B-18A	8.3 ± 2.9**	57.5 ± 16.3**	51.9± 14.3**	6
Kif18A-770	20.4 ± 8.0**	39.1 ± 17.0**	23.5 ± 10.5**	9
Kif18A-L2-K6A	16.2 ± 5.7**	37.6 ± 17.0**	29.4 ± 14.9**	10
Kif18A-ΔL2	13.7 ± 8.4**	30.8 ± 10.7*	22.9 ± 9.9**	6
Kif4A-L2-18A	18.7 ± 9.9** #	25.9 ± 5.0* #	16.9 ± 6.1** #	9

Table 4-1. FRAP measurements of kinesin behavior at K-fiber ends in taxol-treated cells.

(* $p \leq 0.05$ compared to Kif18A-FL, ** $p \leq 0.01$ compared to Kif18A-FL, # $p \leq 0.05$ compared to Kif4A-18A)

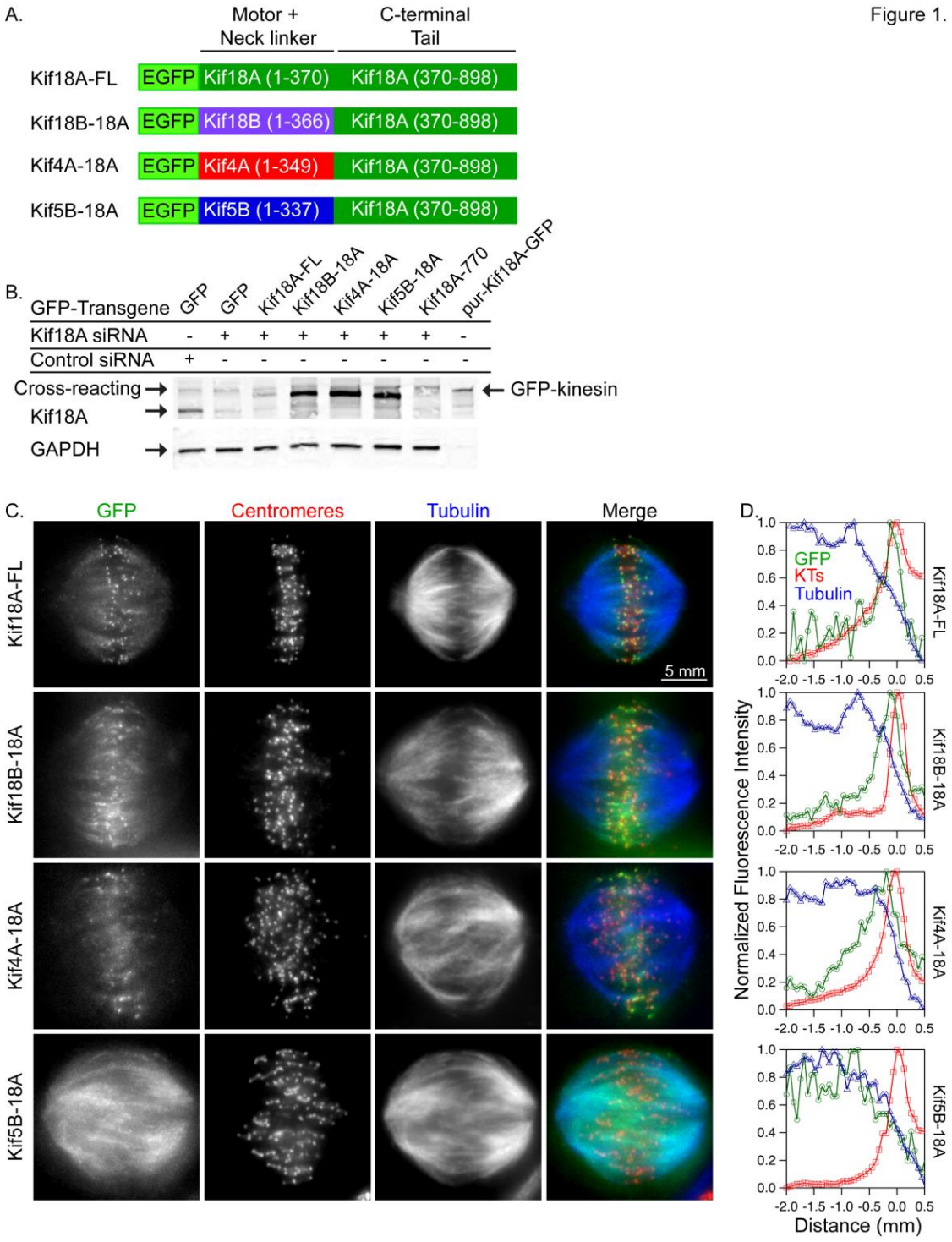

Figure 4-1. The Kif18A C-terminus targets plus-end directed motors to K-fibers but is not sufficient for accumulation at K-fiber ends.

(A) Schematic of Kif18A-tail chimeras. Numbers in parentheses indicate the amino acids used in each fragment. (B) Western blots of lysates transfected with the indicated siRNAs and GFP-tagged transgenes. Purified Kif18A-GFP (30 ng) was included for comparison. Blots were probed with anti-Kif18A (upper panel) and anti-GAPDH (lower panel) antibodies. The amount of Kif18A expressed in Kif18A siRNA treated cells from 3 independent experiments is 9.8 ± 1.3% relative to controls. Note that Kif18A-770 does not contain the epitope recognized by the anti-Kif18A antibody. An anti-GFP blot of this sample is included in Figure S2. (C) Fluorescent micrographs of the indicated GFP-tagged kinesins (green) in Kif18A-depleted HeLa cells immunostained with ACA (centromeres, red) and tubulin (blue) (D) Linescans of GFP-tagged kinesin (green trace) relative to tubulin (blue trace) and ACA fluorescence (red trace) along peripheral K-fibers.

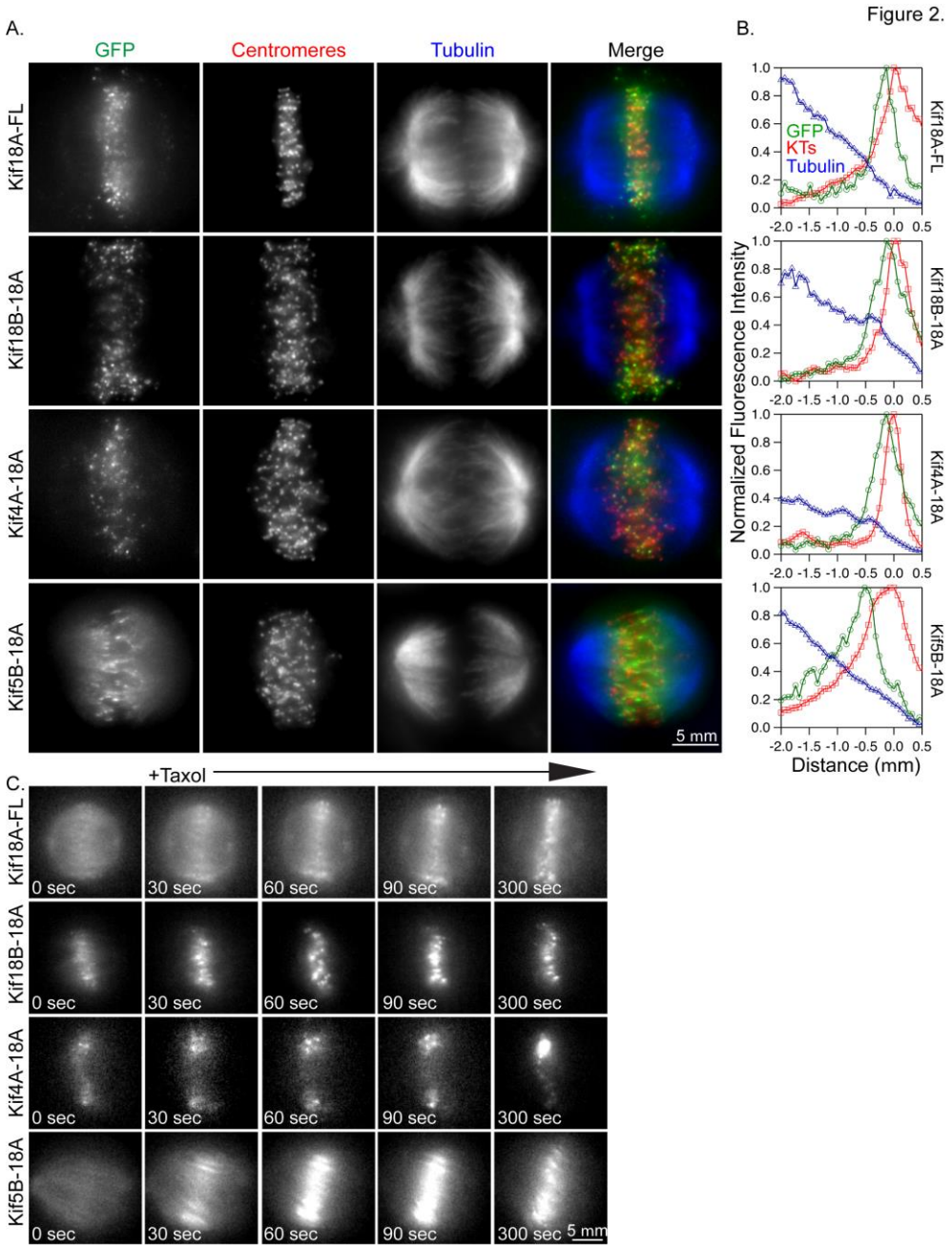

Figure 4-2. Kif18A-tail chimeras rapidly accumulate at K-fiber ends in taxol-treated cells.

(A) Fluorescent micrographs of the indicated GFP-tagged kinesins (green) in Kif18A-depleted HeLa cells following a 5-minute incubation with 10 µM taxol. Cells were immunostained with ACA (centromeres, red) and tubulin (blue). (B) Linescans of GFP-

tagged kinesins (green trace) relative to tubulin (blue trace) and ACA (red trace) along K-fibers in 10 μM taxol-treated cells. (C) Still images from live cell analyses of GFP-tagged kinesin relocalization after the addition of taxol. Taxol was added immediately after the 0 second image was captured.

Figure 3.

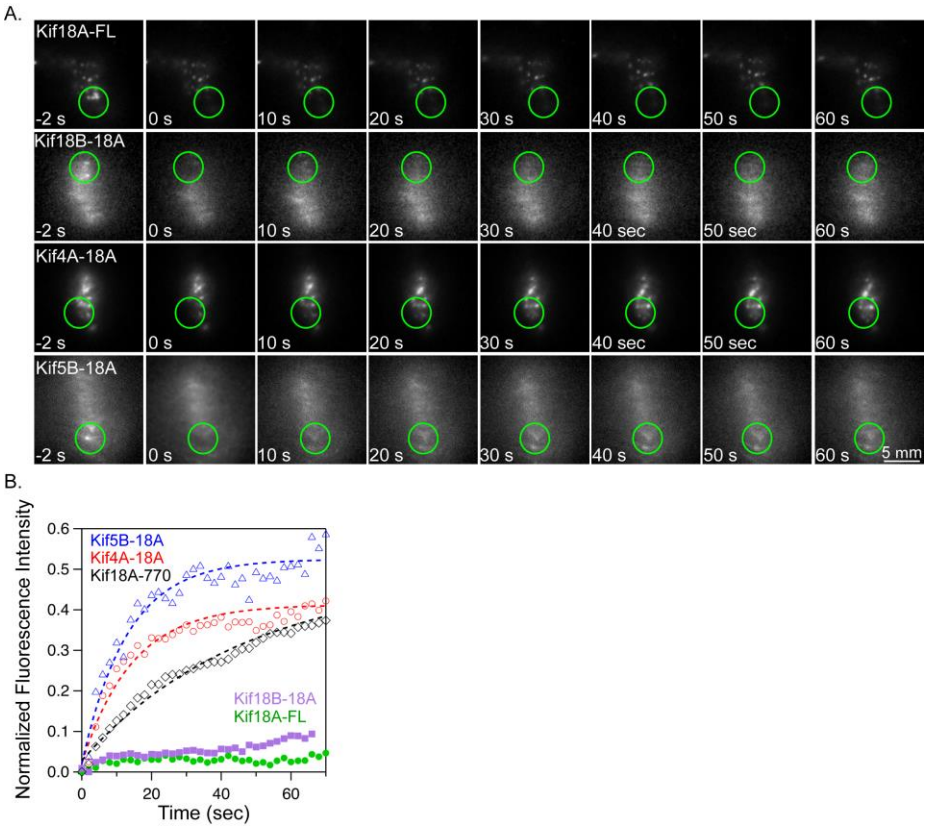

Figure 4-3. A kinesin-8-specific activity is required for stable association with K-fiber ends.

(A) Stills from FRAP assays performed in live taxol-treated, Kif18A-depleted HeLa cells expressing the indicated GFP-tagged kinesin. Fluorescence intensity was measured before (-2 sec) and after (0 - 60 sec) a brief pulse with a 405 nm laser focused to the region indicated by the green circle. (B) Plot of relative GFP-fluorescence as a function of time following a bleaching event for the indicated kinesins. Dashed lines are single exponential fits to the data. Note that the Kif18B-18A and Kif18A-FL data did not fit a single exponential. Quantified data from FRAP experiments are reported in Table 1. Representative images of Kif18A-770 are included in Figure S1.

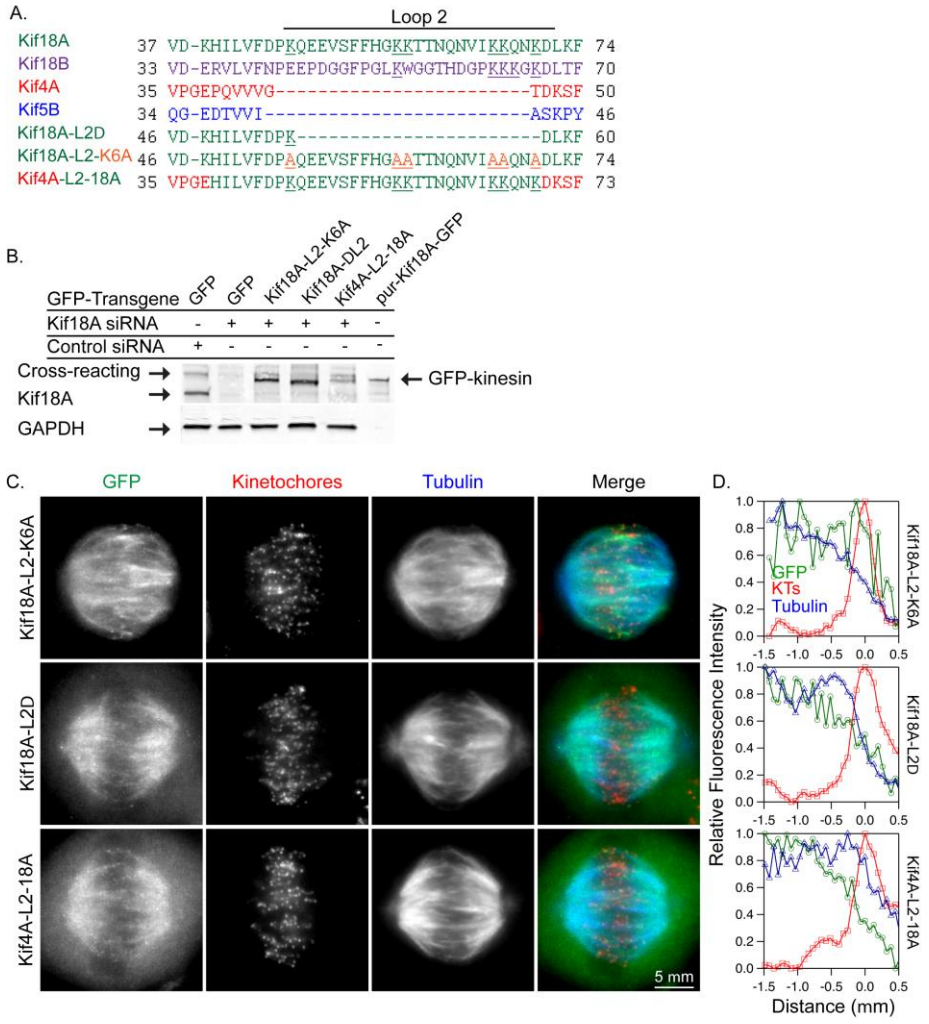

Figure 4-4. Kif18A's loop2 is necessary but not sufficient for motor accumulation at K-fiber ends.

(A) Protein sequence alignment of the loop2 regions for the indicated kinesins. Kif18A's loop2 contains 6 lysine residues (underlined), which were mutated to alanine (orange, underlined) in Kif18A-L2-K6A. (B) Western blots of lysates transfected with the indicated siRNAs and GFP-tagged transgenes. Purified Kif18A-GFP (30 ng) was also loaded for comparison. Blots were probed with anti-Kif18A (upper panel) and anti-GAPDH (lower panel) antibodies. (C) Fluorescent micrographs of the indicated GFP-tagged kinesins (green) in cells immunostained with ACA (centromeres, red) and

tubulin (blue). (D) Linescans of GFP-tagged kinesin (green trace) relative to tubulin (blue trace) and ACA fluorescence (red trace) along peripheral K-fibers.

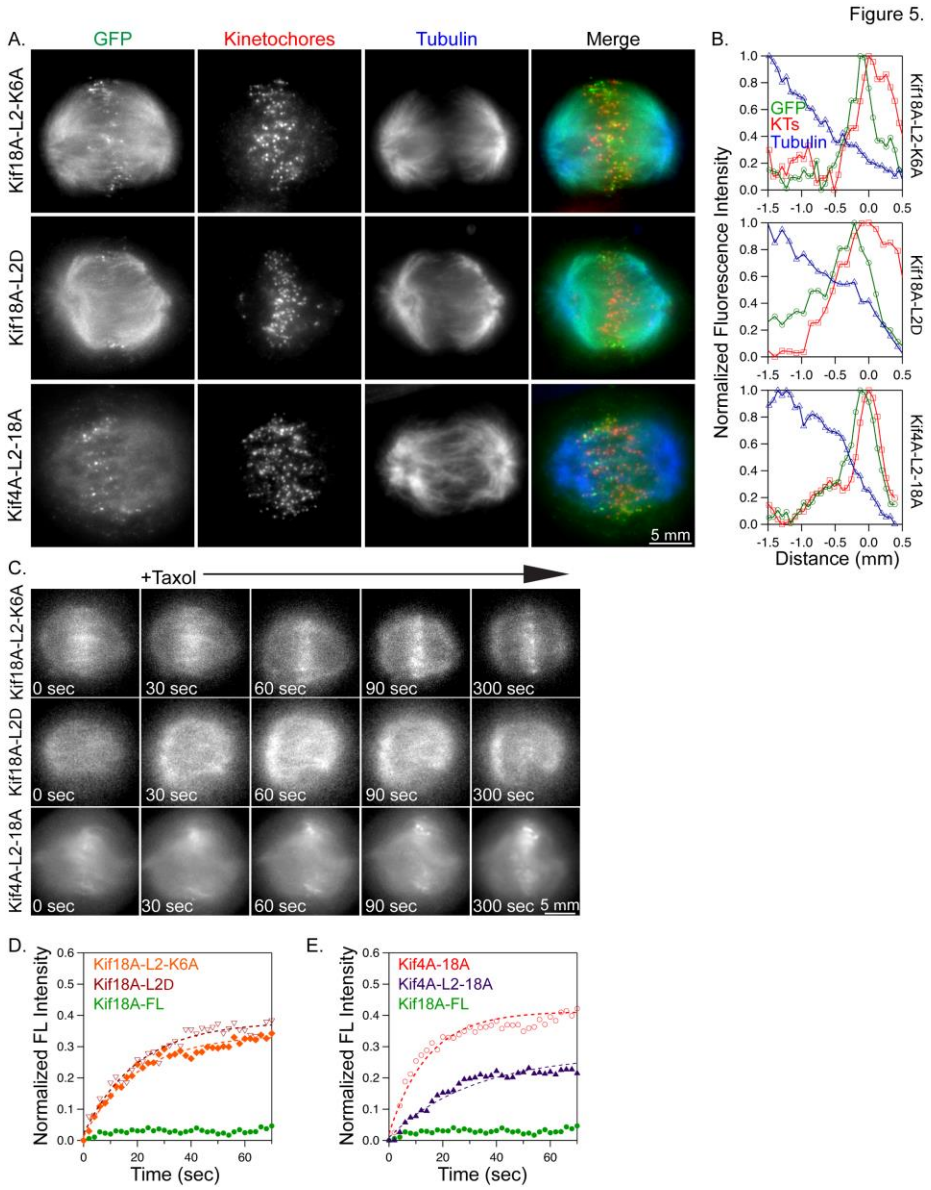

Figure 4-5. Kif18A's loop2 is necessary but not sufficient for stable association with K-fiber ends.

(A) Fluorescent micrographs of the indicated GFP-tagged loop2 mutant kinesins (green) in Kif18A-depleted HeLa cells following a 5-minute incubation with taxol. Cells were immunostained with ACA (centromeres, red) and tubulin (blue). (B) Linescans of GFP-tagged loop2 mutants (green trace) relative to tubulin (blue trace) and ACA (red trace) along K-fibers in 10 μM taxol-treated cells. (C) Still images from live cell analyses of

GFP-tagged kinesin relocalization after the addition of 10 μM taxol. Taxol was added immediately after the 0 second image was captured. (D-E) Plots displaying relative GFP-fluorescence as a function of time following a bleaching event for the indicated kinesins. Dashed lines are single exponential fits to the data. Quantified data from FRAP experiments are reported in Table 1.

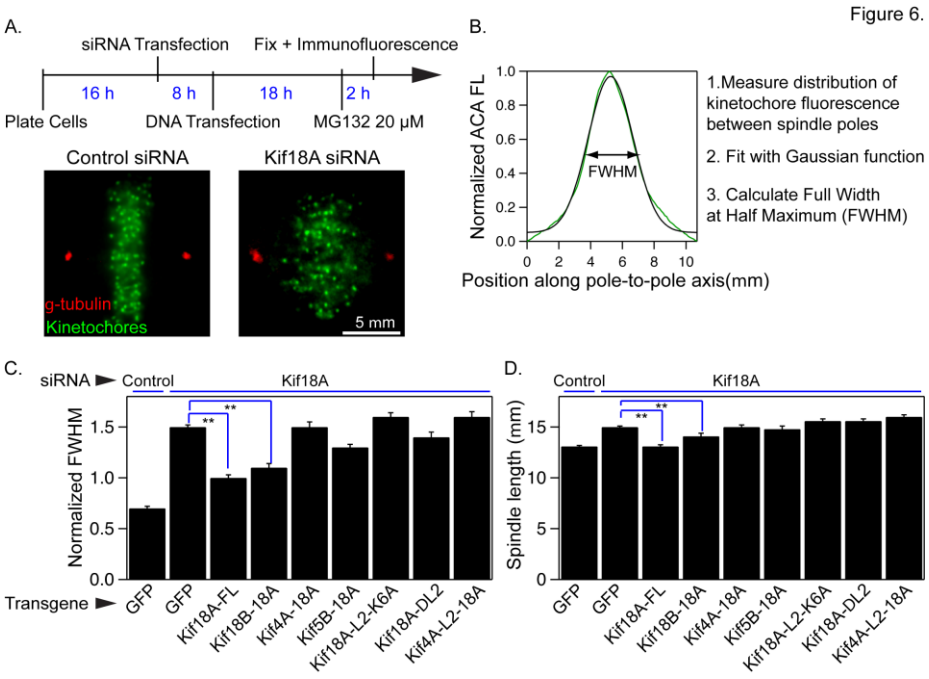

Figure 4-6. Kinesin-8 loop2 is required for mitotic chromosome alignment and spindle length regulation.

(A) Schematic of experimental design. Representative images show control and Kif18A siRNA treated cells immunostained with ACA (centromeres, green) and γ-tubulin (red) antibodies. (B) Representative plot of centromere (ACA) fluorescence distribution as a function of position along the pole-to-pole axis. Fluorescence data were fit with a Gaussian function and the full width at half max (FWHM) was calculated as a metric for centromere alignment. (C-D) Graphs of average FWHM (C) and average spindle length (D) calculated from cells transfected with the indicated siRNAs and transgenes. ** indicates $p<0.01$.

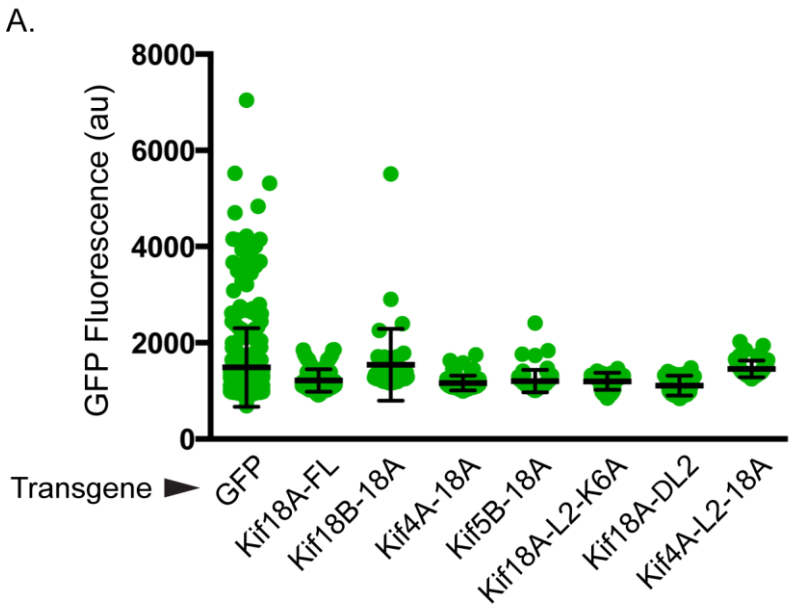

Figure 4-S1. Quantification of GFP-kinesin levels.

(A) Plot of integrated GFP fluorescence intensities in the region of the spindle from individual cells depleted of Kif18A and transfected with GFP or the indicated GFP-tagged kinesin. The population of cells measured was used to evaluate the localization (Figures 1C and 4C), chromosome alignment activity (Figure 6C) and effects on spindle length (Figure 6D) for each kinesin. Bars indicate the mean ± s.d. The number of cells evaluated for each construct (N) is reported above the graph.

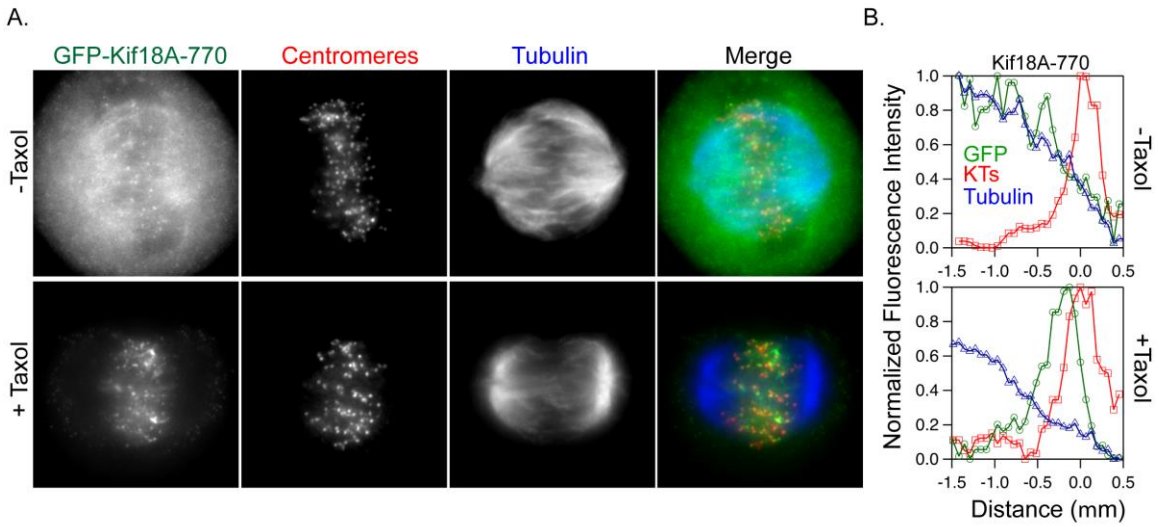

Figure 4-S2. Kif18A-770 concentrates at K-fiber ends in taxol treated cells.

(A) Fluorescent micrographs of GFP-tagged Kif18A-770 (green) in Kif18A-depleted HeLa cells immunostained with ACA (centromeres, red) and tubulin (blue) in the absence (top panels) or presence (bottom panels) of taxol. (B) Linescans of GFP-tagged Kif18A-770 (green trace) relative to tubulin (blue trace) and ACA (red trace) along K-fibers in untreated (top plot) or taxol-treated (bottom plot) cells. (C) Anti-GFP Western blot of a lysate from cells depleted of Kif18A and transfected with GFP-Kif18A-770 (lane 1) compared to 50 ng of purified Kif18A-GFP (lane 2).

CHAPTER 5: DISCUSSION

Data presented in this dissertation elucidates a mechanism for the previously observed temporal coordination of chromosome alignment and silencing of the spindle assembly checkpoint and address its requirement in mammalian development. Our data indicate that the kinesin-8 motor Kif18A has two separable functions that can simultaneously promote stable bioriented attachments and chromosome alignment. We show that Kif18A is required for chromosome alignment in mouse primary embryonic fibroblasts (MEFs) and germline precursor cells, however, it is only necessary for proliferation of germ cells. Our data suggest that primordial germ cells, and certain tumor cells, rely on Kif18A for the stabilization of kinetochore-microtubule attachments and efficient metaphase-to-anaphase transition. We find that Kif18A enhances stable kinetochore-microtubule attachments by recruiting PP1 to the kinetochore-microtubule interface, where it dephosphorylates the kinetochore protein Hec1. Hec1 dephosphorylation enhances electrostatic interactions between kinetochores and microtubules (DeLuca et al., 2005; DeLuca et al., 2006). We propose that this newly characterized function for Kif18A, in combination with its regulation of K fiber dynamics, allows the motor to temporally coordinate stable kinetochore-microtubule attachment and chromosome alignment. Furthermore, Kif18A's ability to directly suppress K fiber plus-end dynamics and restrict chromosome movements to the spindle midzone depends on the motor's unique ability to stably associate with the plus-ends of kinetochore microtubules. Through structure function studies of Kif18A, we identified that the extended Loop2 region in the motor domain of Kif18A is

necessary for stable microtubule plus-end binding. Collectively, this work advances our understanding of the molecular mechanisms controlling the organization and attachment of mitotic chromosomes within the spindle and illuminates interesting cell-type specific dependencies for these mechanisms during mammalian development.

Our work indicates that there are cell lineage dependent requirement for Kif18A during mammalian development. We find that primary embryonic fibroblasts derived from *Kif18A*$^{gcd2/gcd2}$ (Kif18A-R308K) mice divide with almost normal timing even though they require Kif18A for chromosome alignment. In contrast, primordial germ cells in *Kif18A*$^{gcd2/gcd2}$ arrest in mitosis due to kinetochore-microtubule attachment defects, leading to a loss of germ cells and infertility. The question remains as to why certain cell types, even within the same animal, require Kif18A to silence the spindle assembly checkpoint while others do not. This is suggestive of a compensatory mechanism that allows somatic cells to silence the spindle assembly checkpoint and divide without Kif18A, while primordial germ cells rely on Kif18A for proliferation. Incidentally, mouse strains with different genetic backgrounds show variable penetrance in homozygous animals (Reinholdt et al., 2006). It has been reported that inbred strains such as C57/BL6 present with about a 65% phenotypic penetrance, as opposed to the outbred castaneus strains, with over 90% phenotypic penetrance (Reinholdt et al., 2006). Furthermore, Kif18A null mice that were bred in a C57/BL6 background show a sex-specific germline defect, with male mice displaying severe germ line depletion when compared to the female littermates (Liu et al., 2010b).

Interestingly, Kif18A mutations are not the only lesions identified that result in a germline-specific defect. Evidence of germ cell specific mitotic defects have been reported in a mouse model containing a phosphorylation site mutation in the enzyme separase. Separase is a proteinase that cleaves cohesin upon anaphase onset, and remains inactive by its inhibitor securin. The E3 ubiquitin ligase APC ubiquitylates Securin, marking it for degradation upon commitment to enter anaphase (Zou et al., 1999). The phosphosite that has been mutated (S1121A) is an inhibitory phosphorylation site, which has a parallel function in keeping separase inactive (Huang et al., 2008). Separase mutant mice show sexual dimorphism in primordial germ cell development. In male mutant mice, germline cells are completely depleted, while females have a modest depletion of the germline precursor cells (Xu et al., 2011). This study reveals that female PGCs express higher levels of securin, which can compensate for the loss of inhibitory phosphorylation on separase and prevent premature chromosome segregation. Thus, females carrying this separase mutation are able to maintain a germline population. Although the Kif18A mutants in the castaneus background show germline defects in both sexes, the Separase mutant study demonstrates that genetic, or epigenetic, differences between cell types can account for the extent to which phenotypes manifest in different cell types.

Given the data on strain-dependent phenotypic penetrance for functional Kif18A depletion in mice, a genetic screen identifying specific regions that vary between the strains may inform the molecular basis for Kif18A requirement in different mouse backgrounds. Findings from mouse genetic modifier screens could also shed

light on why human somatic cells such as RPE1 and MCF10As are less sensitive to Kif18A depletion, while cells derived from tumors such as MDA-MB-231s and HeLa cells depend on Kif18A for division. In fact, an initial genetic modifier screen has been done in the Reinholdt lab. They isolated the region that differs between the C57/BL6 and the castaneus strains to about a 1 Mb region on chromosome 2 (Czechanski et al., 2015; Reinholdt et al., 2006). Many of the genes have no known cell division roles, but interestingly, a few of the candidate genes do, including the catalytic subunit of PP1ɣ. Other genes of interest include subunits 5 and 7 of the anaphase promoting complex (APC), the E3 ubiquitin ligase that allows metaphase-to-anaphase transition. Unfortunately, there were no detectable differences in transcription or single nucleotide polymorphisms (SNPs) within the gene that codes for the catalytic subunit of PP1ɣ. Potential mutations within the untranslated regions of PP1ɣ could affect overall protein levels, but such mutations have not been found in our initial screen. However, the modifier screen did identify a missense mutation, and a few SNPs in APC5 and APC7 subunits. APC activity is required for the degradation of many cell cycle regulators, including cyclin B and securin, which prompts the cells to transition into anaphase (Fang et al., 1998a; Fang et al., 1998b; Prinz et al., 1998; Sudakin et al., 2001; Thornton and Toczyski, 2003). It is feasible that changes in the expression levels of certain subunits can regulate the efficacy of the E3 ubiquitin ligase activity of APC, and influence cells' sensitivity to Kif18A depletion.

In general, any cell-type specific changes in the regulation of Hec1 affinity for microtubules could also underlie a requirement for Kif18A during division. In support

of this idea, targeting active Aurora B to the outer kinetochore is sufficient to induce microtubule detachment from the kinetochore (Liu and Lampson, 2009). In contrast, tethering PP1 to the outer kinetochore decreases chromosome movement, indicating that additional recruitment of PP1 can suppress microtubule dynamics and normal chromosome movement. Similar suppression of chromosome oscillations can be seen in cells overexpressing Kif18A and cells expressing Hec1-9A (Zaytsev et al., 2014). Therefore, changes in protein levels of Aurora B activity modulators, or even Aurora B or PP1 levels themselves, could account for cell-type specific, Kif18A-dependent kinetochore-microtubule attachments. Since Aurora B affects both the spindle assembly checkpoint mechanism and the phosphorylation state of proteins that electrostatically interact with microtubules, overall Aurora B levels could certainly have an effect on the sensitivity of the spindle assembly checkpoint. It may be informative to compare protein expression profiles of primordial germline cells and somatic cells to determine if regulators of microtubule attachments or the checkpoint vary between the two populations.

The fact that somatic cells lacking Kif18A function can divide without aligning chromosomes challenges the idea that chromosome alignment itself is necessary for normal mitotic progression. However, this observation agrees with studies demonstrating that kinetochore microtubule binding is sufficient to silence the spindle assembly checkpoint (Etemad et al., 2015; Tauchman et al., 2015). Cells expressing a high affinity Hec1 variant, Hec1-9A, are able to enter anaphase in the presence of

chromosome pairs that are not at the metaphase plate or with monopolar spindles that do not contain a metaphase plate at all (Etemad et al., 2015; Tauchman et al., 2015).

While the exact reason as to why cells align their genomic material prior to segregation is currently unclear, emerging evidence suggests a primary function is to preserve the organization of chromosomes into a single nucleus within each daughter cell at the end of cell division. Chromosomes must stay close to each other during late anaphase/telophase to form a contiguous nuclear envelope within the newly formed daughter cells (Hatch et al., 2013). Current research going on in the Stumpff lab shows that chromosome alignment does not necessarily promote genomic integrity by promoting equal segregation of chromosomes, but it does so by preventing micronuclei from forming (Fonseca, 2018). Thus, chromosome alignment may contribute to maintaining genomic stability by spatially compacting separated chromatids during anaphase, leading to the formation of a single nuclear envelope.

Our work also elucidated the mechanism underlying Kif18A's role in promoting kinetochore microtubule attachment. We find that an evolutionarily conserved phosphatase (PP1) binding site in the C-terminal tail of Kif18A (De Wever et al., 2014; Hafner et al., 2014; Meadows et al., 2011) is required for Kif18A-dependent stabilization of kinetochore-microtubule attachments. It might be worth investigating the consequences of disrupting Kif18A-PP1 interaction in a mouse model. If mice carrying the PP1 binding site mutation (Kif18A $A^{612}VVVA^{615}$) recapitulate the germline depletion phenotype that has been observed in our $Kif18A^{gcd2/gcd2}$ model, this

defect can be attributed to Kif18A's role in maintaining kinetochore-microtubule attachments.

While there are several verified mechanisms of recruiting PP1 to kinetochores, none of these can account for the temporal changes in Hec1 phosphorlylation observed during mitotic progression. For instance, the known methods of PP1 recruitment are not microtubule dependent (Rosenberg et al., 2011; Trinkle-Mulcahy et al., 2006). Furthermore, the proteins that recruit PP1 are already incorporated to the kinetochore prior to mitotic entry, which does not explain the time-dependent increase in PP1 localization observed during mitosis (Trinkle-Mulcahy et al., 2006; Vagnarelli et al., 2006; Wurzenberger et al., 2012). However, this temporal change in PP1 accumulation could be explained by a similar time-dependent increase in Kif18A accumulation observed during mitosis (Mayr et al., 2007; Stumpff et al., 2008). Kif18A-PP1 reinforcement of microtubules on the growing K fiber, via dephosphorylation of Hec1, could contribute to the observed increase in microtubules that are bound to the kinetochore between prometaphase and metaphase (Long et al., 2017).

The question remains as to how Kif18A actually recruits PP1 near the kinetochore. Even though changes in the amount of PP1 localization mirrors the kinetics of Kif18A accumulation at the plus-ends, more work has to be done in order to understand if the Kif18A-PP1 interaction is transient or sustained throughout Kif18A's translocation along the microtubule lattice. In addition, it would be interesting to determine if the Kif18A tail activates PP1 or simply recruits it to the kinetochore. Phosphatases are generally activated by the regulatory domain that recruits them with

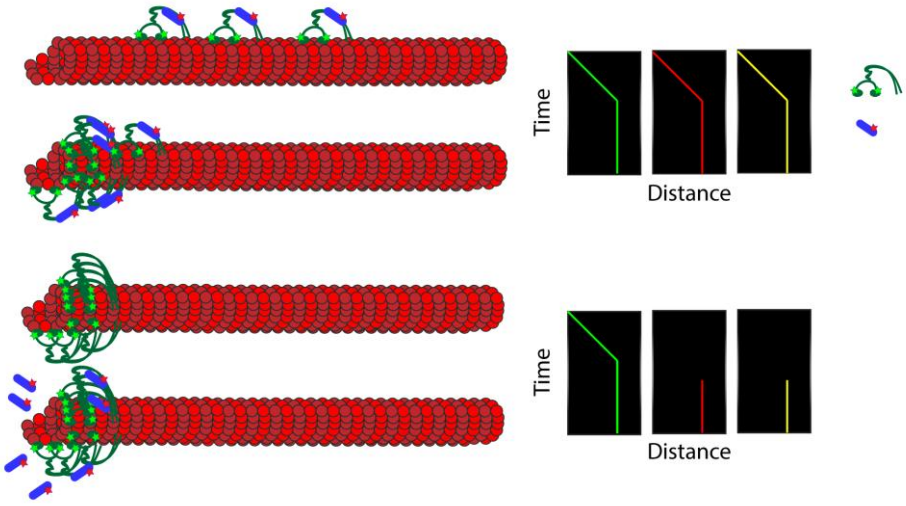

Figure 5-1. Schematic of a single-molecule Kif18A-PP1 co(trans)localization assay. Purified GFP-Kif18AFL combined with purified mCherry-PP1ɣ can be perfused into a flow cell, and plus-end directed motility can be observed. 1.) If Kif18A transports PP1 directly to the microtubule tips, we would expect to see overlapping kymographs with GFP-Kif18A and mCherry-PP1. 2.) If Kif18A simply provides additional binding sites for PP1, then we do not expect to see mCherry-PP1 travel along the microtubule lattice. In fact, we would expect to see mCherry-PP1 visible on the kymograph only after Kif18A has accumulated at the MT plus-ends.

some exceptions, such as Sds22, which binds PP1 via an unconventional binding motif (Tappan and Chamberlin, 2008; Wurzenberger et al., 2012) A short peptide containing the PP1 binding motif is sufficient to enhance phosphatase activity (Tappan and Chamberlin, 2008). However, the peptides containing the conserved PP1 binding motif that have been tested varied in length and showed a wide range of affinities for PP1, from nM to μM (Tappan and Chamberlin, 2008). Therefore, the affinity between PP1 and the conserved binding motif in Kif18A's tail could affect Kif18A-PP1 function at the kinetochore. Two different recruitment mechanisms could explain Kif18A-dependent PP1 recruitment at the kinetochore. First, Kif18A and PP1 associate with high enough affinity that allows the motor to transport PP1 along the entire half-spindle length of several microns. This could be tested using a single-molecule approach with purified proteins to determine if Kif18A carries PP1 along the length of a microtubule (Figure 4-1). Fluorescently tagged PP1 would be combined with purified full-length Kif18A in a single molecule motility assay. If both fluorescent centroids translocate along the microtubule together, this would suggest that Kif18A transports PP1 along the microtubule to the ends (Figure 4-1, 1.). To observe PP1 transport by Kif18A, the interaction between Kif18A and PP1 must occur with high affinity. An alternative recruitment method is for Kif18A to provide a scaffold to which PP1 can bind once Kif18A localizes to the plus-ends. In this case, PP1 fluorescence will colocalize with Kif18A fluorescence transiently and will be observed most frequently where Kif18A accumulates at microtubule plus-ends (Figure 4-1, 2.). This potential mechanism can still provide temporal PP1 recruitment, as Kif18A accumulation increases throughout

mitosis, with the highest accumulation occurring around the metaphase-to-anaphase transition. Furthermore, since PP1 is ubiquitously expressed in the cytoplasm, localization of the activating regulatory element (i.e. PP1 binding motif on Kif18A C-terminus) could explain how PP1 can still exhibit substrate specificity. It will be also interesting to determine the affinity of PP1 with the Aurora B consensus site in Hec1 to determine the potential for a 'hand off 'of PP1 from one binding partner to the next.

Our data demonstrating Kif18A-dependent Hec1 dephosphorylation could explain the time-dependent changes in kinetochore affinity, more specifically Hec1 affinity, to the microtubule lattice. Using the activity of a slow, plus-end directed kinesin like Kif18A to deliver PP1 near the kinetochore provides temporal control over Hec1 affinity. One question that remains to be answered is: Do cells require stable Kif18A-PP1 accumulation for checkpoint silencing or is Kif18A-PP1 accumulation no longer necessary once the checkpoint has been silenced at a particular kinetochore? Utilizing fluorescently labeled MAD2 as a reporter of unattached kinetochores, we can determine the need for transient vs stable association of Kif18A-PP1 at K fiber plus-ends. If transient motor accumulation is necessary, then once all MAD2 is removed from the kinetochores, removing Kif18A would not result in recruitment of the checkpoint protein back to kinetochores. According to a recent study, MAD2 displacement from the kinetochore requires end-on attachments of only about half of the number of microtubules that make up a K fiber (Kuhn and Dumont, 2017). If this is true, once Kif18A-PP1 dependent stabilization occurs, this should be sufficient to maintain checkpoint silencing to keep MAD2 displaced. A way to test this would be by

using a system that can offer temporal control over Kif18A depletion from the spindle, such as a rapamycin-induced dimerization system. One of the dimerization domains would be tethered to Kif18A and the other to a plasma membrane localized polypeptide, as previously described (Wordeman et al., 2016). Cells can be biochemically arrested in MG132, a proteasome inhibitor, to allow all of the MAD2 to be displaced from the kinetochore but prevent anaphase entry. Once the frequency of MAD2 localization at the kinetochores decreases, then rapamycin would be added to remove Kif18A from the spindle. MAD2 localization would then be monitored over time to see if MAD2 foci reappear at kinetochores.

One of the proposed ways in which the spindle assembly checkpoint can be silenced is through induced tension when bioriented end-on attachments occur (Liu et al., 2009). However, tension across sisters can be induced prior to biorientation through a CENP-E dependent lateral attachment with preexisting spindle microtubules. More importantly, interkinetochore stretch via lateral attachments do not remove the checkpoint protein MAD2 from the kinetochore (Kuhn and Dumont, 2017). Only the presence of end-on attachments remove MAD2 from the kinetochore (Kuhn and Dumont, 2017). Consistent with this, our data demonstrate that Kif18A-PP1 promotes checkpoint silencing by enhancing the electrostatic interaction between the Hec1 N-terminal tail and microtubules. Even when interkinetochore stretch is observed, cells expressing Kif18A that cannot bind PP1 still showed attachment defects. It could be that enhanced electrostatic interaction of Hec1 via Kif18A-PP1 dependent

dephosphorylation helps to maintain stable end-on microtubule attachments that promote SAC silencing.

Kif18A's ability to localize to plus-ends and stably associate there is integral for its function as a microtubule dynamics attenuator, both *in vitro* and in cells (Hafner et al., 2014; Kim et al., 2014; Mayr et al., 2007; Stumpff et al., 2008; Weaver et al., 2011). Our data indicate that the unique surface Loop2 in the motor domain is required for stable plus-end binding, which is necessary for Kif18A's function in chromosome alignment. The Loop2 region of kinesin-13 and other kinesin-8 motor domains have been implicated in modifying microtubule plus-ends as well. (Arellano-Santoyo et al., 2017; Chatterjee et al., 2016; Wang et al., 2017). Interestingly, the depolymerizing kinesins Kip3 (kinesin-8, budding yeast), Kif2C/MCAK (kinesin-13, human), and Kif19 (kinesin-8, human) each have an elongated Loop2. However, given that Kif18A and the closely related motor Kif18B do not seem to exhibit depolymerizing activities suggests there must be differences among the activities of different Loop2 regions or that contributions from other regions within the motor domain define the effects of each kinesin on microtubule ends.

Along these lines, there could be other regions in Kif18A that can account for its activity as a microtubule attenuator. The C-terminal tail of Kif18A is important for tethering the motor to the microtubule lattice, enhancing its long dwell time on the microtubule to help the motor traverse to the plus-ends (Stumpff et al., 2011; Weaver et al., 2011). Interestingly, a Kif18A motor that has a C-terminal truncation (Kif18A-Δ770) shows reduced dwell time at microtubule plus-ends even when it can visibly

accumulate there and this is associated with reduced chromosome alignment activity. These data suggest that Kif18A requires both the unique Loop2 in the motor domain AND the C-terminal tail for its plus-end binding and regulation of microtubule dynamics. Cryo-EM studies with the motor domain of closely related Kip3 and microtubules revealed that Kip3 prefers to bind to a curved conformation of the microtubule, which is seen at the plus-ends (Arellano-Santoyo et al., 2017). They have identified Loop11, in addition to Loop2, in the Kip3 motor domain that contribute to Kip3's preference of curved microtubules at the plus-end tips (Arellano-Santoyo et al., 2017). It could be possible that Loop11 in Kif18A also provides specificity for curved tubulin similarly to Kip3, but Kif18A-specific residues tune the activity such that plus-end binding does not induce depolymerization. Thus, elucidating the role of other regions on Kif18A, such as the C-terminal tail and Loop11, which contribute to stable microtubule plus-end binding could provide insight regarding the mechanism of its unique microtubule attenuating activity.

It remains unclear why the closely related kinesin-8 motors Kif18A and Kip3 exhibit different effects on microtubule dynamics. However, it is interesting to note that yeasts do not have any kinesin-13 family members, but still require depolymerase activity to regulate spindle lengths (Hildebrandt and Hoyt, 2000). Phylogenetically, kinesin-8s and kinesin-13s are more closely related to each other than they are to other kinesin families. Therefore, it is possible that as kinesin-13s have evolved to have specific depolymerizing activity in multicellular eukaryotes some kinesin-8s evolved to function as attenuators. Supporting the idea that the fine-tuning of kinesin activities is

functionally relevant, we find that mitotic kinesins that display similar activities of limiting microtubule dynamics are not interchangeable. Additionally, MCAK has a much more robust depolymerizing activity when compared to Kip3 (Arellano-Santoyo et al., 2017; Gupta et al., 2006; Varga et al., 2006; Wordeman and Mitchison, 1995). Therefore, it is unsurprising that kinesins with similar structures, such as elongated surface loops, can have different activities at the plus-ends of microtubules.

While there is a significant amount of data elucidating Kif18A's role in chromosome alignment by dampening microtubule dynamics, an important question that still remains to be answered is how this activity leads to directional switching during chromosome oscillations. Chromosome pairs travel towards one pole, abruptly switch direction, and continue towards the opposite pole. During prometaphase, chromosome movements are eventually limited to right around the midzone (Jaqaman et al., 2010; Skibbens et al., 1993; Stumpff et al., 2012). Currently, some models attribute Kif18A's contentious depolymerase activity to the induction of directional changes, however, there is mounting evidence that it is Kif18A's microtubule attenuating activities at the plus-ends of microtubules that induce directional switches (Stumpff et al., 2012). The latter scenario is more consistent with what we currently know about mammalian Kif18A. We propose that attenuating microtubule dynamics on the growing K fiber, while the poleward moving kinetochore continues on its trajectory, can induce tension that rescues microtubule polymerization inducing a directional switch. As the formerly poleward kinetochore starts traveling towards the opposite pole, the tension is dissipated, and depolymerization on the sister kinetochore is

induced. It has been shown that Hec1 phosphorylation contributes to its interaction on the growing K fiber.Kif18A-PP1interaction can enhance the tension-induced rescue of poleward moving K fiber by stabilizing kinetochore-microtubule attachments on the growing K fiber, facilitating a directional switch.

Taken together, Kif18A's prolonged plus-end binding and its slow, but extremely long run length both contribute to chromosome alignment. These characteristics, combined with the motor's PP1 association work synergistically to coordinate chromosome alignment with fine-tuning of kinetochore affinity for punctual anaphase onset. These separable activities can explain the chromosome misalignment and SAC-dependent metaphase arrest observed in cells lacking Kif18A function.

REFERENCES

Akiyoshi, B., K.K. Sarangapani, A.F. Powers, C.R. Nelson, S.L. Reichow, H. Arellano-Santoyo, T. Gonen, J.A. Ranish, C.L. Asbury, and S. Biggins. 2010. Tension directly stabilizes reconstituted kinetochore-microtubule attachments. *Nature*. 468:576-579.

Arellano-Santoyo, H., E.A. Geyer, E. Stokasimov, G.Y. Chen, X. Su, W. Hancock, L.M. Rice, and D. Pellman. 2017. A Tubulin Binding Switch Underlies Kip3/Kinesin-8 Depolymerase Activity. *Developmental cell*. 42:37-51 e38.

Bernat, R.L., M.R. Delannoy, N.F. Rothfield, and W.C. Earnshaw. 1991. Disruption of centromere assembly during interphase inhibits kinetochore morphogenesis and function in mitosis. *Cell*. 66:1229-1238.

Brouhard, G.J., and A.J. Hunt. 2005. Microtubule movements on the arms of mitotic chromosomes: polar ejection forces quantified in vitro. *Proceedings of the National Academy of Sciences of the United States of America*. 102:13903-13908.

Cai, S., C.B. O'Connell, A. Khodjakov, and C.E. Walczak. 2009. Chromosome congression in the absence of kinetochore fibres. *Nature cell biology*. 11:832-838.

Caldas, G.V., K.F. DeLuca, and J.G. DeLuca. 2013. KNL1 facilitates phosphorylation of outer kinetochore proteins by promoting Aurora B kinase activity. *The Journal of cell biology*. 203:957-969.

Cassimeris, L., C.L. Rieder, G. Rupp, and E.D. Salmon. 1990. Stability of microtubule attachment to metaphase kinetochores in PtK1 cells. *Journal of cell science*. 96 (Pt 1):9-15.

Chatterjee, C., M.P. Benoit, V. DePaoli, J.D. Diaz-Valencia, A.B. Asenjo, G.J. Gerfen, D.J. Sharp, and H. Sosa. 2016. Distinct Interaction Modes of the Kinesin-13 Motor Domain with the Microtubule. *Biophys J*. 110:1593-1604.

Cheeseman, I.M., J.S. Chappie, E.M. Wilson-Kubalek, and A. Desai. 2006. The conserved KMN network constitutes the core microtubule-binding site of the kinetochore. *Cell*. 127:983-997.

Cheeseman, I.M., S. Niessen, S. Anderson, F. Hyndman, J.R. Yates, 3rd, K. Oegema, and A. Desai. 2004. A conserved protein network controls assembly of the outer kinetochore and its ability to sustain tension. *Genes & development*. 18:2255-2268.

Chen, R.H., A. Shevchenko, M. Mann, and A.W. Murray. 1998. Spindle checkpoint protein Xmad1 recruits Xmad2 to unattached kinetochores. *The Journal of cell biology*. 143:283-295.

Ciferri, C., J. De Luca, S. Monzani, K.J. Ferrari, D. Ristic, C. Wyman, H. Stark, J. Kilmartin, E.D. Salmon, and A. Musacchio. 2005. Architecture of the human ndc80-hec1 complex, a critical constituent of the outer kinetochore. *The Journal of biological chemistry*. 280:29088-29095.

Cimini, D., B. Howell, P. Maddox, A. Khodjakov, F. Degrassi, and E.D. Salmon. 2001. Merotelic kinetochore orientation is a major mechanism of aneuploidy in mitotic mammalian tissue cells. *The Journal of cell biology*. 153:517-527.

Cimini, D., B. Moree, J.C. Canman, and E.D. Salmon. 2003. Merotelic kinetochore orientation occurs frequently during early mitosis in mammalian tissue cells and error correction is achieved by two different mechanisms. *Journal of cell science*. 116:4213-4225.

Cimini, D., X. Wan, C.B. Hirel, and E.D. Salmon. 2006. Aurora kinase promotes turnover of kinetochore microtubules to reduce chromosome segregation errors. *Current biology : CB*. 16:1711-1718.

Crasta, K., N.J. Ganem, R. Dagher, A.B. Lantermann, E.V. Ivanova, Y. Pan, L. Nezi, A. Protopopov, D. Chowdhury, and D. Pellman. 2012. DNA breaks and chromosome pulverization from errors in mitosis. *Nature*. 482:53-58.

Czechanski, A., H. Kim, C. Byers, I. Greenstein, J. Stumpff, and L.G. Reinholdt. 2015. Kif18a is specifically required for mitotic progression during germ line development. *Developmental biology*. 402:253-262.

De Wever, V., I. Nasa, D. Chamousset, D. Lloyd, M. Nimick, H. Xu, L. Trinkle-Mulcahy, and G.B. Moorhead. 2014. The human mitotic kinesin KIF18A binds protein phosphatase 1 (PP1) through a highly conserved docking motif. *Biochemical and biophysical research communications*.

DeLuca, J.G., Y. Dong, P. Hergert, J. Strauss, J.M. Hickey, E.D. Salmon, and B.F. McEwen. 2005. Hec1 and nuf2 are core components of the kinetochore outer plate essential for organizing microtubule attachment sites. *Molecular biology of the cell*. 16:519-531.

DeLuca, J.G., W.E. Gall, C. Ciferri, D. Cimini, A. Musacchio, and E.D. Salmon. 2006. Kinetochore microtubule dynamics and attachment stability are regulated by Hec1. *Cell*. 127:969-982.

DeLuca, K.F., S.M. Lens, and J.G. DeLuca. 2011. Temporal changes in Hec1 phosphorylation control kinetochore-microtubule attachment stability during mitosis. *Journal of cell science*. 124:622-634.

Drpic, D., A.J. Pereira, M. Barisic, T.J. Maresca, and H. Maiato. 2015. Polar Ejection Forces Promote the Conversion from Lateral to End-on Kinetochore-Microtubule Attachments on Mono-oriented Chromosomes. *Cell reports*. 13:460-468.

Du, Y., C.A. English, and R. Ohi. 2010. The kinesin-8 Kif18A dampens microtubule plus-end dynamics. *Current biology : CB*. 20:374-380.

Earnshaw, W.C., R.L. Bernat, C.A. Cooke, and N.F. Rothfield. 1991. Role of the centromere/kinetochore in cell cycle control. *Cold Spring Harbor symposia on quantitative biology*. 56:675-685.

Etemad, B., T.E. Kuijt, and G.J. Kops. 2015. Kinetochore-microtubule attachment is sufficient to satisfy the human spindle assembly checkpoint. *Nature communications*. 6:8987.

Fang, G., H. Yu, and M.W. Kirschner. 1998a. The checkpoint protein MAD2 and the mitotic regulator CDC20 form a ternary complex with the anaphase-promoting complex to control anaphase initiation. *Genes & development*. 12:1871-1883.

Fang, G., H. Yu, and M.W. Kirschner. 1998b. Direct binding of CDC20 protein family members activates the anaphase-promoting complex in mitosis and G1. *Molecular cell*. 2:163-171.

Fonseca, C., Malaby, HLH, Sepaniac, LA, Martin, W, Byers, C, Czechanski, A, Messinger, D, Tang, M, Ohi, R, Reinholdt, LG, and Stumpff, JK. 2018. Mitotic chromosome alignment is required for proper nuclear envelope reassembly. *Cell*.

Gupta, M.L., Jr., P. Carvalho, D.M. Roof, and D. Pellman. 2006. Plus end-specific depolymerase activity of Kip3, a kinesin-8 protein, explains its role in positioning the yeast mitotic spindle. *Nature cell biology*. 8:913-923.

Hafner, J., M.I. Mayr, M.M. Mockel, and T.U. Mayer. 2014. Pre-anaphase chromosome oscillations are regulated by the antagonistic activities of Cdk1 and PP1 on Kif18A. *Nature communications*. 5:4397.

Hatch, E.M., A.H. Fischer, T.J. Deerinck, and M.W. Hetzer. 2013. Catastrophic nuclear envelope collapse in cancer cell micronuclei. *Cell*. 154:47-60.

Hildebrandt, E.R., and M.A. Hoyt. 2000. Mitotic motors in Saccharomyces cerevisiae. *Biochimica et biophysica acta*. 1496:99-116.

Hinchcliffe, E.H., C.A. Day, K.B. Karanjeet, S. Fadness, A. Langfald, K.T. Vaughan, and Z. Dong. 2016. Chromosome missegregation during anaphase triggers p53 cell cycle arrest through histone H3.3 Ser31 phosphorylation. *Nature cell biology*. 18:668-675.

Hogge, W.A., A.L. Byrnes, M.C. Lanasa, and U. Surti. 2003. The clinical use of karyotyping spontaneous abortions. *American journal of obstetrics and gynecology*. 189:397-400; discussion 400-392.

Hoyt, M.A., L. Totis, and B.T. Roberts. 1991. Saccharomyces-Cerevisiae Genes Required for Cell-Cycle Arrest in Response to Loss of Microtubule Function. *Cell*. 66:507-517.

Huang, X., C.V. Andreu-Vieyra, J.P. York, R. Hatcher, T. Lu, M.M. Matzuk, and P. Zhang. 2008. Inhibitory phosphorylation of separase is essential for genome stability and viability of murine embryonic germ cells. *PLoS biology*. 6:e15.

Hwang, L.H., L.F. Lau, D.L. Smith, C.A. Mistrot, K.G. Hardwick, E.S. Hwang, A. Amon, and A.W. Murray. 1998. Budding yeast Cdc20: a target of the spindle checkpoint. *Science*. 279:1041-1044.

Irniger, S., S. Piatti, C. Michaelis, and K. Nasmyth. 1995. Genes involved in sister chromatid separation are needed for B-type cyclin proteolysis in budding yeast. *Cell*. 81:269-278.

Itoh, G., M. Ikeda, K. Iemura, M.A. Amin, S. Kuriyama, M. Tanaka, N. Mizuno, H. Osakada, T. Haraguchi, and K. Tanaka. 2018. Lateral attachment of kinetochores to microtubules is enriched in prometaphase rosette and facilitates chromosome alignment and bi-orientation establishment. *Scientific reports*. 8:3888.

Jaqaman, K., E.M. King, A.C. Amaro, J.R. Winter, J.F. Dorn, H.L. Elliott, N. McHedlishvili, S.E. McClelland, I.M. Porter, M. Posch, A. Toso, G. Danuser, A.D. McAinsh, P. Meraldi, and J.R. Swedlow. 2010. Kinetochore alignment within the metaphase plate is regulated by centromere stiffness and microtubule depolymerases. *The Journal of cell biology*. 188:665-679.

Jelluma, N., T.B. Dansen, T. Sliedrecht, N.P. Kwiatkowski, and G.J. Kops. 2010. Release of Mps1 from kinetochores is crucial for timely anaphase onset. *The Journal of cell biology*. 191:281-290.

Kapoor, T.M., M.A. Lampson, P. Hergert, L. Cameron, D. Cimini, E.D. Salmon, B.F. McEwen, and A. Khodjakov. 2006. Chromosomes can congress to the metaphase plate before biorientation. *Science*. 311:388-391.

Kim, H., C. Fonseca, and J. Stumpff. 2014. A unique kinesin-8 surface loop provides specificity for chromosome alignment. *Molecular biology of the cell*.

King, R.W., J.M. Peters, S. Tugendreich, M. Rolfe, P. Hieter, and M.W. Kirschner. 1995. A 20S complex containing CDC27 and CDC16 catalyzes the mitosis-specific conjugation of ubiquitin to cyclin B. *Cell*. 81:279-288.

Kline, S.L., I.M. Cheeseman, T. Hori, T. Fukagawa, and A. Desai. 2006. The human Mis12 complex is required for kinetochore assembly and proper chromosome segregation. *The Journal of cell biology*. 173:9-17.

Kuhn, J., and S. Dumont. 2017. Spindle assembly checkpoint satisfaction occurs via end-on but not lateral attachments under tension. *The Journal of cell biology*. 216:1533-1542.

Lengauer, C., K.W. Kinzler, and B. Vogelstein. 1997. Genetic instability in colorectal cancers. *Nature*. 386:623-627.

Levesque, A.A., and D.A. Compton. 2001. The chromokinesin Kid is necessary for chromosome arm orientation and oscillation, but not congression, on mitotic spindles. *The Journal of cell biology*. 154:1135-1146.

Lewis, C.W., and R.M. Golsteyn. 2016. Cancer cells that survive checkpoint adaptation contain micronuclei that harbor damaged DNA. *Cell Cycle*. 15:3131-3145.

Li, R., and A.W. Murray. 1991. Feedback control of mitosis in budding yeast. *Cell*. 66:519-531.

Liu, D., and M.A. Lampson. 2009. Regulation of kinetochore-microtubule attachments by Aurora B kinase. *Biochemical Society transactions*. 37:976-980.

Liu, D., G. Vader, M.J. Vromans, M.A. Lampson, and S.M. Lens. 2009. Sensing chromosome bi-orientation by spatial separation of aurora B kinase from kinetochore substrates. *Science*. 323:1350-1353.

Liu, D., M. Vleugel, C.B. Backer, T. Hori, T. Fukagawa, I.M. Cheeseman, and M.A. Lampson. 2010a. Regulated targeting of protein phosphatase 1 to the outer kinetochore by KNL1 opposes Aurora B kinase. *The Journal of cell biology*. 188:809-820.

Liu, X.S., X.D. Zhao, X. Wang, Y.X. Yao, L.L. Zhang, R.Z. Shu, W.H. Ren, Y. Huang, L. Huang, M.M. Gu, Y. Kuang, L. Wang, S.Y. Lu, J. Chi, J.S. Fen, Y.F. Wang, J. Fei, W. Dai, and Z.G. Wang. 2010b. Germinal Cell Aplasia in Kif18a Mutant

Male Mice Due to Impaired Chromosome Congression and Dysregulated BubR1 and CENP-E. *Genes & cancer*. 1:26-39.

Loncarek, J., O. Kisurina-Evgenieva, T. Vinogradova, P. Hergert, S. La Terra, T.M. Kapoor, and A. Khodjakov. 2007. The centromere geometry essential for keeping mitosis error free is controlled by spindle forces. *Nature*. 450:745-749.

Long, A.F., D.B. Udy, and S. Dumont. 2017. Hec1 Tail Phosphorylation Differentially Regulates Mammalian Kinetochore Coupling to Polymerizing and Depolymerizing Microtubules. *Current biology : CB*. 27:1692-1699 e1693.

Magidson, V., J. He, J.G. Ault, C.B. O'Connell, N. Yang, I. Tikhonenko, B.F. McEwen, H. Sui, and A. Khodjakov. 2016. Unattached kinetochores rather than intrakinetochore tension arrest mitosis in taxol-treated cells. *The Journal of cell biology*. 212:307-319.

Magidson, V., C.B. O'Connell, J. Loncarek, R. Paul, A. Mogilner, and A. Khodjakov. 2011. The spatial arrangement of chromosomes during prometaphase facilitates spindle assembly. *Cell*. 146:555-567.

Magidson, V., R. Paul, N. Yang, J.G. Ault, C.B. O'Connell, I. Tikhonenko, B.F. McEwen, A. Mogilner, and A. Khodjakov. 2015. Adaptive changes in the kinetochore architecture facilitate proper spindle assembly. *Nature cell biology*. 17:1134-1144.

Maiato, H., C.L. Rieder, and A. Khodjakov. 2004. Kinetochore-driven formation of kinetochore fibers contributes to spindle assembly during animal mitosis. *The Journal of cell biology*. 167:831-840.

Mayr, M.I., S. Hummer, J. Bormann, T. Gruner, S. Adio, G. Woehlke, and T.U. Mayer. 2007. The human kinesin Kif18A is a motile microtubule depolymerase essential for chromosome congression. *Current biology : CB*. 17:488-498.

McEwen, B.F., A.B. Heagle, G.O. Cassels, K.F. Buttle, and C.L. Rieder. 1997. Kinetochore fiber maturation in PtK1 cells and its implications for the mechanisms of chromosome congression and anaphase onset. *The Journal of cell biology*. 137:1567-1580.

Meadows, J.C., L.A. Shepperd, V. Vanoosthuyse, T.C. Lancaster, A.M. Sochaj, G.J. Buttrick, K.G. Hardwick, and J.B. Millar. 2011. Spindle checkpoint silencing requires association of PP1 to both Spc7 and kinesin-8 motors. *Developmental cell*. 20:739-750.

Nagaoka, S.I., T.J. Hassold, and P.A. Hunt. 2012. Human aneuploidy: mechanisms and new insights into an age-old problem. *Nature reviews. Genetics*. 13:493-504.

Nagele, R., T. Freeman, L. McMorrow, and H.Y. Lee. 1995. Precise spatial positioning of chromosomes during prometaphase: evidence for chromosomal order. *Science*. 270:1831-1835.

O'Connell, C.B., J. Loncarek, P. Hergert, A. Kourtidis, D.S. Conklin, and A. Khodjakov. 2008. The spindle assembly checkpoint is satisfied in the absence of interkinetochore tension during mitosis with unreplicated genomes. *The Journal of cell biology*. 183:29-36.

Petrovic, A., S. Pasqualato, P. Dube, V. Krenn, S. Santaguida, D. Cittaro, S. Monzani, L. Massimiliano, J. Keller, A. Tarricone, A. Maiolica, H. Stark, and A.

Musacchio. 2010. The MIS12 complex is a protein interaction hub for outer kinetochore assembly. *The Journal of cell biology*. 190:835-852.

Prinz, S., E.S. Hwang, R. Visintin, and A. Amon. 1998. The regulation of Cdc20 proteolysis reveals a role for APC components Cdc23 and Cdc27 during S phase and early mitosis. *Current biology : CB*. 8:750-760.

Przewloka, M.R., Z. Venkei, V.M. Bolanos-Garcia, J. Debski, M. Dadlez, and D.M. Glover. 2011. CENP-C is a structural platform for kinetochore assembly. *Current biology : CB*. 21:399-405.

Qian, J., M. Beullens, J. Huang, S. De Munter, B. Lesage, and M. Bollen. 2015. Cdk1 orders mitotic events through coordination of a chromosome-associated phosphatase switch. *Nature communications*. 6:10215.

Reinholdt, L.G., R.J. Munroe, S. Kamdar, and J.C. Schimenti. 2006. The mouse gcd2 mutation causes primordial germ cell depletion. *Mechanisms of development*. 123:559-569.

Rieder, C.L., A. Schultz, R. Cole, and G. Sluder. 1994. Anaphase onset in vertebrate somatic cells is controlled by a checkpoint that monitors sister kinetochore attachment to the spindle. *The Journal of cell biology*. 127:1301-1310.

Rosenberg, J.S., F.R. Cross, and H. Funabiki. 2011. KNL1/Spc105 recruits PP1 to silence the spindle assembly checkpoint. *Current biology : CB*. 21:942-947.

Salmon, E.D., D. Cimini, L.A. Cameron, and J.G. DeLuca. 2005. Merotelic kinetochores in mammalian tissue cells. *Philosophical transactions of the Royal Society of London. Series B, Biological sciences*. 360:553-568.

Sarangapani, K.K., B. Akiyoshi, N.M. Duggan, S. Biggins, and C.L. Asbury. 2013. Phosphoregulation promotes release of kinetochores from dynamic microtubules via multiple mechanisms. *Proceedings of the National Academy of Sciences of the United States of America*. 110:7282-7287.

Screpanti, E., A. De Antoni, G.M. Alushin, A. Petrovic, T. Melis, E. Nogales, and A. Musacchio. 2011. Direct binding of Cenp-C to the Mis12 complex joins the inner and outer kinetochore. *Current biology : CB*. 21:391-398.

Shrestha, R.L., and V.M. Draviam. 2013. Lateral to end-on conversion of chromosome-microtubule attachment requires kinesins CENP-E and MCAK. *Current biology : CB*. 23:1514-1526.

Silva, P.M., R.M. Reis, V.M. Bolanos-Garcia, C. Florindo, A.A. Tavares, and H. Bousbaa. 2014. Dynein-dependent transport of spindle assembly checkpoint proteins off kinetochores toward spindle poles. *FEBS letters*. 588:3265-3273.

Sivakumar, S., P.L. Janczyk, Q. Qu, C.A. Brautigam, P.T. Stukenberg, H. Yu, and G.J. Gorbsky. 2016. The human SKA complex drives the metaphase-anaphase cell cycle transition by recruiting protein phosphatase 1 to kinetochores. *eLife*. 5.

Skibbens, R.V., V.P. Skeen, and E.D. Salmon. 1993. Directional instability of kinetochore motility during chromosome congression and segregation in mitotic newt lung cells: a push-pull mechanism. *The Journal of cell biology*. 122:859-875.

Stumpff, J., Y. Du, C.A. English, Z. Maliga, M. Wagenbach, C.L. Asbury, L. Wordeman, and R. Ohi. 2011. A tethering mechanism controls the processivity

and kinetochore-microtubule plus-end enrichment of the kinesin-8 Kif18A. *Molecular cell*. 43:764-775.

Stumpff, J., G. von Dassow, M. Wagenbach, C. Asbury, and L. Wordeman. 2008. The kinesin-8 motor Kif18A suppresses kinetochore movements to control mitotic chromosome alignment. *Developmental cell*. 14:252-262.

Stumpff, J., M. Wagenbach, A. Franck, C.L. Asbury, and L. Wordeman. 2012. Kif18A and chromokinesins confine centromere movements via microtubule growth suppression and spatial control of kinetochore tension. *Developmental cell*. 22:1017-1029.

Sudakin, V., G.K. Chan, and T.J. Yen. 2001. Checkpoint inhibition of the APC/C in HeLa cells is mediated by a complex of BUBR1, BUB3, CDC20, and MAD2. *The Journal of cell biology*. 154:925-936.

Sudakin, V., D. Ganoth, A. Dahan, H. Heller, J. Hershko, F.C. Luca, J.V. Ruderman, and A. Hershko. 1995. The cyclosome, a large complex containing cyclin-selective ubiquitin ligase activity, targets cyclins for destruction at the end of mitosis. *Molecular biology of the cell*. 6:185-197.

Sullivan, K.F., M. Hechenberger, and K. Masri. 1994. Human CENP-A contains a histone H3 related histone fold domain that is required for targeting to the centromere. *The Journal of cell biology*. 127:581-592.

Sundin, L.J., G.J. Guimaraes, and J.G. Deluca. 2011. The NDC80 complex proteins Nuf2 and Hec1 make distinct contributions to kinetochore-microtubule attachment in mitosis. *Molecular biology of the cell*. 22:759-768.

Tappan, E., and A.R. Chamberlin. 2008. Activation of protein phosphatase 1 by a small molecule designed to bind to the enzyme's regulatory site. *Chemistry & biology*. 15:167-174.

Tauchman, E.C., F.J. Boehm, and J.G. DeLuca. 2015. Stable kinetochore-microtubule attachment is sufficient to silence the spindle assembly checkpoint in human cells. *Nature communications*. 6:10036.

Thornton, B.R., and D.P. Toczyski. 2003. Securin and B-cyclin/CDK are the only essential targets of the APC. *Nature cell biology*. 5:1090-1094.

Trinkle-Mulcahy, L., J. Andersen, Y.W. Lam, G. Moorhead, M. Mann, and A.I. Lamond. 2006. Repo-Man recruits PP1 gamma to chromatin and is essential for cell viability. *The Journal of cell biology*. 172:679-692.

Uetake, Y., and G. Sluder. 2010. Prolonged prometaphase blocks daughter cell proliferation despite normal completion of mitosis. *Current biology : CB*. 20:1666-1671.

Umbreit, N.T., D.R. Gestaut, J.F. Tien, B.S. Vollmar, T. Gonen, C.L. Asbury, and T.N. Davis. 2012. The Ndc80 kinetochore complex directly modulates microtubule dynamics. *Proceedings of the National Academy of Sciences of the United States of America*. 109:16113-16118.

Vagnarelli, P., D.F. Hudson, S.A. Ribeiro, L. Trinkle-Mulcahy, J.M. Spence, F. Lai, C.J. Farr, A.I. Lamond, and W.C. Earnshaw. 2006. Condensin and Repo-Man-PP1 co-operate in the regulation of chromosome architecture during mitosis. *Nature cell biology*. 8:1133-1142.

Varga, V., J. Helenius, K. Tanaka, A.A. Hyman, T.U. Tanaka, and J. Howard. 2006. Yeast kinesin-8 depolymerizes microtubules in a length-dependent manner. *Nature cell biology*. 8:957-962.

Wang, W., S. Cantos-Fernandes, Y. Lv, H. Kuerban, S. Ahmad, C. Wang, and B. Gigant. 2017. Insight into microtubule disassembly by kinesin-13s from the structure of Kif2C bound to tubulin. *Nature communications*. 8:70.

Weaver, L.N., S.C. Ems-McClung, J.R. Stout, C. LeBlanc, S.L. Shaw, M.K. Gardner, and C.E. Walczak. 2011. Kif18A uses a microtubule binding site in the tail for plus-end localization and spindle length regulation. *Current biology : CB*. 21:1500-1506.

Wollman, R., E.N. Cytrynbaum, J.T. Jones, T. Meyer, J.M. Scholey, and A. Mogilner. 2005. Efficient chromosome capture requires a bias in the 'search-and-capture' process during mitotic-spindle assembly. *Current biology : CB*. 15:828-832.

Wordeman, L., J. Decarreau, J.J. Vicente, and M. Wagenbach. 2016. Divergent microtubule assembly rates after short- versus long-term loss of end-modulating kinesins. *Molecular biology of the cell*. 27:1300-1309.

Wordeman, L., and T.J. Mitchison. 1995. Identification and partial characterization of mitotic centromere-associated kinesin, a kinesin-related protein that associates with centromeres during mitosis. *The Journal of cell biology*. 128:95-104.

Wurzenberger, C., M. Held, M.A. Lampson, I. Poser, A.A. Hyman, and D.W. Gerlich. 2012. Sds22 and Repo-Man stabilize chromosome segregation by counteracting Aurora B on anaphase kinetochores. *The Journal of cell biology*. 198:173-183.

Xu, J., M. Wang, X. Gao, B. Hu, Y. Du, J. Zhou, X. Tian, and X. Huang. 2011. Separase phosphosite mutation leads to genome instability and primordial germ cell depletion during oogenesis. *PloS one*. 6:e18763.

Yajima, J., M. Edamatsu, J. Watai-Nishii, N. Tokai-Nishizumi, T. Yamamoto, and Y.Y. Toyoshima. 2003. The human chromokinesin Kid is a plus end-directed microtubule-based motor. *The EMBO journal*. 22:1067-1074.

Zaytsev, A.V., and E.L. Grishchuk. 2015. Basic mechanism for biorientation of mitotic chromosomes is provided by the kinetochore geometry and indiscriminate turnover of kinetochore microtubules. *Molecular biology of the cell*. 26:3985-3998.

Zaytsev, A.V., L.J. Sundin, K.F. DeLuca, E.L. Grishchuk, and J.G. DeLuca. 2014. Accurate phosphoregulation of kinetochore-microtubule affinity requires unconstrained molecular interactions. *The Journal of cell biology*. 206:45-59.

Zhang, C.Z., A. Spektor, H. Cornils, J.M. Francis, E.K. Jackson, S. Liu, M. Meyerson, and D. Pellman. 2015. Chromothripsis from DNA damage in micronuclei. *Nature*. 522:179-184.

Zhu, C., J. Zhao, M. Bibikova, J.D. Leverson, E. Bossy-Wetzel, J.B. Fan, R.T. Abraham, and W. Jiang. 2005. Functional analysis of human microtubule-based motor proteins, the kinesins and dyneins, in mitosis/cytokinesis using RNA interference. *Molecular biology of the cell*. 16:3187-3199.

Zou, H., T.J. McGarry, T. Bernal, and M.W. Kirschner. 1999. Identification of a vertebrate sister-chromatid separation inhibitor involved in transformation and tumorigenesis. *Science*. 285:418-422.